THE SOLUBILITY OF POTASSIUM-FELDSPAR IN CALCIC PLAGIOCLASE: EXPERIMENTAL STUDY AND APPLICATION TO NATURAL OCCURRENCES

AI YANG

B.Sc (Changchun College of Geology)

M.Sc (Qualifying, University of Tasmania)

Submitted in partial fulfilment of the requirements

of the degree of Master of Science

at the University of Tasmania

graduating '88

November 1987

Dedicated to My Beloved Country and People,

especially to My Parents.

Thesis Contents

This thesis contains no material which has been accepted for the award of any other degree or diploma in any university and, to the best of my knowledge and belief, contains no copy or paraphrases of material previously published or written by another person, except where due reference is made in the text of this thesis.

艾 楊
aiyang
AI YANG

November, 1987

ACKNOWLEDGEMENTS

I am very grateful to Prof.DH Green for suggesting this study, and for his patient guidance and constant advice at all stages of this work.

Special thanks are due to the following people:

——— Dr.WR Taylor, for his introduction to the high-pressure laboratory and Tasmania wilderness, and for many useful suggestions and valuable discussions.

——— Mr.KL Harris, for his patient instruction in the use of the high-pressure apparatus, for the manufacture of many experimental parts, and for many helpful dicussions.

——— Dr.SM Kuehner and Mr. DN Young, for the samples and unpublished material they provided, especially for detailed explanations of the field geology in the Mawson area (including Departure Rocks).

——— Mr.W Jablonski, for his kind help in the use of the electron microscope and microprobe facilities.

——— Mr.JD Adam, Dr.AJ Crawford, Dr.WR Taylor, and Mrs.ME Wallace, for proof-reading this thesis and for the help in correcting many language mistakes as well as clarifying many ideas (expressions).

——— Prof.S Banno, for his interest in my study and many helpful suggestions and discussions.

——— Dr.E Takahashi, for his suggestion of using the HF-etching technique for SEM observation of the experimental run products.

——— Dr.RJ Ford and Mr.P Robinson, for the help in the use of the XRD instrument. Discussion with Dr. Ford on feldspar crystallography

was very useful.

_____ Mr.S Stephens, for help in the preparation of microprobe mounts and thin sections.

_____ Ms.J Pongratz, for many helpful suggestions in drafting.

_____ Drs.GE Wheller and R Varne, for instructions in the use of a BBC microcomputer, which was used to prepare this thesis; and for helpful discussions.

_____ Drs.TJ Falloon, SF Foley, P Bertrand, EJ Reid, and Messrs SM Eggins, Khin Zaw, NWA Odling, B Harahap, T Wongwanich, S Dwipa, MR Hermanto, for various help and discussions.

_____ Mr.ZJ Lin (Geography Department), for his introduction of, and help in, the use of Macintosh computer.

_____ Many other fellow students, post-doctoral fellows, and staff members in the Geology Department (University of Tasmania), for providing an enjoyable, comfortable, and stimulating study environment. Discussions at the petrology group meetings were very beneficial in improving my English and geology background.

_____ Many Chinses students and visiting scholars in Hobart area, with whom I have shared lots of enjoyable occasions, esppcially some special holidays such as the Chinese New Year's Day and Middle Autumn Festival.

_____ Members of the "ping-pong (table tennis) team" and the "badminton team" of the Chinese Students & Visiting Scholars Association in Tasmania, members of the "volleyball team" of the Geology Department (University of Tasmania), for many enjoyable and relaxing hours spent in the university gymnasium.

——— Mr. & Mrs. Fuglsang (my host family), Prof. & Mrs. Green, Mrs. Parker and friends from the Australia-China Friendship Society (Hobart branch), for providing hospitality and friendship.

——— Drs. PS Law, AC Yong and their families, and other Malaysian friends, for extending their understanding and friendship through all sorts of activities.

An overseas postgraduate scholarship from the State Education Commission of the People's Republic of China is greatly acknowledged. Research fund from the University of Tasmania (to Prof.DH Green) is appreciated.

List of Tables

List of Figures

List of Plates

ABSTRACT

Unusual feldspar intergrowths were found in two metamorphosed basalt dykes from Departure Rocks, Antarctica. They are composed of host calcic plagioclase (Kf_{0-3} An_{75-91} Ab_{9-25}) and potassium-rich alkali feldspar (Kf_{90-96} An_{0-5} Ab_{0-8}) lamellae. Their bulk composition is estimated to be Kf_{21} An_{65} Ab_{14}. The complex and yet regular lamella textures of these intergrowths suggest that they are exsolution products. This requires the existence of a formerly homogeneous plagioclase, compositionally equivalent to the estimated bulk composition of these intergrowths. Experimental studies in the binary system anorthite -- K-feldspar and in the albite-poor ternery feldspar system have proven the existence of such homogeneous plagioclase, which has been synthesized at 1150°C and 10 Kbar under dry conditions. The unusual feldspar intergrowths were homogenized under these same conditions, further supporting the hypothesized exsolution origin of these intergrowths. In an experiment of plagioclase crystallization in a synthetic rock system, a K-rich plagioclase ($Kf_{19.6}$ An_{70} $Ab_{10.4}$) was obtained from a K-rich melt at 1140°C and 10 kbar, indicating that the proposed parental plagioclase for the unusual feldspar intergrowths can be formed in a complex (rock) system. Such K-rich melt could be generated through interaction of the dyke magma and its surrounding charnockitic magma.

It is concluded that limits of solid solutions in feldspar systems are increased at high pressures due to the increase of feldspar melting temperatures. Pressure may have an effect on the extend of feldspar solid solutions, but it is considered to be very small.

INTRODUCTION

In 1985, Dr.SM Kuehner found some texturally and chemically unusual feldspar intergrowths in two basalt dyke samples that he collected from Mawson, Antarctica. These have unusually low Na contents and relatively high K and Ca contents. Texturally they show very complicated twinning and intergrowth lamellae. The complex intergrowth textures are suggestive of exsolution. However, the average bulk composition of these feldspars plots well within the two-feldspar field in the An ($CaAl_2Si_2O_8$) - Ab ($NaAlSi_3O_8$) - Kf ($KAlSi_3O_8$) diagram for the ternary feldspar system. This apparently precludes the existence of a formerly homogeneous feldspar, from which the lamellae may have exsolved.

The two-feldspar field is separated from the one-feldspar field by an empirical curve which defines the limit of ternary feldspar solid solutions. The curve is located on the basis of the analyzed compositions of both natural and synthetic feldspars (Vogt, 1926, pp.48 - 52; Tuttle & Bowen, 1958, p.131, Fig.64; Parsons & Brown, 1983, Fig.7). Most of the natural feldspars analyzed are either formed or re-equilibrated at low temperatures (<1000°C) and pressures (<6 Kbar). Synthetic feldspars are also usually made at low pressures, and low to moderate temperatures, often with various amount of water present. Therefore, the limit of ternary feldspar solid solutions is well known only at low pressures and relatively low to moderate temperatures. Since at high isostatic pressures in dry conditions, the melting temperatures of the feldspar end members are much higher than at atmospheric pressure (or under various water pressures), feldspars with higher solid solutions may stably exist at very high temperatures (>1000°C) in dry and high pressure (10 - 30 kbar) conditions. If such high temperature feldspars can form extensive solid solutions

(Carmichael et al., 1974, p.223), then this would provide an explanation for the existence of K-rich plagioclases, and for the unusual Antarctic feldspar intergrowths described above.

An experimental study under dry conditions at high pressures provides one test of this model. Four sets of experiments have been performed. The first set was in the anorthite -- K-feldspar system, as the mutual solubilities between anorthite and K-feldspar are the least in the ternary feldspar system. If the mutual solubilities between anorthite and K-feldspar can be increased at high pressure, high temperature conditions, then the two-feldspar field in the ternary feldspar system will be considerably reduced as increased Na enhances the one-feldspar field. The second set of experiments was in the Na-poor part of the ternary feldspar system, to bracket the natural intergrowth compositions which are less than 20 mol% albite component. The third set of experiments involved homogenization of the natural feldspar intergrowths under the conditions for one-feldspar field as defined by the foregoing experiments. Finally, a set of plagioclase crystallization experiments was conducted to crystallize the proposed parental plagioclase in complex rock systems.

The results of the first set of experiments are discussed in the second chapter of this thesis and those of the second and third sets are discussed in the third chapter. The final (fourth) set of experiments is described in the fourth chapter. An origin for these unusual feldspar intergrowths is suggested on the basis of the petrographic observations and experimental results. Before detailing the experimental study, it is necessary to understand the geological setting and manner of occurrence of these intergrowths. Geological and mineral-chemical evidence suggests high temperature, high pressure conditions of crystallization, and this aspect will be the main topic of the first chapter.

CHAPTER ONE

GEOLOGICAL BACKGROUND

CONTENTS

CHAPTER ONE

GEOLOGICAL BACKGROUND

1.1 Geological Setting

Eastern Antarctica can tectonically be divided into two regions: the Archaean high-grade metamorphic terranes and the Proterozoic mobile belt between these terranes (Fig 1.1). The Archaean terranes include the early Archaean granulite-facies Napier Complex in Enderby Land, the Archaean Vestfold Hills of Princess Elizabeth Land, and the later Archaean to early Proterozoic Prince Charles Mountains (Sheraton & Black, 1981). The Proterozoic mobile belt between these terranes consists of the Rayner Complex of Enderby Land, and correlates in Kemp Land, MacRobertson Land, Prydz Bay and most of Princess Elizabeth Land (Blacket al., 1981).

Detailed studies of field geology, petrology, geochemistry and geochronology have shown that these Archaean terranes have experienced several complex metamorphic and tectonothermal events (Sheraton et al., 1980; Ellis, 1980; Sheraton & Black, 1983; Black et al., 1983). The evolution of the Proterozoic mobile belt started much later and was relatively simple (Black et al., 1987). Within the Proterozoic mobile belt of the Mawson area of MacRobertson Land, charnockite occurs over an area of at least 2000 Km^2. The charnockite, named Mawson Charnockite after the ANARE station "Mawson" (Trail, 1970), is dark brown, medium to coarse-grained, and mainly composed of quartz, hypersthene, and feldspars, with or without garnet, biotite, and hornblende. Mawson Charnockite is further divided into porphyroblastic and even-grained types, depending on the presence or absence of large feldspar

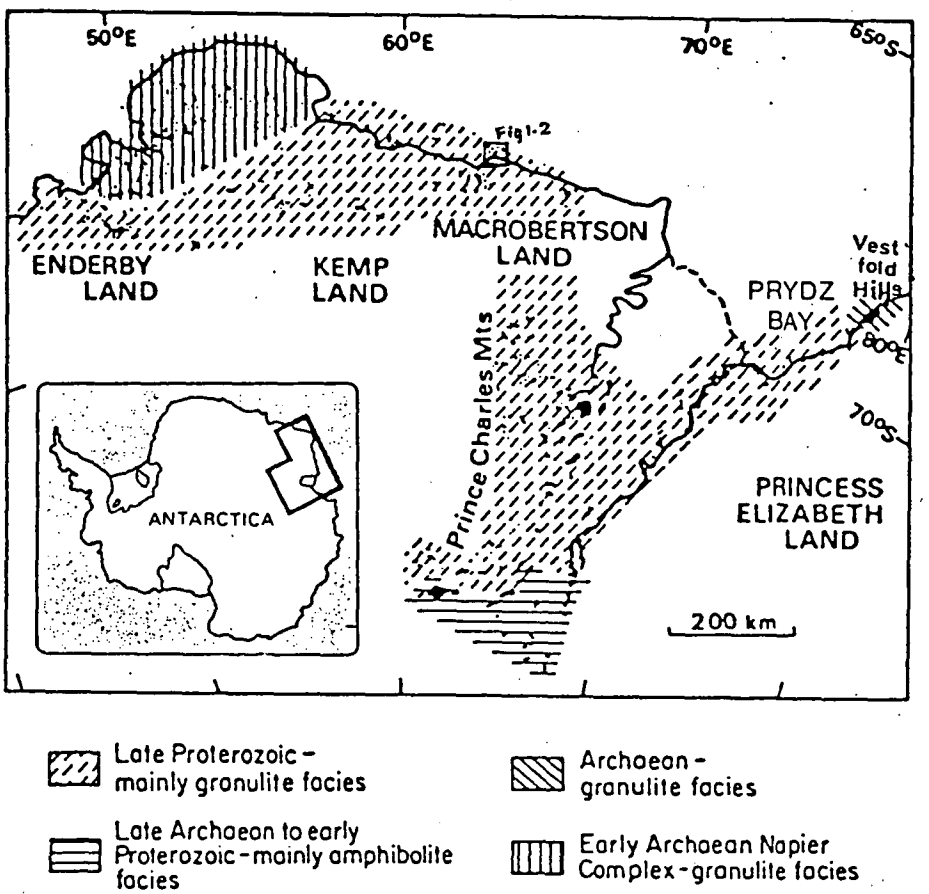

Fig 1.1 Simplified Geological Map of Eastern Antarctica (Modified from Sheraton & Black, 1981).

(alkali feldspar or/and plagioclase) porphyroblasts (McLeod et al., 1966). Intrusive contacts occurs between Mawson Charnockite and its "gneiss inclusions" (Crohn, 1959). The even-grained charnockite is also intruded by the porphyroblastic charnockite (Sheraton, 1982). The Mawson Charnockite is therefore interpreted to have an igneous origin. The "gneiss inclusions" are pyroxene-bearing gneisses (garnet and biotite are often present with or without amphibole). An integrated geochronological, geochemical and petrological study of the Proterozoic mobile belt by Black et al. (1987) has shown that Mawson Charnockite intruded its "gneiss inclusions" slightly later than 963 m.a. BP, when the gneisses were formed during a transitional amphibolite- to granulite-facies metamorphism (about 7 - 8 Kbar, 750^{o}C). Soon after its intrusion, Mawson Charnockite was itself intruded by some basaltic dykes. Localized melting caused the intrusion of some aplites and garnet-bearing pegmatites at about 770 m.a. BP. A regional upper greenschist metamorphism took place at about 540 m.a. BP, accompanied by localized shearing and faulting.

1.2 Mafic Dykes from Mawson Area

A number of basalt dykes in the Mawson area were sampled during the 1984 - 85 ANARE summer season by Dr.S.Kuehner. Among these dykes, six are from some of the small islands very close to Mawson station (Fig 1.2). Two of these dykes contain feldspar intergrowths which are rich in K and Ca, and yet poor in Na. This kind of feldspar intergrowth is classically called antiperthite. In order to emphasize the oddness of this feldspar intergrowth it will be called "unusual feldspar intergrowth" although it will become apparent later that it should be called "unusual" antiperthite.

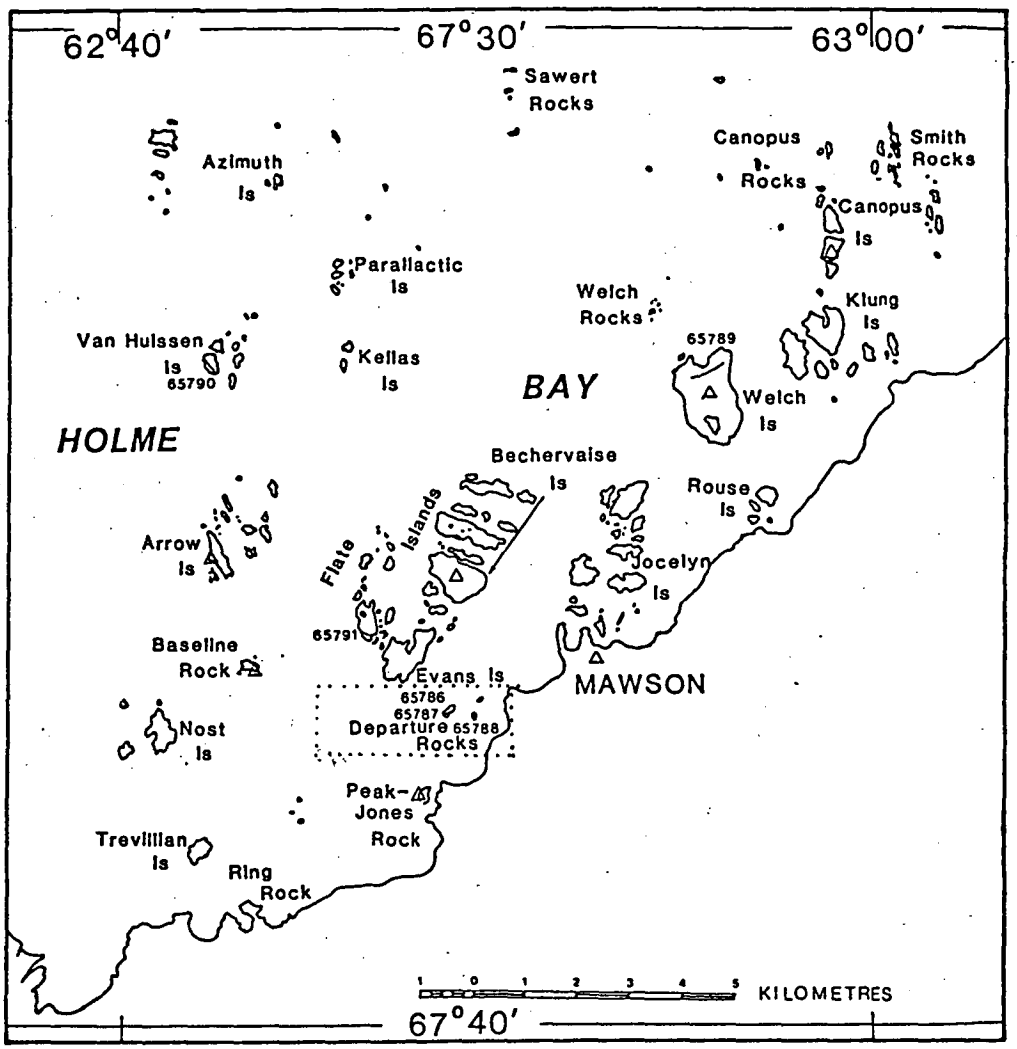

Fig 1.2 Localities of Mafic Dykes in the Mawson Area. Numbers are of the dyke samples housed in the Department of Geology, University of Tasmania (based on Kuehner (unpub.)).

Most of the six dykes are made up of orthopyroxene, clinopyroxene, plagioclase, and Fe -Ti oxides with accessory apatite (Table 1.1). Three dykes contain phlogopite. The unusual feldspar intergrowths occur in the dykes that do not contain phlogopite, which suggests that these dykes were formed in relatively dry condition. One dyke sample (65788) contains only 0.20 wt% K_2O, which is the least among all the Mawson dykes (Table 1.2). This dyke contains plagioclase showing no intergrowth of K-feldspar and has the character of a two-pyroxene plus plagioclase granoblastic granulite. It is not possible to ascertain if the differences in K-content between this dyke and the other five dyke samples (average K_2O = 0.90%) reflect primary magmatic difference or differences resulting from chemical interaction between dykes and wall-rocks.

All Mawson dykes have suffered deformation and recrystallization. None of the crystals in these dykes have regular igneous shapes; and small crystals are often found to be recystallization products along large crystal boundaries. Such deformation and recrystallization features are even clearer in their host rocks. Mafic minerals (usually orthopyroxene) in the host rocks are alligned, showing obvious lineation, and felsic minerals (plagioclase, alkali feldspar and quartz) are flattened, with elongated crystal shapes. The deformation and recrystallization event post-dates or is synochronous with dyke emplacement. In later paragraphs the dyke mineralogy is used to define these conditions of recrystallization.

The two dykes that have the unusual feldspar intergrowths are mainly composed of feldspars (about 52%) and pyroxenes (about 33%). Quartz, magnetite, ilmenite, and apatite are about 10 - 15% in total. Feldspar crystals may be as large as 5 mm x 3 mm but are generally between 2.5 mm x

Table 1.1 Mineralogy of Mawson Dykes

Dyke No.	65786	65787	65788	65789	65790	65791
Olv	-	-	-	-	-	+
Opx	+	+	+	+	+	+
Cpx	+	+	-	+	-	+
Plag	+	+	+	+	+	+
Kf	+	+	-	-	-	-
Phl	-	-	-	+	+	+
Qz	+	+	+	+	+	-
Mt	+	+	-	-	-	-
Ilm	+	+	+	-	+	-
Apt	+	+	+	-	+	-
S	-	-	-	-	-	+
texture	recrystallized porphyritic					equi-granular

*)abbreviations: Olv - Olivine; Opx - Orthopyroxene; Cpx - Clinopyroxene; Plag - Plagioclase; Kf - Potassium Feldspar; Phl - Phlogopite; Qz - Quartz; Mt - Magnetite; Ilm - Ilmenite; Apt - Apatite; S - Iron (Nickel) Sulfides.

**)symbols: + present; - absent.

2 mm to 1.5 mm x 1 mm. Pyroxene crystals are relatively smaller, ranging from 1.5 mm x 1 mm to 1 mm x 0.6 mm. The texture of these dykes show obvious deformation and recrystallization (plate 1.1). It is likely that the large crystals are relict phenocrysts but have been modified by the later metamorphism.

1.3 Mafic Dykes from Departure Rocks

Departure Rocks, about 3 Km from Mawson station, are formed by two tiny islands, West Rock and East Rock (Fig 1.3). East Rock is mainly charnockite, but also contains boudins of gneiss and one deformed, boudinaged basalt dyke (65788). This dyke does not contain either the unusual feldspar intergrowths or phlogopite. West Rock is composed of charnockite and orthopyroxne-bearing gneiss, which are separated by a clear-cut, intrusive contact. In some places, the gneiss was partially melted, apparently due to heat input from the intruding charnockite. Felsic leucosomes or veins of Opx-bearing melt are thus formed along the intrusive boundary (DN Young, written communication, 1987), which is now parallel to regional S_3 fabric (334°). Field observation suggests that early intense folding events D_1 and D_2 took place before the intrusion of charnockite into the Opx-bearing gneiss, and that the early fabrics (mainly $S_0 = S_1$) rotated into parallelism with S_3 (DN Young, written communication, 1987). A few boudins of Opx-bearing gneiss have also been found within the charnockite. Both the gneiss and charnockite are intruded by two basalt dykes (65786 & 65787; Fig 1.3). The two dykes have almost identical chemical and mineralogical compositions (Table 1.2 & Table 1.1) and may in fact be parts of a single dyke. The curvature of dyke 65787 in the Opx-bearing gneiss along S_3

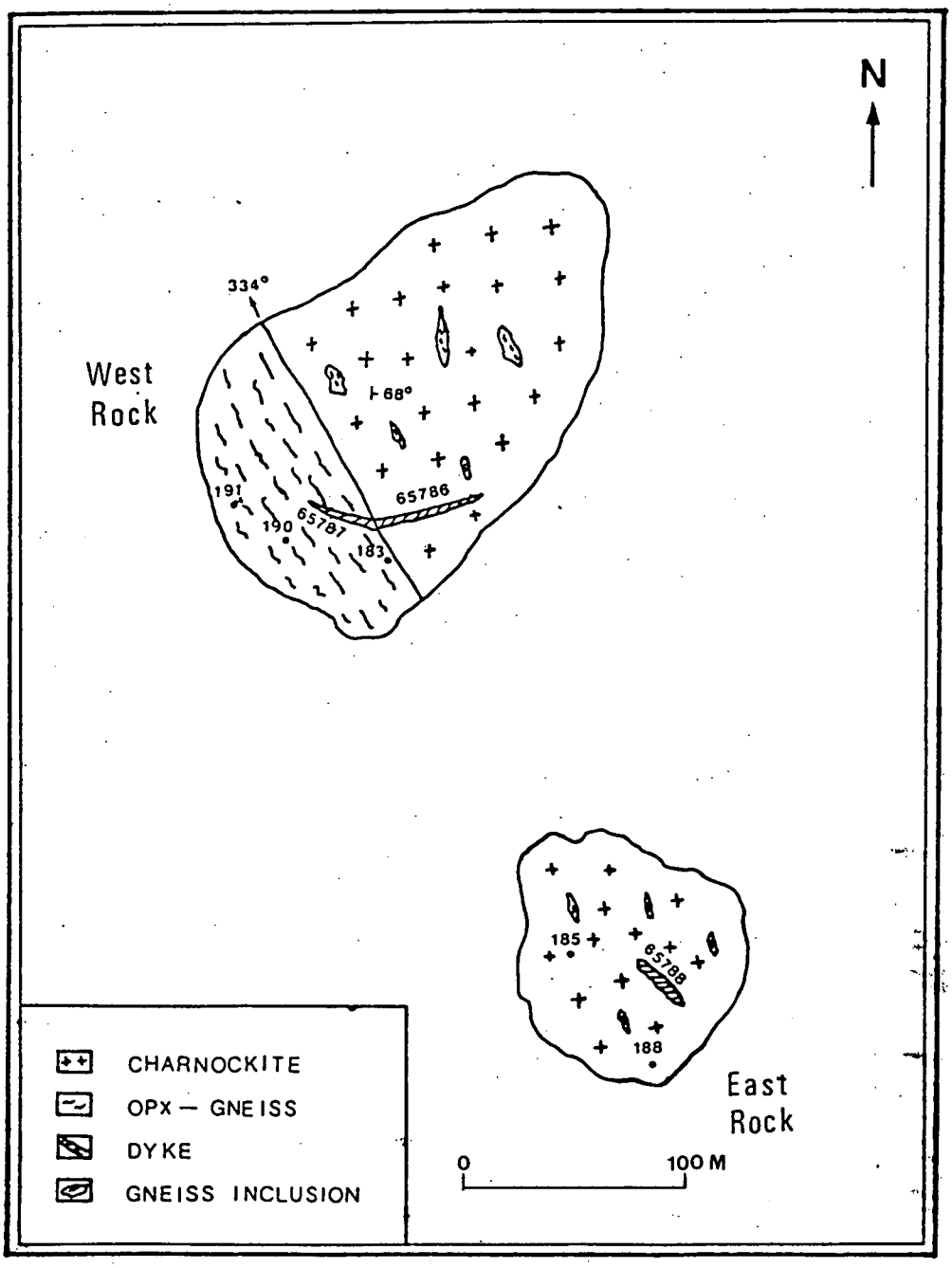

Fig 1.3 Sketch Map Displaying the Main Geological Features of Departure Rocks (based on field data supplied by SM Kuehner & DN Young).

Table 1.2 Chemical Compositions of Mawson Dykes and Host Rocks

	Mawson Dykes*						Host Rocks**				
	65786	65787	65788	65789	65790	65791	183	190	191	185	188
major elements (wt%)											
SiO2	52.27	51.81	51.86	49.49	51.42	44.27	73.00	60.42	78.33	63.47	64.46
TiO2	2.10	1.81	1.99	0.86	2.11	0.75	0.49	0.64	0.16	1.00	0.88
Al2O3	15.97	16.69	16.67	15.50	16.57	8.14	12.73	16.31	11.05	15.56	15.85
Fe2O3	1.52	1.47	1.60	1.27	1.28	1.61	0.79	1.77	0.56	0.60	0.90
FeO	10.11	9.77	10.68	8.48	8.56	10.76	3.00	6.24	0.69	5.94	4.76
MnO	0.29	0.27	0.28	0.22	0.20	0.22	0.10	0.10	0.02	0.12	0.10
MgO	4.98	5.53	5.83	9.44	6.49	26.61	2.07	4.88	0.56	2.86	2.26
CaO	9.45	9.59	8.22	9.52	7.58	4.94	4.63	5.26	1.07	4.44	4.42
Na2O	0.68	0.68	1.03	1.58	1.17	1.01	1.93	2.63	1.66	2.68	2.54
K2O	0.80	0.56	0.20	1.08	1.62	0.46	0.59	0.69	5.43	2.25	2.77
P2O5	0.36	0.30	0.32	0.10	0.70	0.11	0.10	0.06	0.04	0.10	0.17
LOI	-0.45	-0.51	-0.62	-0.26	-0.09	0.25	0.04	0.01	0.01	0.11	0.07
H2O-	0.23	0.27	0.23	0.23	0.22	0.22					
Sum	99.43	99.32	99.48	98.46	98.79	100.05	99.47	99.01	99.58	99.13	99.18
trace elements (in ppm)											
Zr	187	157	129	88	452	74	227	91	180	247	181
Sr	297	295	279	131	412	128	83	89	88	195	164
Nb	15	14	13	5	31	4	14	11.5	2	16.5	24
Y	44	39	35	23	39	15	40	17	7	20	20
Rb	15	13	2	60	193	16	5.5	7.5	153	49.5	67
Ba	660	391	270	461	2300	208	170	230	945	685	550
V	178	177	196	262	236	127	29	74	8	108	82
La	24	22	23	36	76	11	64	32	29	45	45
Ce	49	37	47	71	166	20	142	61	48	84	94
Sc	38	38	41	39	34	21	15	23	6	20	16
Ni	20	18	31	209	59	1289	4	37	2	26	17
Cr	59	63	61	622	242	598	6	100	3	53	29
Nd	30	25	26	32	81	12					

@) 65786 & 65787 contain the unusual feldspar intergrowths.

*) Analyses of Mawson Dykes were done by Dr.S. Kuehner.

**) Host Rocks from Departure Rocks (D. Young, unpub.).

is probably caused by the deformation event D_3, because the gneiss is less competent than the charnockite.

Both alkali feldspar and plagioclase are found in the charnockite. The alkali feldspars are very rich in K, almost identical in composition to the alkali feldspar lamellae in the unusual feldspar intergrowths in the dykes. The plagioclases are less Ca-rich than those in the unusual feldspar intergrowths in the dykes (Fig 1.4). It could be possible that the unusual

Table 1.3 Ba Abundances (wt%) in Feldspars in Dyke 65786 and Host Charnockite 185

Sample No.	65786			185		
analy No.	1	2	3	1	2	3
K_2O	13.26	14.76	14.83	14.03	13.64	14.52
BaO	1.25	1.18	1.23	0.40	0.31	0.41

feldspar intergrowths might have come from the charnockite. However, the barium contents in the alkali feldspar lamellae in the unusual intergrowths are much higher than those in the alkali feldspar of similar K_2O content in the charnockite (Table 1.3), although the barium abundances in the dykes are similar to or even slightly lower than those in the charnockite (Table 1.2). This apparently excludes the possibility of the unusual feldspar intergrowths being xenoliths from the host charnockite.

In an experimental investigation by Watson & Jurewicz (1984), a molten oceanic tholeiite was kept in contact with a partially molten granite. It was found that interdiffusion of melt components was limited for structure-controlling species such as Si^{+4} and Al^{+3}, and also for divalent cations. However, interdiffusion of alkali ions was very rapid, resulting in consi-

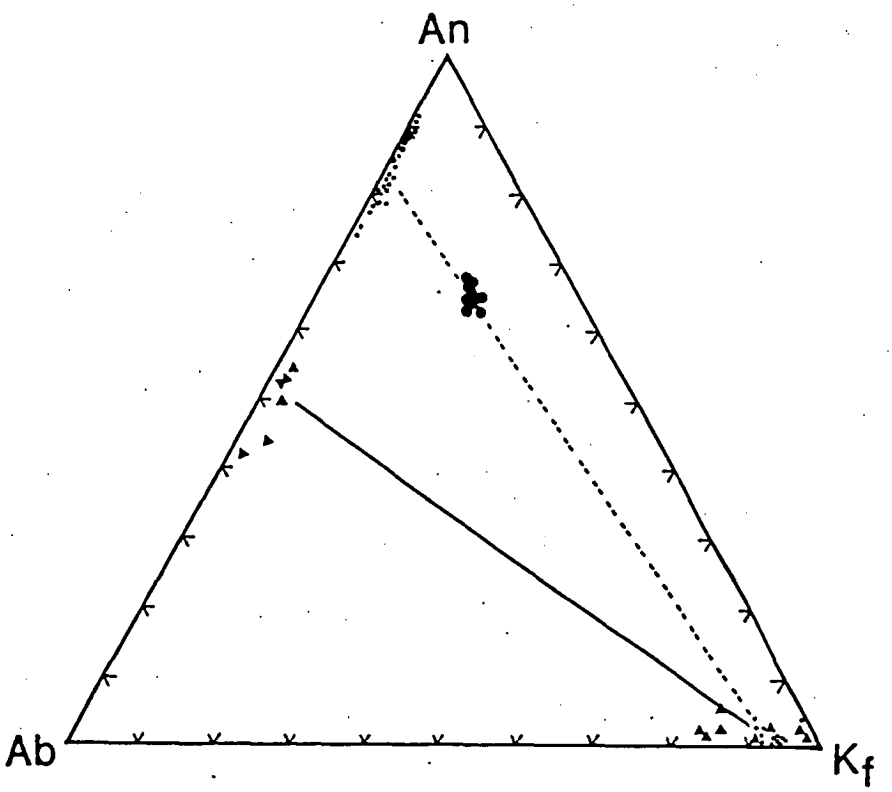

Fig 1.4 Compositions of Feldspars from the Two Dykes in West Rock (dots) and from the Host Charnockite (triangles) Plotted in the Ternary Feldspar Diagram. K-feldspars from the dykes are lamellae in the An-rich plagioclase host. Their bulk compositions are shown by the large dots, obtained by defocused-beam EMP area scans. The K-feldspar lamellae and their host plagioclases are connected by a broken line. K-feldspars and plagioclases from the charnockite are separate crystal grains. They are connected by a solid line, indicating coexistence of these feldspars. (Note: The large dots shown in the diagram are only the representative area scan analyses.)

derable up-take of K by the basaltic melt and loss of Na from the basalt to the granite. This raises the possibility that the K in the K-rich plagioclase-bearing dykes may have come from the surrounding charnockite through a diffusional process. At present there is no strong evidence for or against such process in operation. This problem remains to be explored.

1.4 Estimation of Temperatures and Pressures

Most of the dykes contain two pyroxenes, plagioclase, and Fe - Ti oxides in a fine-grained granoblastic texture in which mineral grains do not show chemical zoning. It may be assumed that this is an equilibrated metamorphic assemblage and equilibration temperatures and pressures can be calculated using mineral geothermometers and geobarometers. There are a number of two-pyroxene thermometers available at present (Wood & Banno, 1973; Ross & Huebner, 1975; Wells, 1977; Powell, 1978; Kretz, 1982; Fonarev & Graphchikov, 1982; Lindsley, 1983; Bertrand & Mercier, 1985). Detailed evaluations of pyroxene thermometers, by Stephenson (1984) and Carswell & Gibb (1987), concluded that none of these is universally satisfactory. Best temperature can be assessed by consideration of a combination of the most satisfactory thermometer formulations, based on both the two-pyroxene solvus and the Fe^{2+} - Mg exchange reactions (Carswell & Gibb, 1987). The most recent version, by Bertrand & Mercier (1985), (not evaluated by Carswell & Gibb, 1987), appears to be the most self-consistent and to give the most reasonable results when applied to these dykes from the Mawson area. There is one thermometer for coexisting Fe - Ti oxides (Spencer & Lindsley, 1981), and only one barometer for coexisting plagioclase - clinopyroxene (Ellis, 1980), which are applicable to these rocks. In this study the two-pyroxene

thermometers of Wells (1977), Kretz (1982) and Bertrand & Mercier (1985), the Fe - Ti oxide thermometer of Spencer & Lindsley (1981) (with the recalculation scheme of Stormer, 1983) and the plagioclase - clinopyroxene barometer of Ellis (1980) are used. The results are shown in Table 1.4 and Fig 1.5.

As discussed above the textures of these dykes and their host rocks clearly indicate that they experienced a metamorphic event, and that the equilibrium temperatures and pressures of minerals in these rocks should reflect that event. For coexisting pyroxenes, temperatures calculated by the Wells (1977) method are generally 150°C higher than those calculated by other methods, probably because it uses the ideal solution model of Wood & Banno (1973) and thermodynamic data extrapolated from experimental results obtained at high temperatures. Other methods give a reasonable temperature around 750° +/- 50°C, which is probably the temperature during peak metamorphism. The calculated temperatures of coexisting Fe - Ti oxides are around 600° +/- 50°C, probably reflecting the temperatures during waning of the metamorphic event. The coexisting Fe - Ti oxides in the host charnockite yield an equilibrium temperature of about 600°C. Therefore such temperature may well be the preserved regional metamorphic temperature. Because of the absence of clinopyroxenes in the host rocks, temperature can not be estimated from them using the two-pyroxene thermometers.

Neglecting the temperatures calculated using the Wells (1977) method, some are still higher than 750° +/- 50°C. They may be caused by several factors, such as non-equilibrium between the two pyroxenes chosen and limitations in the thermometers used. Nonetheless, the majority are very close to 750° +/- 50°C. Using this temperature, and compositions of coexisting

Table 1.4 Estimated Temperatures and Pressures

	Temperature (°C)					Pressure (Kbar)	
	Two-Pyroxene Thermometers				Fe-Ti Oxide	Cpx - Plag	
Sample No.	Wells	B & M	Kretz trans	Kretz exch	Thermometer S & L	Barometer No.	Barometer Ellis
65786-1	894	775	669	693	657	65786-1	6.4
65786-2	844	730	560	636	641	-2	4.0
65786-3	862	686	656	803	713	-3	4.6
65786-4	895	731	714	807	707	-4	2.8
65786-5	1152	1152	1203	1421	583	-5	6.4
65786-6	913	754	755	880	579	-6	4.8
65786-7	1061	987	1082	951	605	-7	2.7
65786-8	870	716	670	811	617	-8	4.7
65786-9					733	-9	6.0
65786-10					589	-10	3.0
65787-1	941	790	788	868	580	-11	10.4
65787-2	920	746	742	810	619	-12	10.5
65787-3	908	754	776	824	577	-13	6.2
65787-4	884	745	672	648	632	-14	6.9
65787-5	903	757	700	768	586	-15	6.4
65787-6	922	744	731	1011	635	-16	7.8
65787-7	906	764	741	906			
65787-8	1086	994	1106	995		65787-1	6.4
65789-1	1055	955	1073	1042		-2	1.4
65789-2	1093	1022	1130	988		-3	8.3
65789-3	874	777	710	659		-4	1.9
65789-4	927	762	763	715		-5	6.5
65789-5	931	740	734	877		-6	8.5
65789-6	942	785	785	718		-7	6.6
65791-1	835	723		1105		-8	3.3
65791-2	837	733		1044		-9	5.1
184-1					623	-10	5.4
184-2					640		

*) References for the thermometers and barometer used:

Wells (1977); B & M (Bertrand & Mercier, 1985); Kretz (1982); S & L (Spencer & Lindsley, 1981); Ellis (1980).

**) trans: Ca-transfer thermometer;

exch: Fe - Mg exchange thermometer.

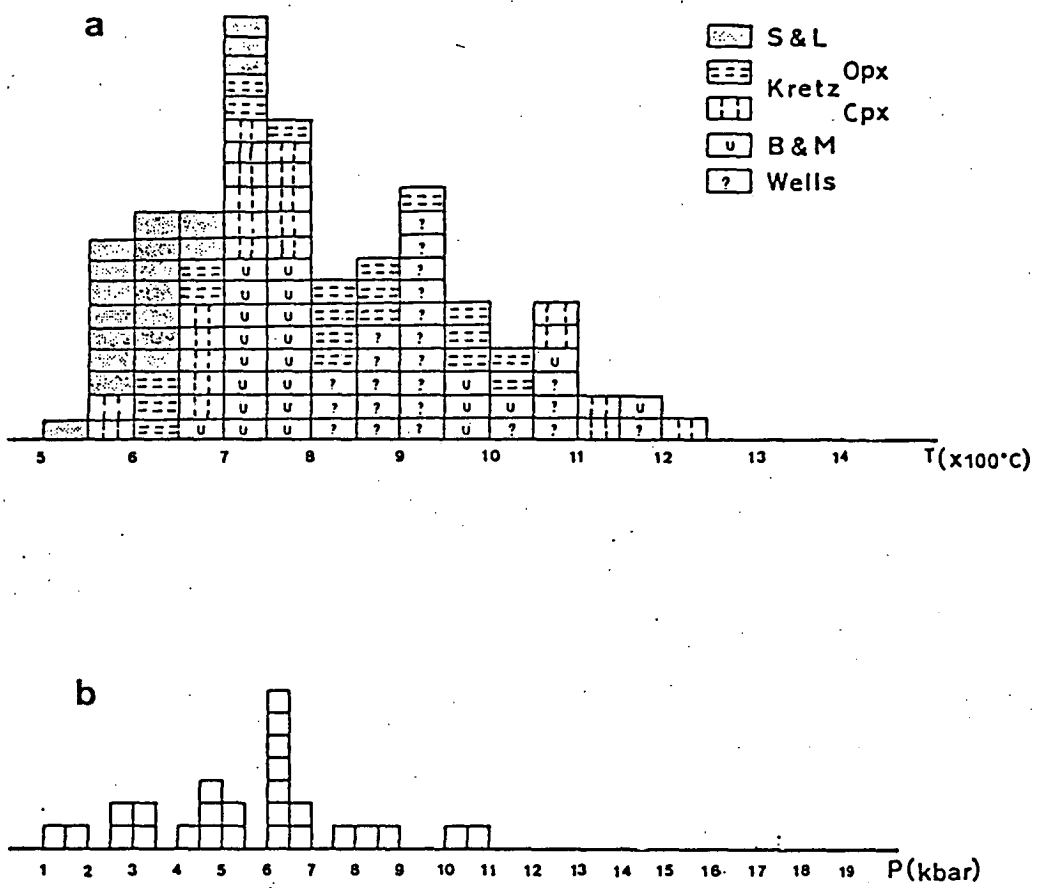

Fig 1.5 Estimated Equilibrium Temperatures (a) and Pressures (b) for Minerals in the Mawson Dykes (data in Table 1.4).

plagioclases and clinopyroxenes, pressures can be calculated following the method of Ellis (1980). A pressure of 6 +/- 1 kbar is obtained and may represent the regional metamorphic pressure. (If the lower temperature of 600°C is used, the calculated pressure will increase 1 - 2 Kbar).

Some representative analyses of coexisting pyroxenes, Fe - Ti oxides, and plagioclases and clinopyroxenes are listed in Appendix I. The detailed formulations of the thermometers and barometer used in this study are given in Appendix II.

1.5 Unusual Feldspar Intergrowths

1.5.1 A Review of Feldspar Intergrowths

Plagioclase and alkali-feldspars are the commonest feldspar groups. At high temperatures they are homogeneous and can have monoclinic crystal structure, which is the highest symmetry for this group of minerals. At low temperatures they have lower crystal symmetry (triclinic) and often form very complex intergrowths. The intergrowths may be primary, when the feldspars are formed at low temperatures; or may be secondary, when the homogeneous high temperature feldspars re-equilibrated at lower temperatures. Three main types of intergrowths have been recognized in natural plagioclases and are collectively called micrometer intergrowths (Smith, 1974). The three main types are Peristerite, Boggild, and Huttenlocher intergrowths.

Peristerite intergrowth has a bulk composition ranging from An_2 to An_{16}. The X-ray diffraction pattern shows two sets of spots whose positions suggest the presence of two components: one with the composition nearly pure albite, and the other around An_{25}. Plagioclases with Peris-

terite intergrowth are usually found in regional metemorphic rocks and pegmatites. Such intergrowth is interpreted as exsolution of high temperature homogeneous plagioclase (oligioclase).

Boggild intergrowth has the bulk composition about An_{46} to An_{60}, often with more than 2 wt% Kf. It is suspected to be made up of sodic "e"-type plagioclase (see Appendix III for explanation of the "e"-type plagioclase) and calcic "e"-type plagioclase, with compositions of An_{44} and An_{58} respectively (Ribbe, 1983). Plagioclases with this kind of intergrowth are often found in Precambrian metamorphic rocks.

Huttenlocher intergrowth is usually found in non-volcanic plagioclases, with the bulk composition An_{66} to An_{90}. It consists of sodic "e"-type plagioclase and a kind of anorthite solid solution. Most of the plagioclases with Huttenlocher intergrowth are from deep-seated metamorphic rocks. Both Huttenlocher and Boggild intergrowths are explained as coherent spinodal decomposition inside the crest of the plagioclase solvus (Smith, 1974; 1983; 1984).

In natural alkali-feldspars, three main types of intergrowths have also been distinguished, according to whether a K-rich phase or a Na-rich phase is dominant in the intergrowth. When a K-rich phase is dominant (as host), the intergrowth is called Perthite; when a Na-rich phase is dominant over a K-rich phase, the intergrowth is called Antiperthite; when the two phases are equally dominant, the intergrowth is called Mesoperthite (Barth, 1969, Fig 1.14). The three main types are further sub-divided into three groups according to the size of the lamellae. They are macro-, micro-, and crypto-(perthite/mesoperthite/antiperthite) (Laves & Soldatos, 1963). Macroperthites are those with lamellae thicker than 0.05 mm and therefore easily visible

with a simple hand-lens; microperthite covers perthites distinguishable with an optical microscope, and whose lamellae are thinner than 0.05 mm. Cryptoperthite includes perthites not distinguishable microscopically, which can only be recognized by other methods, such as X-ray diffraction, electron microscopy, and sometimes iridescence (Smith, 1974; Vol.2, p.404).

Because of the variety of alkali-feldspar intergrowths, many mechanisms are suggested to explain their origin. Among these, three are considered to be important: heterogeneous nucleation, metasomatism (or replacement), and exsolution. Heterogeneous nucleation takes place at high temperatures, where nucleation occurs most easily. Metasomatism is a likely process for the formation of coarse patchy mesoperthites in metasomatic rocks (Smith, 1974). Exsolution is the favoured mechanism to explain most alkali-feldspar intergrowths. However, it is now realized that exsolution in feldspars is very complex.

Two kinds of solvus have been recognized in the alkali-feldspar system. One is an equilibrium solvus, which is the one normally refered to; the other is the coherent solvus, which is related to the formation of coherent phases. The coherent phases have a continuous structure across the lamellae interface, as shown in Fig 1.6. Each solvus is associated with another solvus-like curve, called a spinodal. The relationship between these can be best explained with the aid of the G - X and T - X diagrams shown in Fig 1.7. In a binary system A - B, the change of Gibbs free energy, G, during mixing (or unmixing) at fixed pressure and temperature is shown as a continuous curve [the solid curve in Fig 1.7 (a)] with two minima and one maximum, corresponding to the most stable (equilibrium) and the most unstable state. The compositions of the two minima define a curve in the T - X

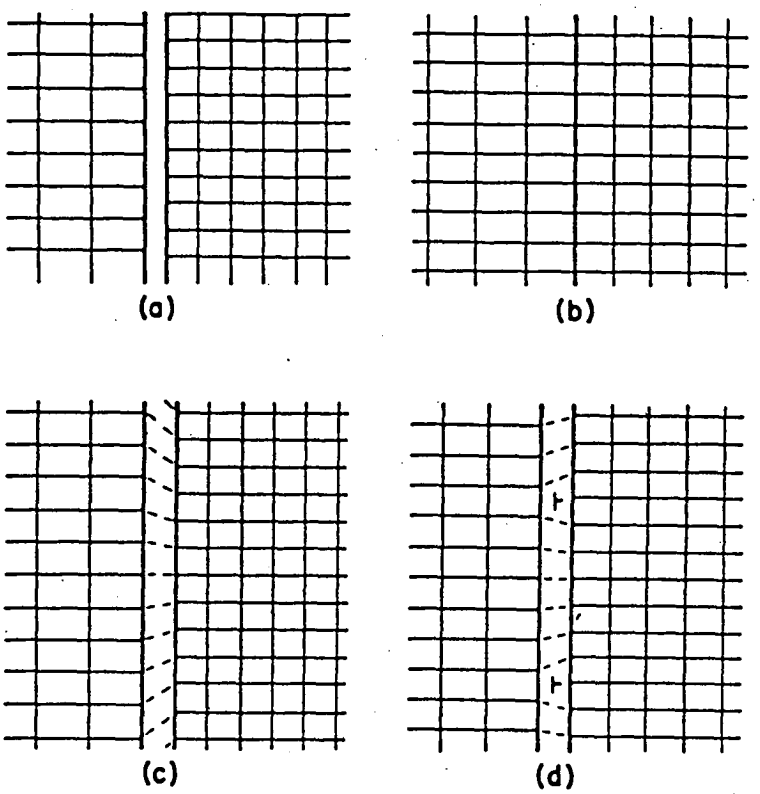

Fig 1.6 Schematic Illustration of Noncoherent, Coherent, and Semicoherent Phase Boundaries. (a) Two lattices of different spacing because of compositional difference. If pushed together they would form a noncoherent boundary. (b) Same lattices (phases) as in (a) but joined with perfect coherency and homogeneous strain. (c) Impossible way to achieve coherency. (d) Semicoherent boundary with dislocations: the strain is inhomogeneous in the interface region. (after Yund & Tullis, Fig 7, 1983).

Fig 1.7 (a) Gibbs Free Energy as a Function of Composition during Subsolidus Mixing/Unmixing of Two Phases in a Hypothetical Binary System A - B at Fixed Temperature and Pressure. Because of the addition of the coherency strain energy the coherent phases have higher stable energy (indicated by the dashed curve) than the non-coherent phases (shown by the solid curve). "s_1" and "s_2" are the inflection points or spinodes, which make the spinodal in the T - X diagram (b).

(b) Schematic T - X Diagram Showing the Relation between Equilibrium (Strain-free) Solvus (M) and Coherent Solvus (M′). Dotted lines are the equilibrium spinodal (S) and coherent spinodal (S′).

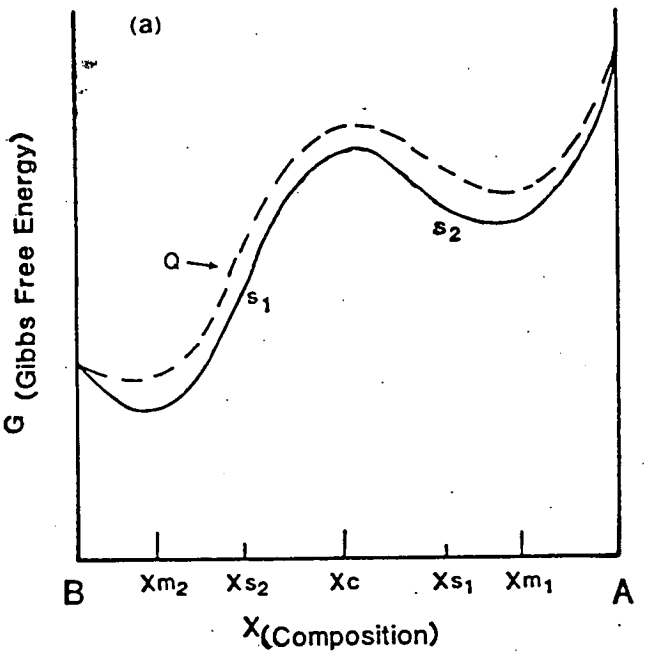
(a)
G (Gibbs Free Energy)
Q
s_1
s_2
B
Xm_2
Xs_2
Xc
Xs_1
Xm_1
A
X (Composition)

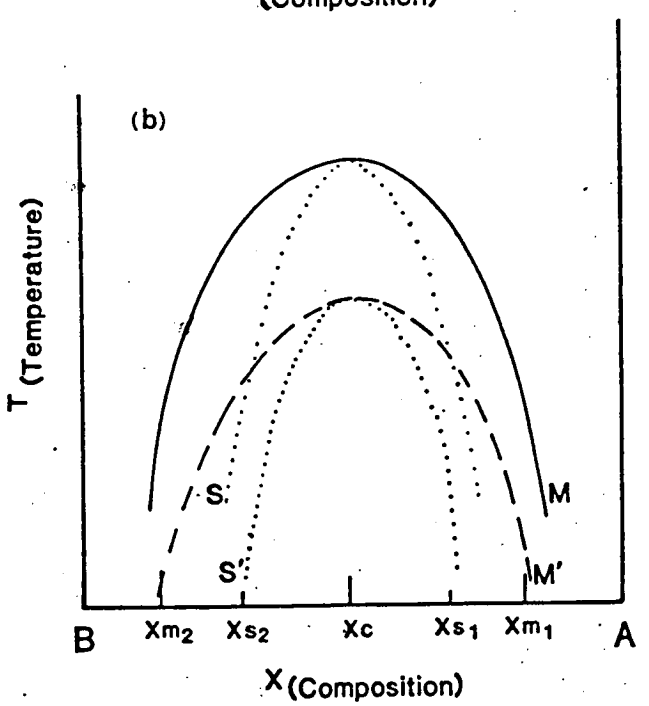
(b)
T (Temperature)
S
S'
M
M'
B
Xm_2
Xs_2
Xc
Xs_1
Xm_1
A
X (Composition)

diagram [the solid curve M in Fig 1.7 (b)]. This is the equilibrium (or chemical or strain-free) solvus. This curve connects two most stable phases that have the lowest Gibbs free energy at the fixed pressure and temperature. There are another three inflection points on this curve. One is the maximum. The other two (s_1 & s_2) are between the maximum and the two minima. Whereas the maximium is the most unstable point on this curve, the other two inflection points s_1 & s_2 may be metastable, provided there is an extra amount of energy to help maintain the stability of the phases. It is therefore at least theoretically possible that the two phases whose compositions corresponding to s_1 and s_2 may be stable at a given pressure and temperature. These s_1 and s_2 points define a curve called a spinodal in the T - X diagram [dotted curve S in Fig 1.7 (b)]. (More sophisticated treatment of spinodal decomposition theory can be found in Cahn, 1968; Hillard, 1970; and Langer, 1973). In a similar way the coherent solvus [M' in Fig 1.7 (b)] and spinodal [S' in Fig 1.7 (b)] can be drawn in the T - X diagram, corresponding to the Q - X curve [broken curve in Fig 1.7 (a)] in the G - X diagram. The energy Q is the sum of the Gibbs free energy and the coherency strain energy, resulting from the coherent growth of the two phases. This coherent spinodal is more realistic than the equilibrium (strain-free) spinodal because such coherency strain energy is practically available as long as the phases grow coherently.

Recent experimental studies of alkali-feldspar exsolution have shown that cryptoperthite can be duplicated in laboratory conditions and that most of the cryptoperthites may well be the result of coherent spinodal decomposition (Yund, 1983; and references therein). For coarse perthites the interpretation is more difficult. Some may have formed by initial coherent spino-

dal/solvus decomposition, but later the coherency is lost during coarsening (Ribbe, 1983; Yund, 1983). The coarsening process of perthite lamellae is complex and governed by many factors, two of which are the Ca contents of the alkali-feldspars and H_2O. Parsons (1978) and others emphasize that water is likely to play an important role in the development of coarse perthites, especially in many granitic rocks. In a micro-structural study of perthites from the granulite complex of Finland, Yund et al. (1980) noticed that many grains of perthite contain coherent lamellae together with a third feldspar phase which is coarser, non-coherent, Ca-rich, and occurs in the form of blebs. Their interpretation is that the Ca-rich blebs formed at high temperature by heterogenerous nucleation and that the Ca-poor lamellae formed by spinodal decomposition at lower temperatures. The preservation of these microstructures is attributed to the low water content of these granulite-facies rocks.

Feldspars that contain more than 5 mol% of each of the components An, Ab, and Kf are called ternary feldspar. A feldspar intergrowth whose bulk composition corresponds to a ternary feldspar is therefore termed a ternary feldspar intergrowth. The most common examples of ternary feldspar intergrowths are mesoperthite and antiperthite. These often have a Na-rich phase dominant, which usually contains more than 5 mol% An (and > 5 mol% of Ab), and a K-rich phase which always exceeds 5 mol%. Most mesoperthites occur in charnockite and granulite-facies metamorphic rocks. Exsolution and metasomatism are the two main mechanisms proposed to explain their origin (Smith, 1974). At present detailed studies are lacking. The study of antiperthites, however, has received much attention recently. Two representative examples should be mentioned. The first is a study by Kay (1977), who investigated

antiperthites in anorthosites from Laramie Range and Adirondacks, New York, by various methods (including optical observation, electron microprobe analysis, transmission electron microscope observation, universal stage measurement, single crystal X-ray diffraction, and heating experiments). She convincingly demonstrated that these antiperthites originated by an exsolution mechanism involving nucleation and growth from originally homogeneous ternary feldspars. The main reasons are as follows:

1). An content of the host plagioclase increases near the K-feldspar lamellae, indicating slow diffusional transport of Ca and Al in exchange for alkalis and Si away from the bleb site.

2). The flattened sides of the Kf lamellae are orientated near $(\bar{3}01)$, $(0\bar{4}1)$, and (100) and subparallel to planes with minimal elastic strain in peristerite, which is the host plagioclase.

3). The crystallographic axes of the non-coherent blebs and the plagioclase host are subparallel.

4). Heating experiments suggest that "at high enough temperatures over long periods of time, diffusion rates of Al and Si are adequate to produce antiperthites by exsolution". (Kay, 1977, p.915).

In Kay's (1977) heating experiments, antiperthites were not homogenized even after six months of heating at 1000°C and 1 atm. The reason may be that the temperature is not high enough. It could not simply be raised because the lamellae would melt at temperatures higher than 1060°C at one atm (the eutectic point in the anorthite -- potassium feldspar system). This in fact happened, as Kay's (1977) runs at 1100°C yielded K-rich melt. In order to raise the temperature high enough to homogenize antiperthite and not to cause melting, higher isostatic pressure is necessary. Details will

be further discussed in the next chapter.

The second example is a study of "moonstone" from Labrador, Canada by transmission electron microscopy (TEM) (Ried & Korekawa, 1978). The "moonstone" is made up of two parts: part A contains fine plagioclase lamellae of thickness usually less than 1 micrometre and bulk composition about $An_{27.2}\ Ab_{69.2}\ Kf_{3.6}$; part B shows no lamellae under the petrographic microscope, but TEM reveals that it consists of fine lamellar intergrowths of plagioclase and K-feldspar. The suggested bulk composition of part B is $An_{20}\ Ab_{50}\ Kf_{30}$. TEM observation of part A shows the presence of two types of twinning {following albite (010) and pericline [010] laws} which partly have sharp and distinct boundaries along (010) and partly penetrate each other, forming a typical "M-twinning". The significance of "M-twinning" is that it indicates the presence of initial monoclinic plagioclases. This is because it is commonly seen in microclines that have inverted from monoclinic sanidine. In part B some exsolved Kf lamellae 150 Å to 15000 Å thick, are oriented parallel to $(\bar{8}01)$. They are partly coherent with the host plagioclase. But in most areas of part B both bright field and dark field images show no sharp boundaries between fine albite-twinned plagioclase and the exsolved Kf. Therefore, the Kf lamellae are better explained by replacement of Na (Ca) by K. Based on the detailed TEM and single crystal X-ray diffraction studies, Ried & Korekawa (1978) suggest the following crystallization history for the "moonstone":

1). Formation of a homogeneous phase with monoclinic symmetry. The composition of this phase is close to the bulk composition of part A but with slightly higher Kf content.

2). Replacement of Na(Ca) by K in some parts of the crystal, resulting

in formation of a monoclinic homogeneous part B with composition An_{20} Ab_{50} Kf_{30}.

3). Structural change in part A from monoclinic to triclinic, causing the formation of "M-twinning".

4). Nucleation of exsolved Kf seems to occur at twin boundaries in part A. The remaining part A has the composition $An_{27.2}$ $Ab_{69.2}$ $Kf_{3.6}$.

5). Concurrent exsolution of Kf in part B leads to lamellae with compositions An_5 Ab_{20} Kf_{75} and An_{28} Ab_{71} Kf_1. The transition of the latter lamellae from monoclinic to triclinic symmetry leads to polysynthetic twinning on a fine scale, reducing strain and preserving coherency with the monoclinic Kf whose lamellae are parallel to $(\bar{8}01)$.

Summarizing the above discussion, the feldspar intergrowths are divided into Peristerite, Boggild, and Huttenlocher intergrowth in plagioclase; and Perthite, Mesoperthite, and Antiperthite in alkali-feldspars, mainly on the basis of their chemical compositions. Mesoperthite and antiperthite are usually ternary feldspar intergrowths because their bulk compositions correspond to ternary feldspar (Fig 1.8). These intergrowths can be either primary or secondary, depending on how they formed. The primary intergrowths can form by simultenous nucleation; secondary intergrowths can be caused by solvus/spinodal decomposition with or without coherency when the homogeneous high temperature feldspars are cooled down to low temperatures; the secondary intergrowths can also be formed by replacement process during metasomatism.

1.5.2 Optical Observation of the Unusual Feldspar Intergrowths

All feldspar intergrowths in the two dykes from West Rock are plagioclase in composition. Some of them show albite (010) twinning and some show

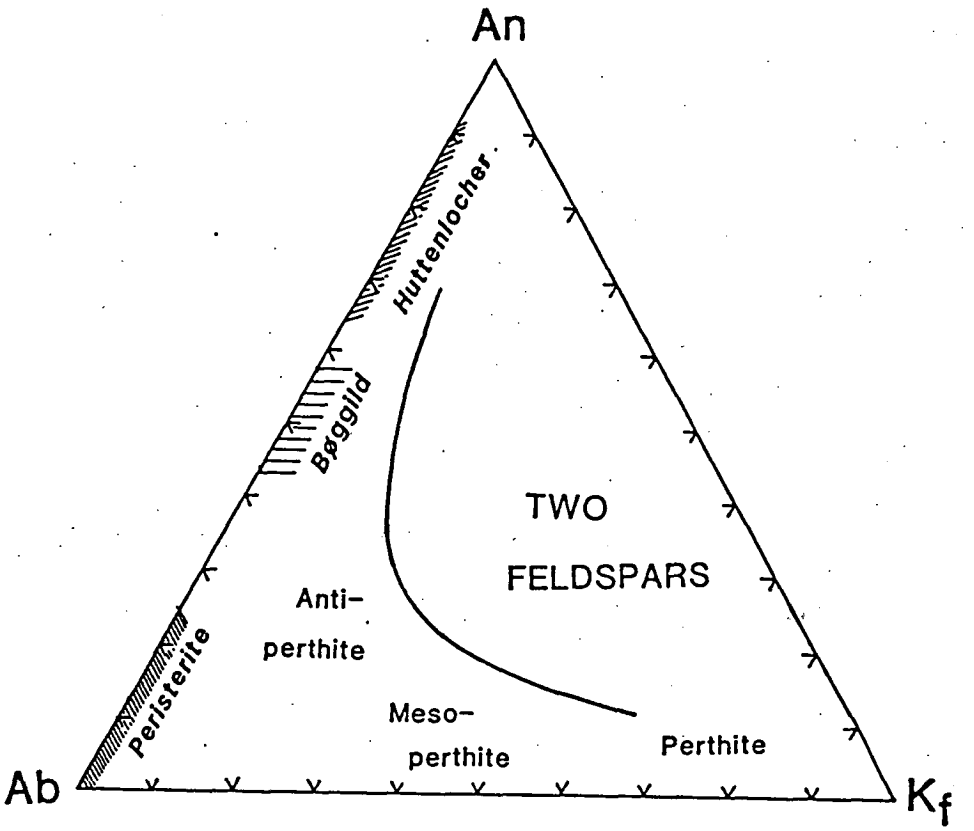

Fig 1.8 Feldspar Intergrowths at Low Temperature and Pressure (Modified from Smith, 1974).

both albite (010) and pericline [010] twinning (plate 1.2). The albite and pericline twin lamellae cross cut each other, forming the so-called "M-twinning" that suggests the feldspars are converted from original monoclinic plagioclase (Ried & Korekawa, 1978). It is very probable, therefore, that the feldspars originated at high temperatures.

Two types of lamellae in these feldspars can be distinguished according to their shapes. One type is fairly regular and very thin, more than 0.2 mm long and less than 0.004 mm thick. The other type is relatively irregular and thick. The first type will be called regular lamellae and the second, irregular lamellae. There are at least three sets of regular lamellae, orientated in three different directions. Usually only two sets can be clearly seen in one crystal section. If the other set is present, it appears very weak and occurs only in parts of the crystal section. The exact orientations of these regular lamellae are not clear, as universal stage studies have not been attempted. However, the relative positions between the regular lamellae and the cleavages can be found in suitably orientated section. In one crystal section (plate 1.3) two cleavages are present, intersecting each other with an angle of about 37°. The (010) cleavage appears clearer and more often than the perfect (001) cleavage. This section can not be (110) but should be very close to (118). Three sets of regular lamellae can be found in the same section, cut by the two cleavages. Two sets are dominant over the other. One dominant set is nearly parallel to (001) cleavage, with an intersection angle of about 10°. The other dominant set intersects (010) cleavage with an angle of 75°. The weaker set is cut by the (010) cleavage, with an angle of about 20°.

The irregular lamellae can be further divided into two kinds. One kind

is obviously caused by two sets of regular lamellae overlapping each other where one cleavage cuts both sets (plate 1.4). The other kind is the result of K addition to the existing regular lamellae. The additional K may be from the neighbouring regular lamellae, as shown by the difference in relative thickness between the lamellae, and from the host, when it further decomposes. This is inferred from the occurrence of these irregular lamellae and their relation with the regular lamellae. These irregular lamellae are present together with the regular lamellae. The regular lamellae seem to be thinner and less abundant than those in the feldspars where irregular lamellae are absent. The irregular lamellae typically have a greater width to length ratio (plate 1.5), but not as great as that of the first kind of irregular lamellae. Besides, there seems to be a gradual change in the lamellar thickness between the irregular lamellae.

These irregular lamellae are less abundant than the regular lamellae. They are not parellel to any cleavage or parting or twin plane. Thus they are unlikely to be the result of any metasomatic process. Also, the dyke shows no obvious signs of metasomatic alteration, such as the presence of OH-bearing phases (phlogopite, amphibole, etc).

Because the regular lamellae are regular both in individual lamellar shape and collective lamellar orientation, and not parallel to any of the two cleavages, they can not have formed by replacement of Na (Ca) by K during metasomatism. Since sponteneous heterogeneous nucleation and growth can not produce such regular and yet complex intergrowths the only possible origin of these regular lamellae is exsolution. Further detailed TEM study should provide information about the fine structures of the lamellae and the host and of their relations (such as whether they are coherently related

or not). This will be helpful for understanding of the exact exsolution process: solvus or spinodal decomposition with or without coherency?

1.5.3 Chemical Composition of the Unusual Feldspar Intergrowths

Electron microprobe analysis results of the unusual feldspar intergrowth are shown in Fig 1.9 and Table 1.5. They were obtained using defocused beam area scans with a magnification less than a thousand times. These analyses can generally be divided into two groups: one is relatively K-rich, the other is relatively K-poor. Both groups are very rich in K compared with any reported Huttenlocher intergrowths. Because the lamellae are K-feldspar and the host is plagioclase, the intergrowth should obviously belong to the antiperthite category. However, the antiperthite area is located near the Na end of the ternary feldspar diagram, whereas these analyses are near the Ca end. These intergrowths are, therefore, unusual antiperthites, but will be simply called unusual feldspar intergrowths.

The analyses in Table 1.5 do not define a unique bulk composition for the intergrowths. The difference between the two groups of analyses is probably caused by the heterogeneity in the distribution of the different kinds of lamellae. It is important to know the exact bulk composition of the unusual feldspar intergrowths when attempting to elucidate their origin. An estimation of Kf_{21} An_{65} Ab_{14} is made on the basis of optical observation and the microprobe analyses shown in Fig 1.9. Considering the analytical accurracy, this estimated bulk composition seems reasonable.

Following the method of Kay (1977), the change in relative Ca, Na, and K contents from host to lamellae was studied very carefully. An example is given in Fig 1.10. The vertical axis in this diagram indicates the relative Ca, Na, and K contents (total 100). The horizontal axis shows the electron

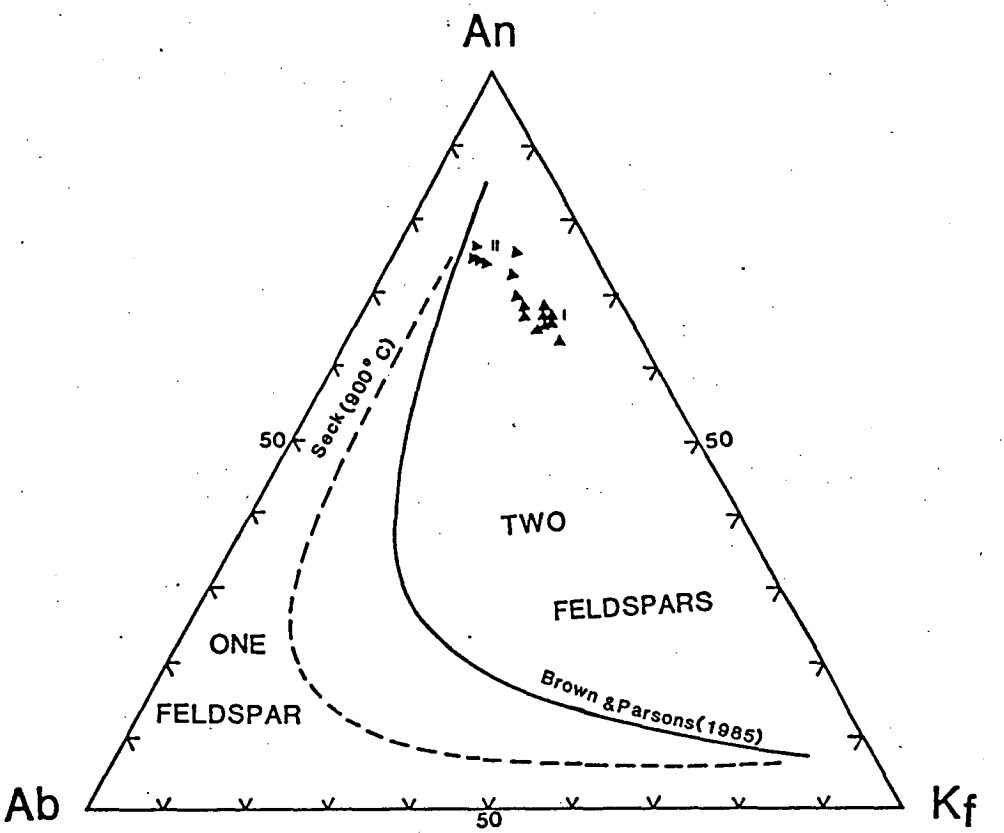

Fig 1.9 Defocused-beam Area Scan Analyses of the Unusual Feldspar Intergrowths in the Two Mafic Dykes from Departure Rocks. Solid curve is the limit of the ternary feldspar solid solutions proposed by Brown & Parsons (1985). Broken curve is the 900°C isotherm of Seck (1971) which connects two coexisting feldspars in his experiments at 0.5 Kbar water pressure.

Table 1.5 Representative Area Scan Analyses of the Unusual Feldspar Intergrowths

65786	1		2		3		4	
	wt%	cat*	wt%	cat	wt%	cat	wt%	cat
SiO2	50.62	2.3294	52.98	2.4249	49.58	2.2548	50.78	2.3589
Al2O3	28.84	1.5640	27.53	1.4851	32.44	1.7388	29.18	1.5978
FeO	2.55	0.0983	2.64	0.1012	0.40	0.0152	1.62	0.0631
MgO	1.18	0.0809	1.35	0.0923	0	0	0	0
CaO	13.41	0.6612	11.60	0.5688	15.05	0.7335	13.19	0.6566
Na2O	1.26	0.1124	1.06	0.0938	1.79	0.1578	1.49	0.1338
K2O	2.64	0.1550	3.88	0.2265	1.88	0.1091	3.34	0.1978
Sum	100.50	5.0013	101.04	4.9926	101.14	5.0093	99.59	5.0079
Ca:Na:K	71.2	12.1 16.7	64.0	10.6 25.5	73.3	15.8 10.9	66.4	13.5 20.0
65786	5		6		7		8	
SiO2	50.86	2.3208	51.09	2.3651	52.02	2.3746	50.40	2.2748
Al2O3	31.27	1.6815	29.94	1.6335	30.12	1.6204	32.40	1.7236
CaO	13.85	0.6769	13.20	0.6549	13.37	0.6539	15.17	0.7337
Na2O	1.42	0.1257	1.18	0.1059	1.16	0.1029	1.73	0.1516
K2O	3.31	0.1927	3.78	0.2230	3.95	0.2298	1.92	0.1108
Sum	100.71	4.9976	99.19	4.9825	100.61	4.9815	101.63	4.9945
Ca:Na:K	68.0	12.6 19.4	66.6	10.8 22.7	66.3	10.4 23.3	73.3	15.2 11.1
65786	9		10		11		12	
SiO2	52.02	2.3603	51.75	2.3898	50.57	2.2968	49.58	2.2702
TiO2	0.19	0.0064	0.19	0.0066	0	0	0	0
Al2O3	30.35	1.7050	29.42	1.6013	31.64	1.6938	31.65	1.7082
FeO	0.23	0.0086	0	0	0.26	0.0100	0.66	0.0251
CaO	13.20	0.6417	12.27	0.6070	14.44	0.7027	14.92	0.7318
Na2O	1.43	0.1257	1.38	0.1231	1.44	0.1271	1.80	0.1598
K2O	4.10	0.2375	4.64	0.2734	3.08	0.1787	2.07	0.1208
Sum	101.52	5.0033	99.65	5.0012	101.44	5.0091	100.67	5.0159
Ca:Na:K	63.9	12.1 24.0	60.5	12.3 27.2	69.7	12.6 17.7	72.3	15.8 11.9
65787	1		2		3		4	
SiO2	52.34	2.3576	49.76	2.2820	50.93	2.3667	48.57	2.2443
TiO2	0	0	0	0	0.16	0.0057	0	0
Al2O3	31.00	1.6455	31.81	1.7196	29.74	1.6290	31.96	1.7404
CaO	13.56	0.6545	14.94	0.7340	12.83	0.6386	15.18	0.7515
Na2O	1.14	0.0997	1.09	0.0971	1.15	0.1035	1.39	0.1244
K2O	3.90	0.2241	2.53	0.1479	4.09	0.2424	2.31	0.1363
Sum	101.95	4.9814	100.13	4.9806	98.90	4.9859	99.40	4.9969
Ca:Na:K	66.9	10.2 22.9	75.0	9.9 15.1	64.9	10.5 24.6	74.2	12.3 13.5

*) cations per 8 oxgens.

beam position. Each number in the horizontal axis represents one focused beam analysis (beam size about 1 to 2 micrometres in diameter). The distance between each analysis is not exactly constant because the beam was moved manually. However it is believed to be about 2 to 5 micrometers. The important information evident from this diagram is that the Ca contents near the K-feldspar lamellae are relatively higher than those away from the lamellae. Similar evidence was used by Kay (1977) to support an exsolution origin of Kf lamellae in the antiperthites from Laramie Range and the Adirondacks, since it suggests slow diffusional transport of Ca and Al in exchange for alkalis and Si away from the lamellae. It is also evident from Fig 1.10 that the lamellae are very rich in K, but very poor in both Na (about 10%) and Ca (about 1%), and that the host is very rich in Ca but very poor in Na (about 14%) and K (<1%). The very low concentration of Ca in the lamellae and of K in the host indicate that they were separated almost completely at low temperature.

1.5.4 Possible Origin

Optical observation of these unusual feldspar intergrowths suggests that there are two types of K-feldspar lamellae: one is the regular lamellae and the other is the irregular lamellae. Most of the feldspars contain regular Kf lamellae and only a few contain the irregular Kf lamellae. Where irregular lamellae are present there are less regular lamellae, which seem to be thinner. The gradual change in lamellar thickness indicates that some irregular lamellae may be a result of further growth of some regular lamellae. The shape of some other irregular lamellae clearly shows that they are the result of overlapping between two sets of regular lamellae. Where such overlapping occurs, at least one cleavage is present and cuts both sets of

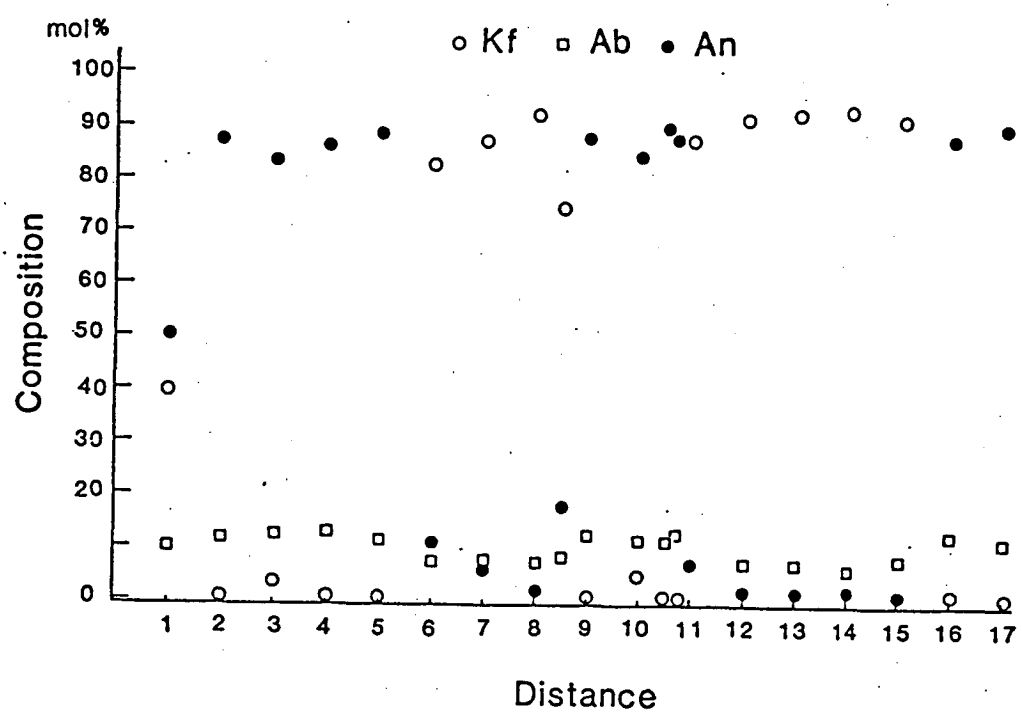

Fig 1.10 Compositional Change in One of the Feldspar Crystals in Dyke 65786 as a Function of Distance across Lamellae (scale is about 2 - 5 micrometer per unit).

the overlapping lamellae.

The complex, yet regular occurrence of the regular lamellae implies that they formed by exsolution. Whether they formed by solvus or spinodal decomposition and with or without coherency is not certain and needs be studied by the TEM method. The presence of "M-twinning" in some of the intergrowths strongly supports their high temperature origin. The chemical composition of the original undecomposed plagioclose should not be very different from the estimated bulk composition of these intergrowths since there is no evidence suggesting subsolidus ion movement between the feldspars and other phases in the two dykes and their host rocks. This bulk composition (Kf_{21} An_{65} Ab_{14}) is well within the two-feldspar field of the ternary feldspar system. In order to permit the exsitence of feldspars with such ternary composition, the one-feldspar field in the ternary feldspar diagram needs to be expanded at the expense of the two-feldspar field.

It is well documented that feldspar solid solutions are very limited at low temperatures (Carmichael et al., 1974). The extent of feldspar solid solutions increases with increasing temperature. The maximum solid solution occurs when temperature is increased to a maximum value which is determined by the feldspar stabilities. At high pressure (10 - 30 Kbar) feldspar melting temperatures are increased so that they can be stable at very high temperatures (>1000°C). At such high temperatures homogeneous feldspars of ternary composition (such as Kf_{21} An_{65} Ab_{14}) may possibly exist. From the homogeneous plagioclase of composition Kf_{21} An_{65} Ab_{14}, the complex regular lamellae-bearing feldspar intergrowths may have evolved. The irregular lamellae-bearing intergrowths are the result of further development of the regular lamellae-bearing intergrowths, by way of overlapping and solid state

intercrystal diffusion. The existence of such homogeneous ternary feldspar (plagioclase) has been tested by three sets of experiments: first in the anorthite -- K-feldspar binary system, then in the sodium-poor ternary feldspar system, and, finally by homogenization of the natural feldspar intergrowths. These experimental studies are discussed in detail in the following chapters.

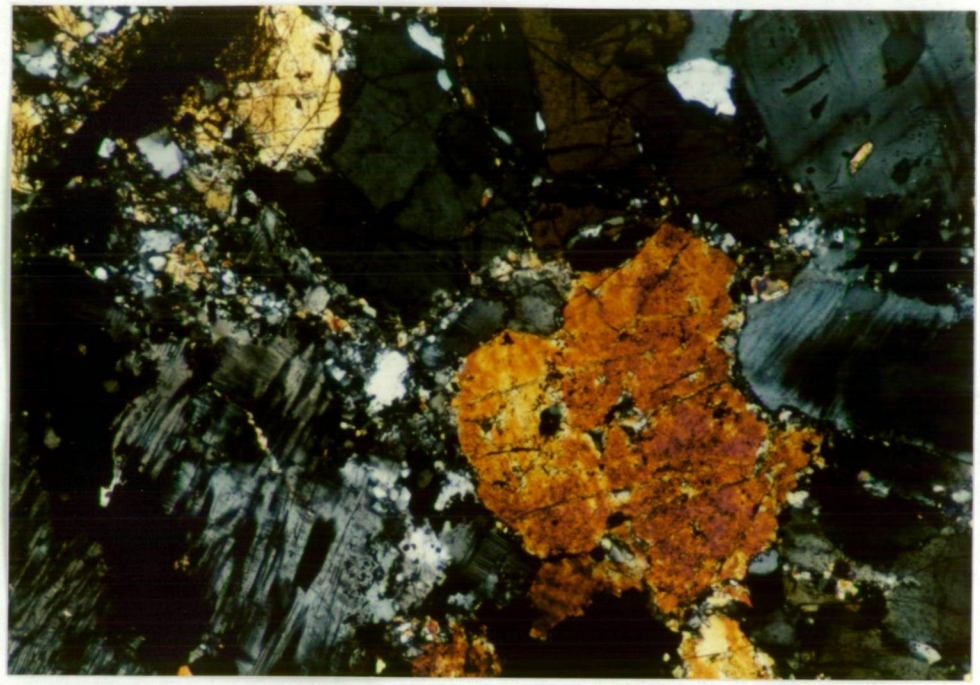

Plate 1.1 Recrystallized, Deformed Texture

in Dyke 65786 (cross nicols x 20)

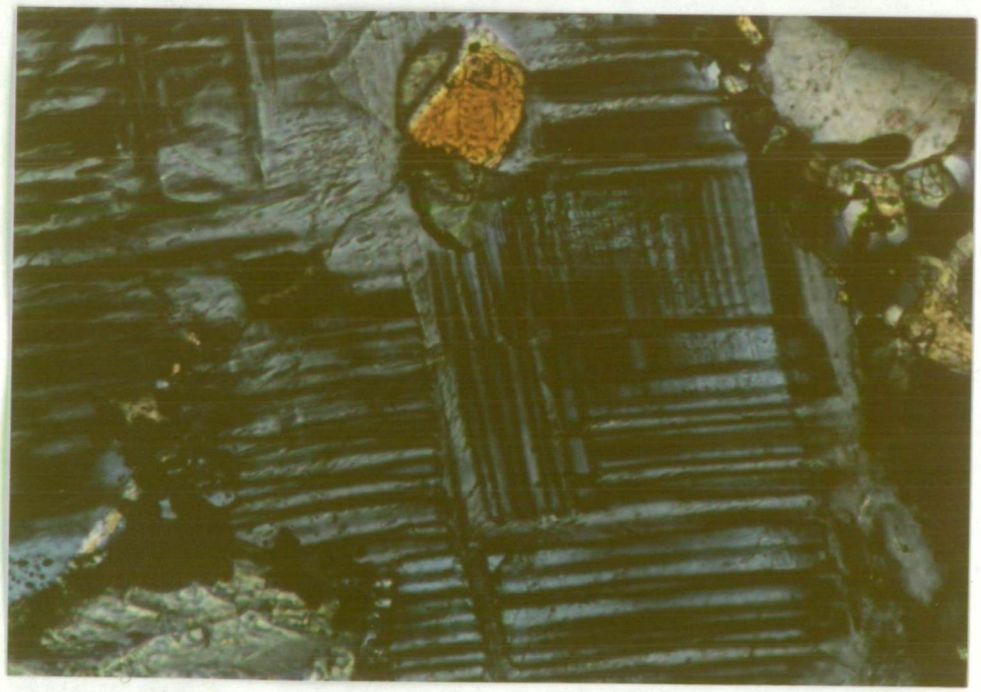

Plate 1.2 M-twinning in a Large Feldspar Crystal

in Dyke 65786 (cross nicols x 80).

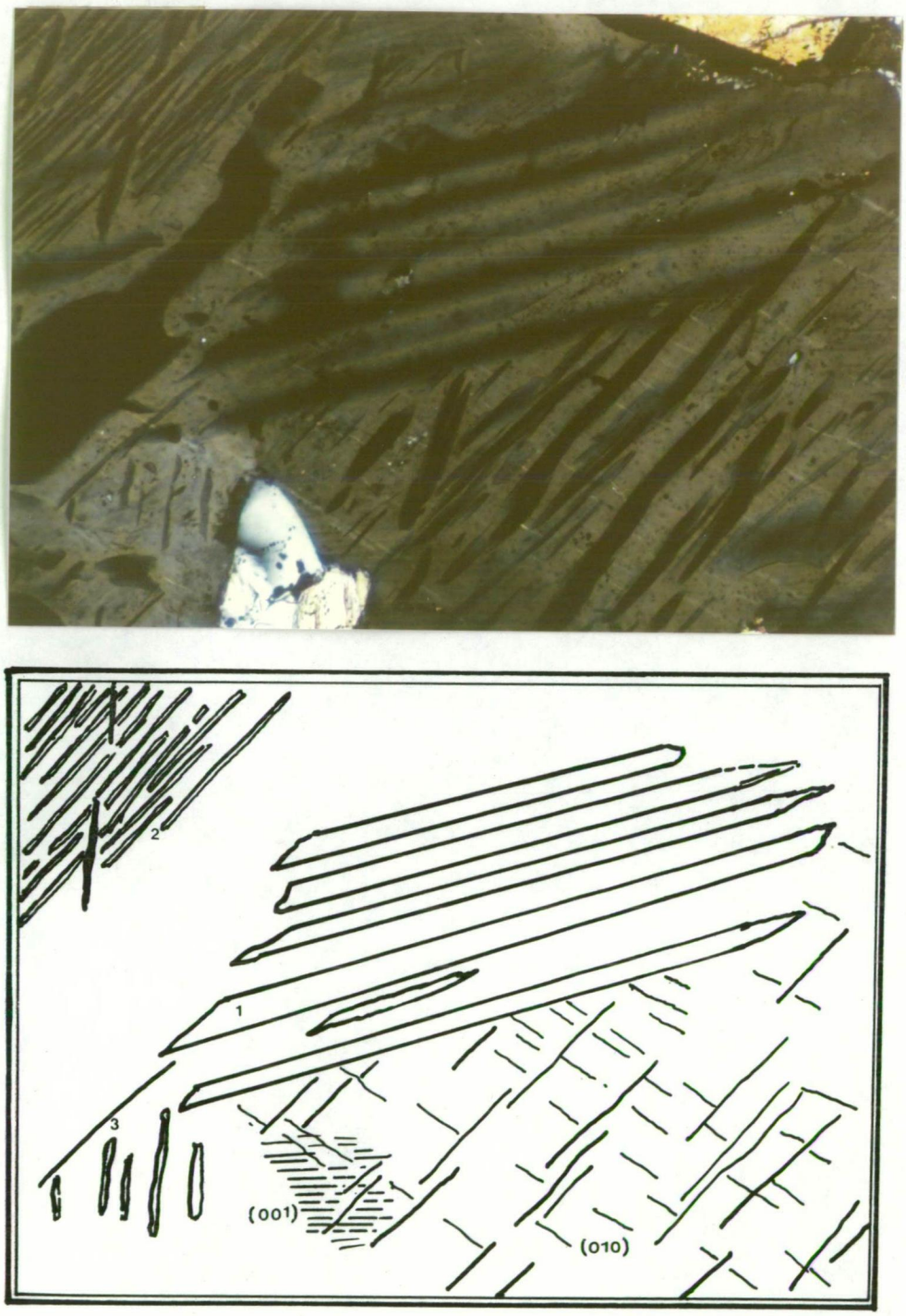

Plate 1.3 One large Feldspar Crystal with Two Cleavages [(010) & (001)], Three Sets of Regular Lamellae (labelled 1, 2, & 3) and One Kind of Irregular Lamellae (cross nicols x 40).

Plate 1.4 Overlapping of Two Sets of Regular Lamellae, Forming the First Kind of Irregular Lamellae. The background is the host plagioclase showing multiple twinning (cross nicols x 40).

Plate 1.5 the Second Kind of Irregular Lamellae, Formed by Further Growth of Formerly Regular Lamellae (cross nicols x 40).

CHAPTER TWO

PHASE RELATIONS IN THE SYSTEM ANORTHITE -- POTASSIUM FELDSPAR AT 10 KBAR PRESSURE WITH EMPHASIS ON THEIR SOLID SOLUTIONS

CONTENTS

CHAPTER TWO

PHASE RELATIONS IN THE SYSTEM ANORTHITE - POTASSIUM FELDSPAR AT 10 KBAR PRESSURE WITH EMPHASIS ON THEIR SOLID SLOUTIONS

2.1 Introduction

Homogeneous feldspars of compositions similar to the bulk composition of the unusual feldspar intergrowths from Departure Rocks can not exist according to the present understanding of the ternary feldspar system. However, such feldspars may possibly be formed under some unusual conditions, for example, at very high temperatures (>1000°C). In order for such homogeneous feldspar to exist, the solid solution of potassium feldspar in plagioclase should be increased, so that the homogeneous feldspar lies at least on the limit of ternary feldspar solid solutions (Fig 1.9). This may be achieved at high temperatures, because increasing temperature causes extensive solid solutions in the ternary feldspar system. However, because of the intersection of the feldspar solvus with the solidus for the binary or ternary feldspar systems, such high temperature can only be reached at high pressures. In this study, the pressure for experimental investigation is fixed at 10 kilobars for the following reasons:

(a) The geological background and possible origin of the two dykes that contain the unusual feldspar intergrowths, and of their host rock Mawson Charnockite, suggest that the dykes originated from mantle. There may have been a mantle diapir beneath the Mawson Charnockite (Ellis, 1980), which during the Proterozoic time was part of the base of the east Antarctic

crust. This mantle diapir was probably the source of the two dykes. The original feldspar phenocrysts in the dykes might have crystallized close to the base of the Proterozoic crust. At the base of normal, stable continental crust, the isostatic pressure is generally equivalent to 10 Kbar.

(b) All the feldspar end members (i.e. anorthite, albite, potassium feldspar) are stable at 10 kbar pressure and thus there are no complexities of breakdown reactions of end-members.

(c) After intrusion, the two dykes and their host rocks experienced a regional upper greenschist- to amphibolite-facies metamorphism. The metamorphic pressure is estimated to have been no less than 6 Kbar (Chapter One). This metamorphic event obviously took place after the formation of the feldspar phenocrysts in the two dykes. These phenocrysts should, therefore, have crystallized at pressures of 6 Kbar or greater.

Anorthite, albite, and potassium feldspar are the major components of most natural feldspars. Anorthite and albite form a complete solid solution series (Fig 2.1, the plagioclase loop of Bowen, 1913). Albite and K-feldspar can also form complete solid solution (Fig 2.2). The solid solutions between anorthite and K-feldspar are, however, very limited. It is reasonable, therefore, to suggest that the limit of ternary feldspar solid solutions is largely controlled by the mutual solubilities of anorthite and K-feldspar. Thus the system anorthite -- K-feldspar is important to the understanding of ternary feldspar solid solutions. In addition, the estimated bulk composition of the unusual feldspar intergrowths is very close to the anorthite apex in the ternary feldspar diagram. The solubility of K-feldspar in anorthite-rich feldspar is therefore particularly interesting.

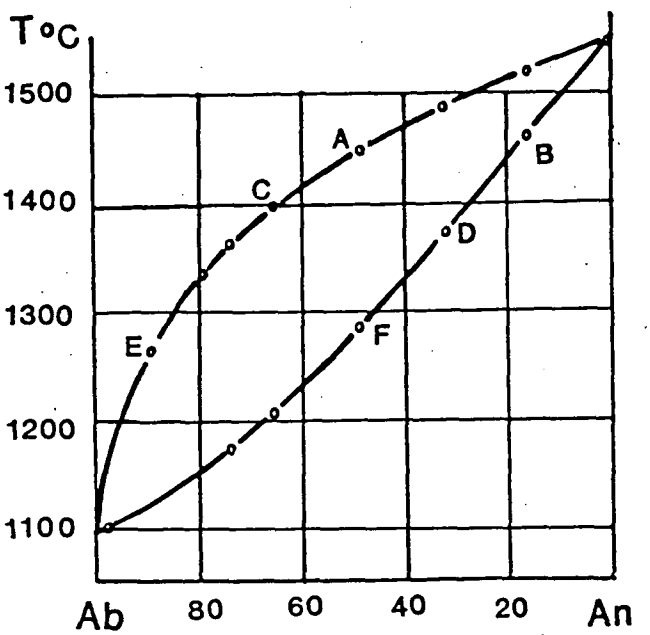

Fig 2.1 Phase Relations in the Plagioclase System at 1 atm (Bowen, 1913).

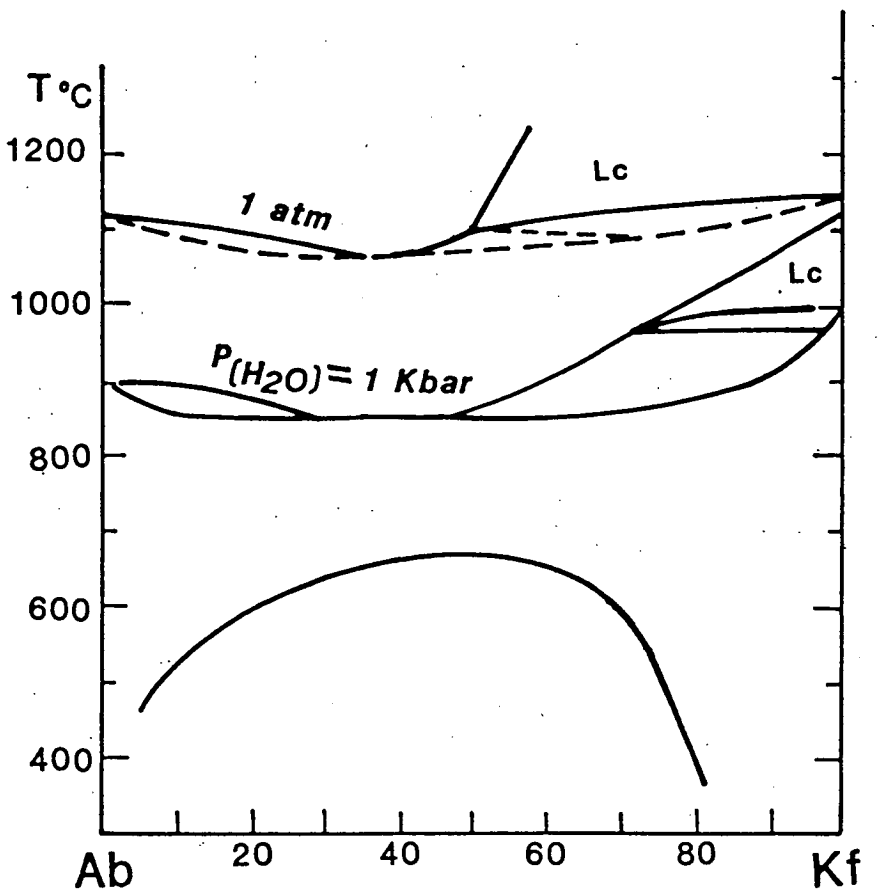

Fig 2.2 Phase Relations in the Alkali Feldspar System

(Tuttle & Bowen, 1958)

2.2 Previous Studies

There has been no previous experimental work performed on the pure anorthite -- K-feldspar binary system. Phase relations for this system have been inferred from the study of more complex systems. Two projections are shown in Fig 2.3. The upper diagram (a) is projected from the experimental data of Schairer & Bowen (1947) in the anorthite -- leucite -- silica system at atmospheric pressure. The lower diagram (b) is projected from the experimental data of Yoder et al. (1957) in the ternary feldspar system at 5 kbar water pressure. Both show the eutectic character of the anorthite -- K-feldspar binary system with an eutectic point very close to the K-feldspar end. The mutual solubilities between anorthite and K-feldspar are so limited in the first diagram that it could not be detected by Schairer & Bowen, who used the refractive index method to examine their run products. The maximum K-feldspar solid solution in anorthite in the second diagram is given as less than 5 mol%, and the maximum anorthite content in K-feldspar is less than 2 mol%; these values are very uncertain due to the insensitivity of the X-ray diffraction method used, and are thus indicated by broken lines.

Experiments done in the water-saturated ternary feldspar system have demonstrated that anorthite solubility in K-feldspar is 5 - 7 mol% (Hamilton, 1969), and K-feldspar solubility in anorthite is less than 10 mol% (Norris, 1972) at 900°C, 0.5 Kbar water pressure. K-feldspar solubility in albite-poor plagioclase in the ternary feldspar system is about 4.4 mol% and anorthite solubility in albite-poor alkali feldspar is about 3 mol% according to the experimental results of Seck (1971) at 900°C, 0.5 Kbar water pressure (Fig 1.9). (Note: the molar ratio of anorthite and K-feldspar are almost the same

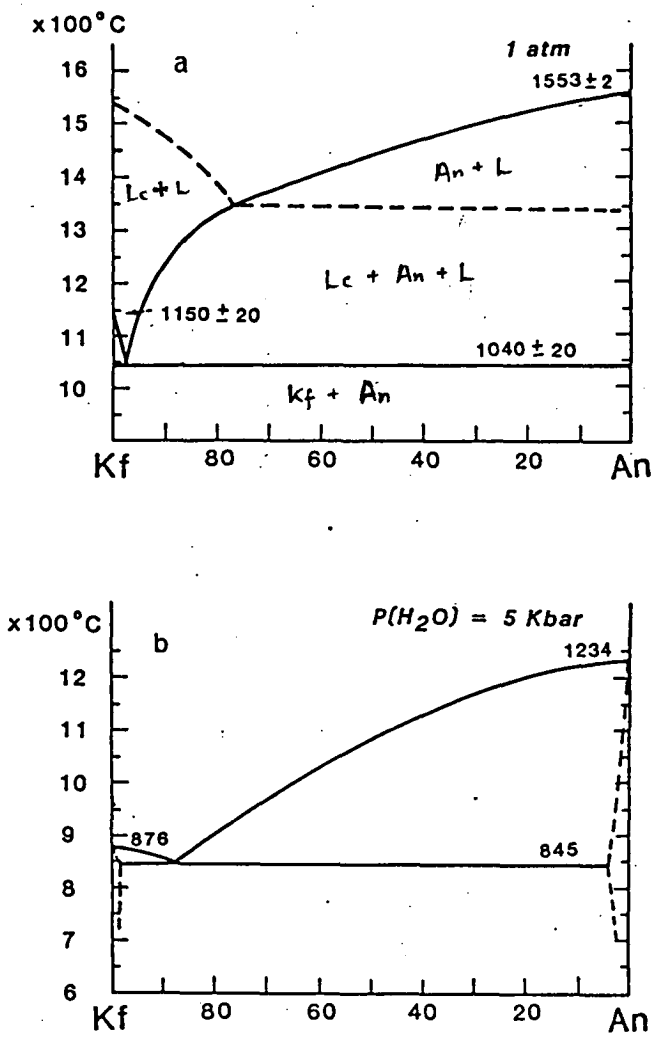

Fig 2.3 Phase Relations in the Anorthite -- K-feldspar System Projected from Experimental Data from More Complex Systems (a) Schairer & Bowen, 1947; (b) Yoder et al., 1957.

as their weight ratio because anorthite has nearly the same molecular weight as K-feldspar).

The survey of K-feldspar contents of natural plagioclases by Sen (1959) gives the maximum K-feldspar content of 3% in albite-poor plagioclase in granulite-facies rocks and of 0.6% in amphibolite-facies rocks. The maximum anorthite content in natural albite-poor alkali feldspar is 2.5% (Spencer, 1937). The solid solution limit in the ternary feldspar system given by Brown & Parsons (1985) also suggests that the mutual solubilities between anorthite and K-feldspar are less than 10% in the albite-poor region (Fig 1.9). These results are basically consistent with the above experimental data because the natural feldspars examined were homogeneous and the result of low temperature (<1000°C) and low pressure (<5 Kbar) reactions.

The effect of high pressure under dry conditions on ternary feldspar solid solutions is virtually unknown, but is considered to favor extensive solid solution, as outlined below.

Fig 2.4 is a generallized binary phase diagram of eutectic type. Dotted lines represent the liquidus, separating a melt field from a melt-plus-crytal field. Broken lines indicate the solidus, separating the melt-plus-crystal field from a crystal-only field. Solid lines are the solvus, separating the one-phase field from the field of two coexisting solid phases. The point "e" is the eutectic, where the liquidus, solidus, and solvus meet at the same temperature. At this temperature maximum solid solution occurs between the two solid phases. Because the shape of the solvus is convex, increasing temperature enlarges the gap between the solvus and temperature axis, increasing the solid solutions between the two coexisting phases.

In the alkali feldspar system, pressure is believed to have little

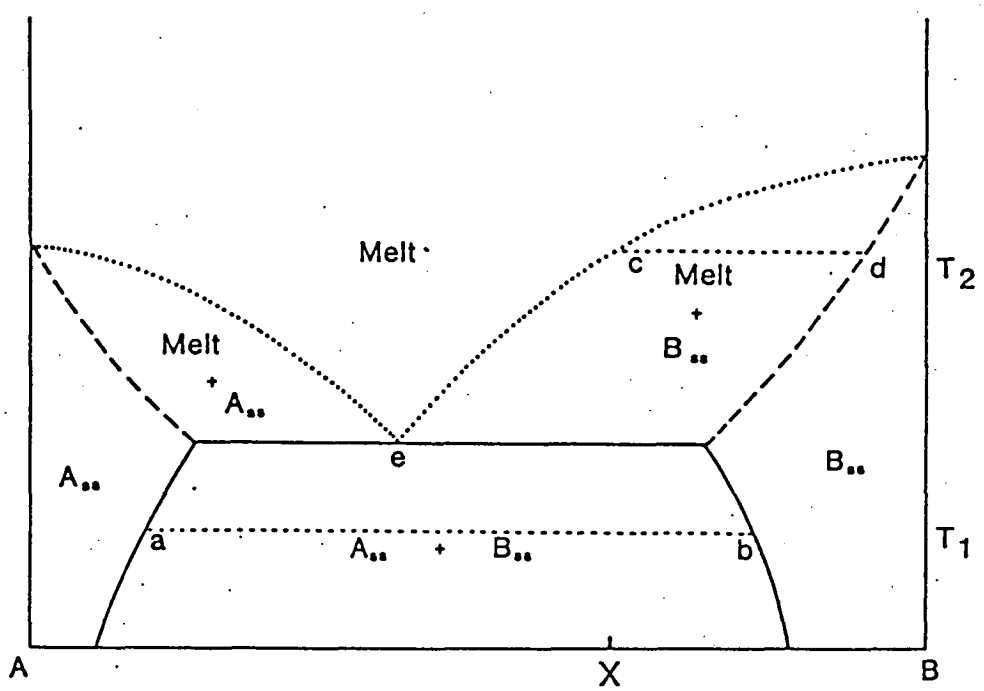

Fig 2.4 An Ideal Phase Diagram of a Binary System with Limited Solid Solutions and an Eutectic Point.

effect on the position of solvus (Tuttle & Bowen, 1958, Fig 1.7). However, the melting temperatures of plagioclases and alkali feldspars are increased at high isostatic pressures (Lindsley, 1966; 1969). Thus pressure has an effect of increasing melting temperatures. This, in turn, will increase the feldspar solid solutions as discussed above. The anorthite -- K-feldspar system is expected to be similar to the alkali feldspar system. High pressures and temperatures are deduced to be favoured conditions where extensive solid solutions occur. This conclusion is supported by the survey of Sen (1959), because in granulite-facies rocks, which were formed at high pressures and temperatures, K-feldspar content in albite-poor plagioclase is more than that in plagioclase in amphibolite-facies rocks. This evidence is not very strong because the feldspars in those rocks have exsolved at lower pressures and temperatures and the metamorphic temperatures are not high compared with igneous temperatures. Thus these feldspars can not represent those formed at both very high temperatures and high pressures.

2.3 Experimental Methods

All experiments were done in a solid-media piston-cylinder apparatus. Internal pressure on the first stage ram was fixed at 4450 p.s.i. when talc/pyrex (dry) assemblies were used; and at 4050 p.s.i. when salt/pyrex assemblies were used. Both are equlivalent to 10 kilobars on the 0.5" second stage piston (a 10% pressure correction is made for the talc/pyrex assembly relative to the salt/pyrex assembly due to friction). The measured pressure has been calibrated against SiO_2 polymorph transitions and the reaction (albite = jadeite + quartz). Pressure uncertainty is about +/- 0.5 kbar, which is an accepted value for most piston-cylinder apparati. Pressure

variation during experiments is negligible.

Temperature was measured by platinum/platinum (90%) rhodium (10%) thermocouple and was controlled within +/- 15°C for long runs (> 1 day) and within +/- 10°C for runs lasting only a few hours. The effect of pressure on the E.M.F (electron motive force) of the thermocouple is not considered.

The starting material for most runs was glass melted from a sintered oxide mix on an iridium strip heater. The oxide mixes were prepared according to the desired proportions of anorthite to K-feldspar. They were mixed under acceton in an agate mortar for more than 20 minutes and then melted on the iridium strip heater. The detailed procedures are given in Table 2.1.

Electron microprobe analyses of these glasses show that they are homogenous (Table 2.2 & Fig 2.5), and also, that the glasses contain slightly less K than the original compositions of the oxide mixes. This may have been caused by alkali volatization during preparation and melting of the oxide mixes, and during microprobe analysis. The maximum K loss for starting compositions with Kf# > 25 [Kf# = 100*Kf/(Kf + An)] is about 5% but is insignificant for compositions with Kf# < 25, as suggested by the defocused beam area scan analyses of the run products (Fig 2.6). The exact potassium loss is important for determination of Kf solubility in anorthite, especially for starting compositions Kf# < 25, because these compositions are close to phase boundaries. Fortunately, the loss is minor for these compositions and should not have a great effect on the determined Kf solubility in anorthite.

For most of the runs, a layered sample assembly was used. i.e. glasses of different compositions were put in one platinum capsule and separated by 2 - 3 platinum discs to ensure complete separation. Before each experiment the sample was kept in an oven at 120°C overnight in order to release any

I

1. $SiO_2 + Al_2O_3 + CaCO_3$

2. $SiO_2 + Al_2O_3 + K_2CO_3$

mixed with acetone in agate mortar for at least 20 minutes to ensure complete mixing

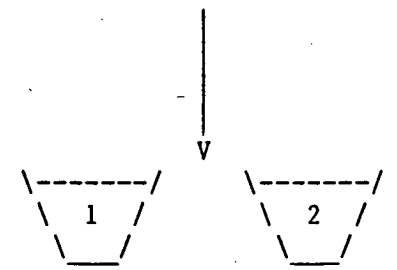

mix 1 & 2 were put in two large platinum crucibles

II the two mixes were heated separately in the oven

1. 600°C (2 hours) --- 850°C (13 hours) for mix 1

2. 800°C (3 hours) --- 950°C (10 hours) for mix 2

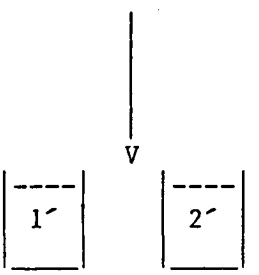

1′. sintered oxide mix of anorthite composition
2′. sintered oxide mix of K-feldspar composition

III the sintered oxide mixes 1′ and 2′ were mixed again in different proportions and melted on an iridium strip to get glass starting material for high pressure runs

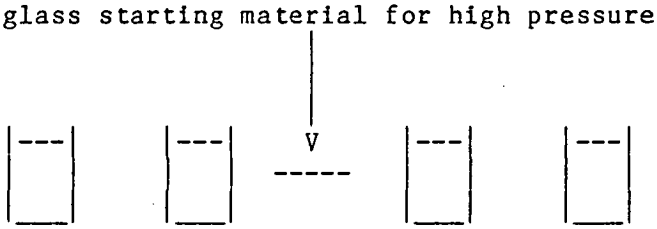

$(Kf_5\ An_{95})$ $(Kf_{10}\ An_{90})$ $(Kf_{80}\ An_{20})$ $(Kf_{90}\ An_{10})$

glass starting material

Table 2.1 Procedures for Preparing Glass Starting Material

Table 2.2 Representative Compositions of the Glass Starting Material

	SiO_2	Al_2O_3	CaO	K_2O	Sum	SiO_2	Al_2O_3	CaO	K_2O	Sum
wt%	42.91	36.61	20.15	0.33	100	43.16	36.31	20.16	0.37	100
cat	1.9920	2.0027	1.0022	0.0195	5.0163	2.0035	1.9863	1.0025	0.0217	5.0140
Kf#		1.9					2.1			
wt%	43.86	35.29	20.48	0.36	100	43.88	35.30	20.49	0.32	100
cat	2.0366	1.9313	1.0190	0.0214	5.0083	2.0317	1.9311	1.0193	0.0192	5.0068
Kf#		2.1					1.9			
wt%	43.70	35.55	20.42	0.33	100	43.82	35,54	20.27	0.37	100
cat	2.o285	1.9450	1.0155	0.0197	5.0087	2.0255	1.9360	1.0035	0.0215	4.9939
Kf		1.9					2.1			
wt%	45.40	34.42	19.27	0.91	100	44.04	35.70	19.43	0.84	100
cat	2.1007	2.8775	0.9554	0.0537	4.9873	2.0418	1.9508	0.9608	0.0494	5.0074
Kf#		5.3					4.9			
wt%	44.93	35.07	19.18	0.81	100					
cat	2.0785	1.9122	0.9507	0.0477	4.9892					
Kf#		4.8								
wt%	45.10	34.19	19.52	1.20	100	45.31	34.27	19.35	1.07	100
cat	2.0938	1.8707	0.9709	0.0708	5.0062	2.0999	1.8720	0.9605	0.0632	4.9956
Kf#		6.8					6.2			
wt%	44.80	34.67	19.51	1.03	100	44.57	34.96	19.44	1.04	100
cat	2.0783	1.8955	0.9697	0.0610	5.0050	2.0678	1.9116	0.9703	0.0613	5.0070
Kf#		5.9					6.0			
wt%	45.68	34.04	18.55	1.73	100	45.71	33.78	18,66	1.85	100
cat	2.1182	1.8604	0.9216	0.1025	5.0027	2.1222	1.8483	0.9284	0.1094	5.0083
Kf#		10.0					10.5			
wt%	45.48	34.07	18.76	1.70	100					
cat	2.1107	1.8638	0.9327	0.1004	5.0076					
Kf#		9.7								
wt%	46.86	33.28	17.40	2.45	100	46.88	33.07	17.56	2.48	100
cat	2.1700	1.8161	0.8634	0.1449	4.9943	2.1726	1.8063	0.8719	0.1469	4.9976
Kf#		14.4					14.4			
wt%	46.63	33.47	17.48	2.42	100	46.89	33.31	17.36	2.44	100
cat	2.1599	1.8272	0.8678	0.1430	4.9979	2.1706	1.8171	0.8609	0.1444	4.9930
Kf#		14.2					14.4			

Table 2.2 Representative Compositions of the Glass Starting Material (continued)

	SiO_2	Al_2O_3	CaO	K_2O	Sum	SiO_2	Al_2O_3	CaO	K_2O	Sum
wt%	47.21	32.05	17.33	3.42	100	47.62	31.70	17.16	3.53	100
cat	2.1980	1.7586	0.8645	0.2030	5.0241	2.2138	1.7413	0.8562	0.2084	4.0197
Kf#		19.0					19.6			
wt%	49.25	30.82	16.41	3.52	100	48.11	32.17	16.38	3.35	100
cat	2.2799	1.6815	0.8139	0.2078	4.9832	2.2276	1,7556	0.8124	0.1976	4.9933
Kf#		20.3					19.6			
wt%	49.23	30.69	15.70	4.38	100	48,94	31.83	15.16	4.07	100
cat	2.2852	1.6793	0.7808	0.2593	5.0047	2.2631	1.7350	0.7511	0.2401	4.9893
Kf#		24.9					24.2			
wt%	48.37	32.08	15.63	3.92	100	48.84	32.00	15.22	3.94	100
cat	2.2406	1.7515	0.7758	0.2315	4.9993	2.2575	1.7433	0.7537	0.2326	4.9871
Kf#		23.0					23.6			
wt%	49.73	30.82	14.52	4.93	100	49.26	31.30	14.73	4.70	100
cat	2.3044	1.6830	0.7210	0.2915	4.9998	2.2827	1.7094	0.7314	0.2778	5.0014
Kf#		28.8					27.5			
wt%	49.79	30.95	14.29	4.97	100	50.07	30.80	14.36	4.77	100
cat	2.3055	1.6888	0.7090	0.2936	4.9969	2.3151	1.6785	0.7113	0.2814	4.9863
Kf#		29.3					28.3			
wt%	51.01	29.59	12.97	6.42	100	51.62	28.99	12.74	6.65	100
cat	2.3681	1.6191	0.6449	0.3804	5.0125	2.3958	1.5853	0.6334	0.3939	5.0084
Kf#		37.1					38.3			
wt%	54.03	27.09	11.72	7.07	100	50.82	30.07	12.54	6.57	100
cat	2.4962	1.4785	0.5814	0.4168	4.9729	2.3577	1.6445	0.6235	0.3887	5.0143
Kf#		41.8					38.4			
wt%	53.08	28.00	10.46	8.46	100	54.01	27.20	10.40	8.38	100
cat	2.4652	1.5323	0.5205	0.5012	5.0192	2.5034	1.4860	0.5164	0.4957	5.0014
Kf#		49.1					49.0			
wt%	54.43	27.14	10.24	8.19	100	54.76	26.72	10.35	8.16	100
cat	2.5165	1.4789	0.5070	0.4830	4.9855	2.5314	1.4559	0.5126	0.4813	4.9813
Kf#		48.8					48.4			

Table 2.2 Representative Compositions of the Glass Starting Material
(continued)

	SiO_2	Al_2O_3	CaO	K_2O	Sum	SiO_2	Al_2O_3	CaO	K_2O	Sum
wt%	55.94	25.77	8.73	9.56	100	55.73	25.75	8.98	9.54	100
cat	2.5883	1.4056	0.4328	0.5642	4.9910	2.5816	1.4060	0.4458	0.5636	4.9971
Kf#		56.6					55.8			
wt%	56.70	25.08	8.44	9.78	100	57.77	24.39	7.85	9.99	100
cat	2.6215	1.3669	0.4181	0.5770	4.9835	2.6646	1.3261	0.3878	0.5879	4.9663
Kf#		58.0					60.3			
wt%	57.99	25.70	6.91	9.40	100	61.49	22.76	6.01	9.75	100
cat	2.6540	1.3859	0.3387	0.5490	4.9276	2.7970	1.2203	0.2928	0.5655	4.8756
Kf#		61.8					65.9			
wt%	61.27	21.81	6.03	10.88	100	60.90	22.02	5.47	11.62	100
cat	2.8088	1.1786	0.2963	0.6363	4.9200	2.8002	1.1930	0.2693	0.6814	4.9414
Kf#		68.2					71.7			
wt%	61.66	22.64	5.46	10.24	100	58.33	25.21	5.80	10.66	100
cat	2.8070	1.2148	0.2663	0.5949	4.8830	2.6780	1.3643	0.2855	0.6240	4.9518
Kf#		69.1					68.6			
wt%	50.55	33.31	3.19	12.95	100	57.99	24.16	3.83	14.02	100
cat	2.3557	1.8297	0.1592	0.7697	5.1142	2.7012	1.3264	0.1912	0.8333	5.0521
Kf#		82.9					81.3			
wt%	56.74	25.30	3.00	14.97	100	72.23	13.59	2.00	12.18	100
cat	2.6551	1.3952	0.1503	0.8933	5.0939	3.2390	0.7185	0.0961	0.6966	4.7501
Kf#		85.6					87.9			
wt%	57.81	26.07	2.51	13.61	100	57.75	26.34	2.83	13.07	100
cat	2.6719	1.4204	0.1244	0.8023	5.0190	2.6637	1.4320	0.1398	0.7693	5.0048
Kf#		86.6					84.6			
wt%	62.76	20.14	2.18	14.91	100	60.64	21.81	1.99	15.56	100
cat	2.9026	1.0979	0.1080	0.8797	4.9883	2.8222	1.1964	0.0992	0.9234	5.0413
Kf#		89.1					90.3			
wt%	63.07	19.56	2.36	15.01	100	64.43	18.80	1.99	14.78	100
cat	2.9197	1.0670	0.1169	0.8865	4.9901	2.9683	1.0206	0.0982	0.8688	4.9558
Kf#		88.4					89.8			

1) wt% : weight percent

2) cat : cations per 8 oxygen

3) Kf# : 100 * Kf/(Kf + An)

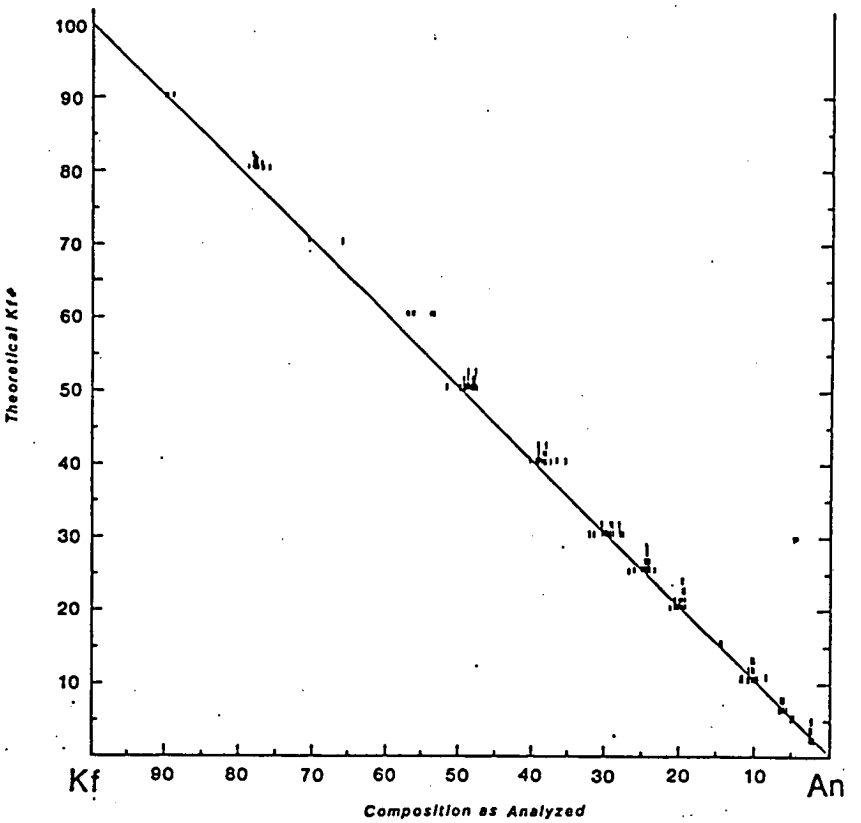

Fig 2.5 Compositions of the Glass Starting Material (each small vertical stroke represents one defocused beam area scan analysis).

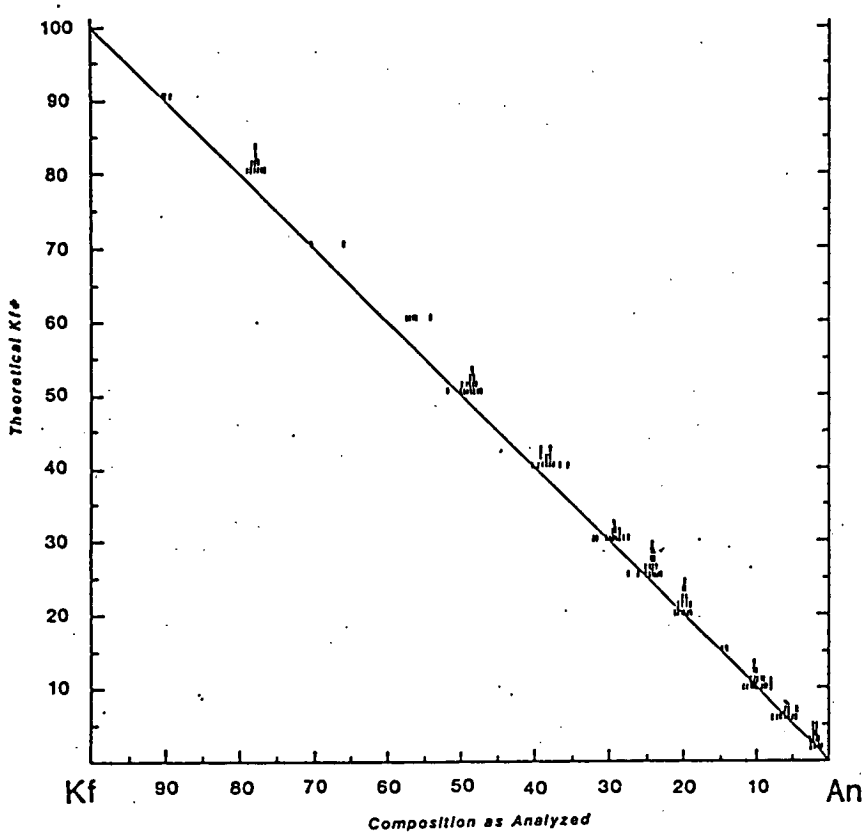

Fig 2.6 Defocused-beam Area Scan Analyses of Run Products.

trace of water possibly absorbed by the sample during assembly preparation.

Since experiments were done under dry conditions, and feldspar melts have large viscosities, crystallization rates during experiments were extremely slow, even at temperatures as high as 1200°C. As an example, the effect of run time on the run product is shown in Fig 2.7. The starting compositions for the two runs (No. T-3151 & T-2151) are identical: Kf# = 25. Both runs were carried out at 1200°C. The run time for T-2131 is only three hours and for T-2151 is more than eleven (11) days (Table 2.4). The T-2131 run produced only small, poorly-formed anorthite crystals, suggested by weak anorthite peaks in the X-ray diffraction chart [Fig 2.7(a)]. The anorthite peaks in the product of run T-2151 [Fig 2.7(b)] are obviously much stronger than those in that of the previous run. More important is that the XRD chart of run T-2151 reveals the presence of K-feldspar crystals, which is not seen in the chart of run T-2131 (K-feldspar peaks are shaded in Fig 2.7(b)]. Thus appropriate run times needed to be carefully chosen at each temperature. Based on the experience of Schairer & Bowen (1947) in doing experiments in the anorthite -- leucite -- silica system, and on experience gained in the first few experiments, it was found that suitable run time is a few hours at temperatures between 1400°C and 1600°C, a few days at temperatures between 1200°C and 1300°C, and 10 - 20 days at temperatures less than 1200°C.

2.4 Experimental Results

2.4.1 Microscopic examination

Run products were first examined with an optical microscope. If feldspar crystals were present they could be observed under high magnification, but it was very difficult to distinguish anorthite from K-feldspar (although

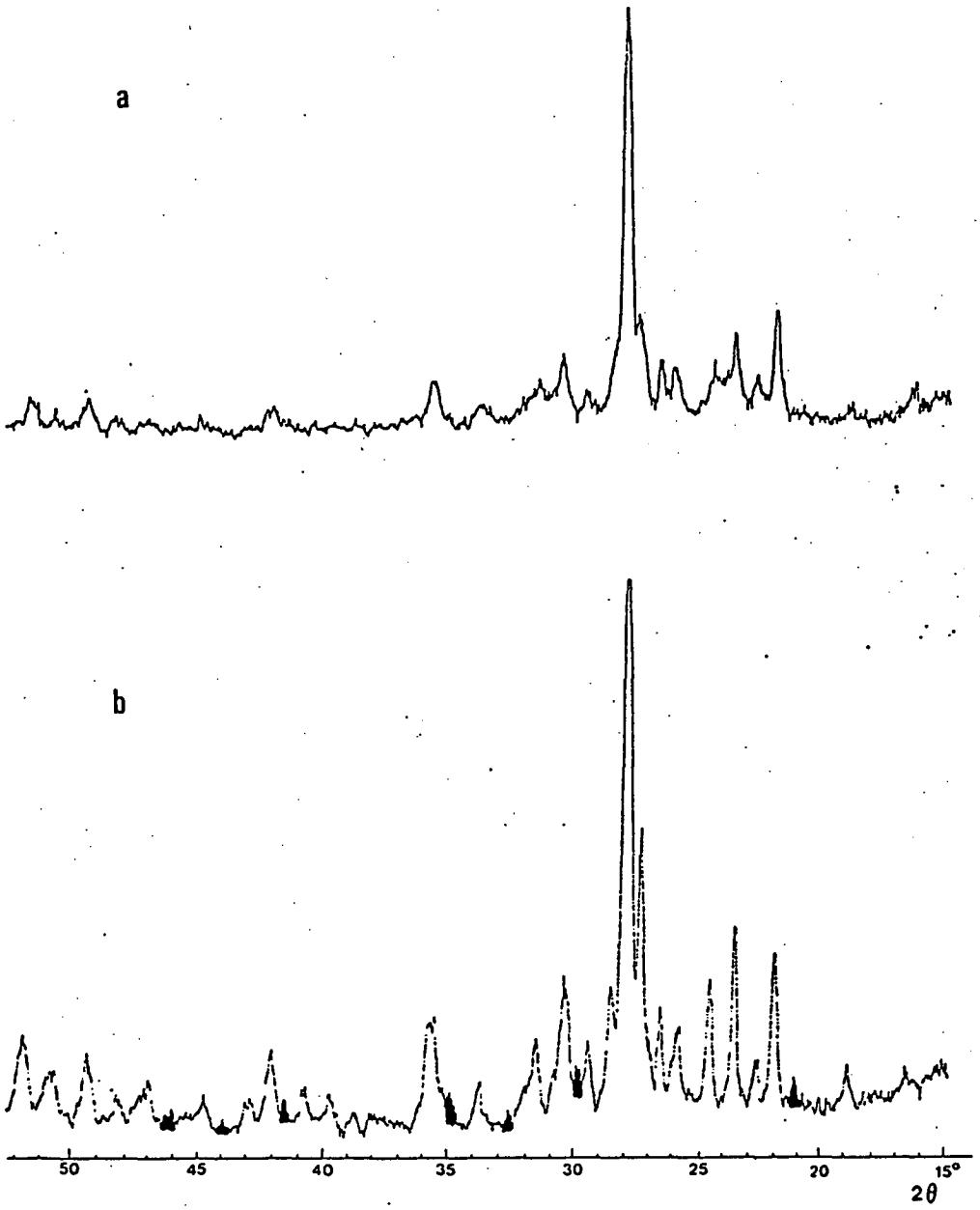

Fig 2.7 The XRD Patterns of Two Runs at 1200°C with Identical Starting Compositions, Showing Time Effect on the Run Products (a) T-2131 (run for three hours); (b) T-2151 (run for 11 days).

sometimes they could be distinguished by differences in relief). The refractive index of the oil used was chosen as 1.550. Pure K-feldspar has a refractive index of 1.53. Anorthite has a refractive index as high as 1.580. Such a difference sometimes showed up but often did not due to the small size of crystals and possibly due to solid solution, which tends to decrease the RI of anorthite (and increase that of K-feldspar). The presence and amount of melt were very difficult to estimate microscopically. However, large amounts of melt could be recognized. The glass was very brittle, so when crushed very small pieces were readily obtained. If many crystals were present in a charge, the sample needed to be crushed many times to be broken into sufficiently small pieces.

2.4.2 XRD analysis

After microscopic observation, the crushed powder was examined by X-ray diffraction techniques. An internal standard was not used in order to keep the samples pure for further infra-red investigation. The consistency of the XRD results was checked by repetitive analysis of the same sample. All diffraction patterns indicate that no other minerals except feldspars are present in the run products. All run products are, therefore, believed to contain only feldspars and/or their equivalent glasses.

For each sample, about 5 - 10 milligram of powder was used. Samples were scanned between 15^{o} and 52^{o} (2θ) on a Philips diffractometer using CuK radiation. Typical XRD patterns are shown in Fig 2.8. The first pattern [Fig 2.8(a)] shows the presence of K-feldspar only. The second [Fig 2.8(b)] indicates both anorthite and K-feldspar present in the run product. The third [Fig 2.8(c)] is identical to the pure anorthite pattern.

Since the strongest K-feldspar peaks (2θ between 27^{o} and 28^{o}) are

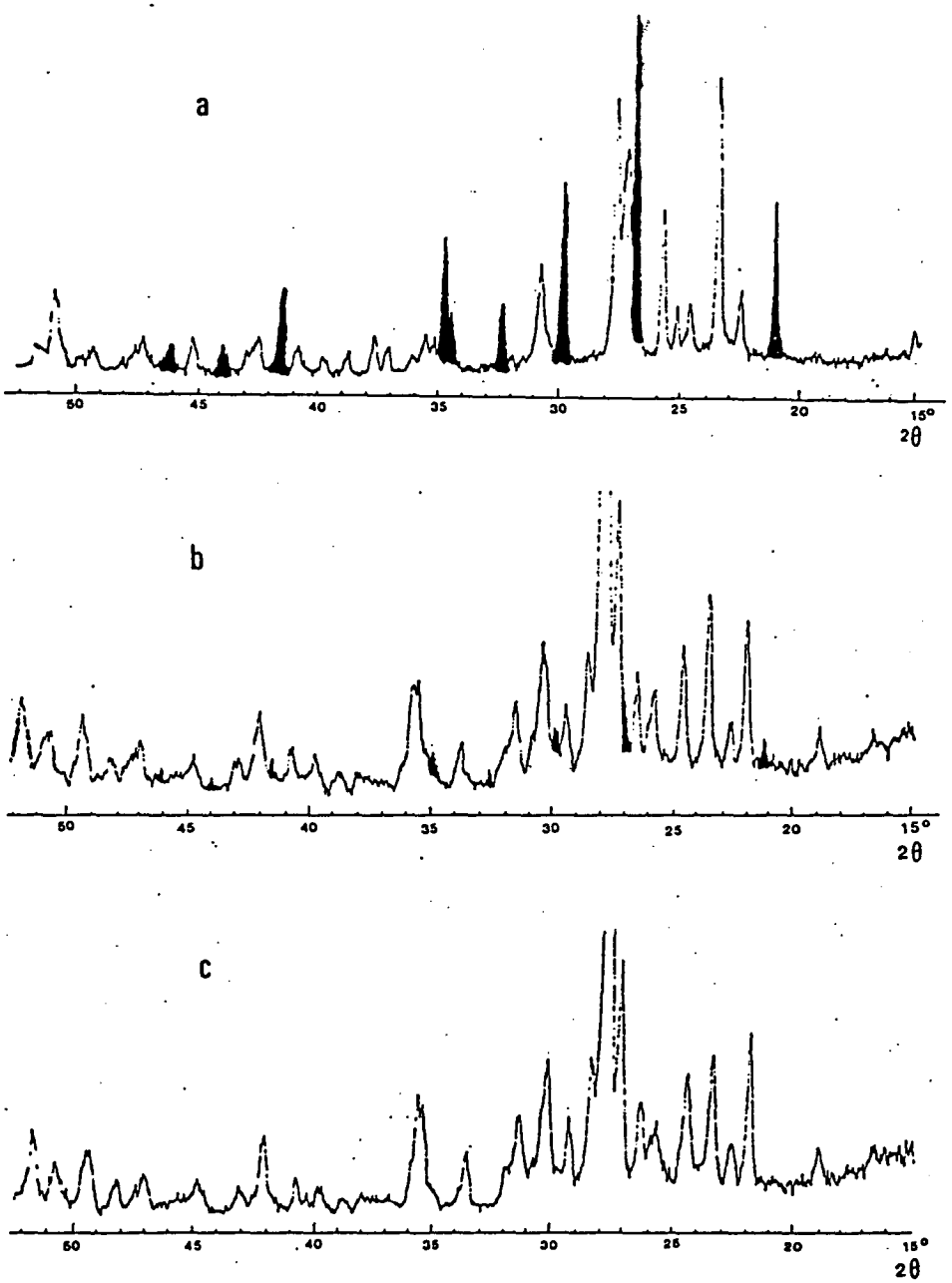

Fig 2.8 Three Typical XRD Charts

(a) T-2152 1200°C, Kf_{90} K-feldspar only;

(b) T-2151 1200°C, Kf_{25} anorthite and K-feldspar;

(c) T-2155 1200°C, Kf_{20} anorthite only.

often obscured by the strongest anorthite peaks, they are not diagnostic. Fortunately other peaks do not all overlap, and some of them can be used as diagnostic features. These diagnostic peaks are listed in Table 2.3. Some of the diagnostic K-feldspar peaks are shaded in Fig 2.8.

Among these diagnostic peaks, the 21° [2θ of $(\bar{2}01)$] K-feldspar peak and the 22° [2θ of $(\bar{2}02)$] anorthite peak are the "characteristic" peaks for K-feldspar and anorthite respectively. It is often necessary to check the presence of other peaks besides the two characteristic peaks before making a final conclusion as to which feldspar is present and which is not, especially when the peaks are very weak {either due to small amount of sample available or small amount of crystals present}.

Several methods have been proposed to determine synthetic feldspar composition by the XRD powder method, such as the [2θ $(\bar{2}01)$ of feldspar -- 2θ $(10\bar{1}0)$ of quartz] -- K-feldspar wt% method of Tuttle & Bowen (1958); the [4θ $(\bar{2}04)$ -- 4θ (060)] -- anorthite% method of Viswanathan (1971); etc. These methods have been used by some researchers in their experimental studies (e.g. Seck, 1971; Yoder et al., 1957); but their accuracy has been questioned by others (e.g. Norris, 1972). In this study, the XRD method is used to check the phases present in the run products. The compositions of these phases, however, were determined by electron microprobe analysis, which will be discussed later in this section.

By looking for the absence of feldspar crystals, or the presence of one or two feldspars in a XRD chart of a run product, the liquidus and solvus can be fixed. The only problem is the detection limit of this X-ray method. In order to evaluate this limit, natural feldspars of known composition (sanidine and An-rich plagioclase) were mechanically mixed in different

Table 2.3 Diagnostic Peaks of Anorthite and K-feldspar

anorthite						K-feldspar	
2θ	hkl	2θ	hkl	2θ	hkl	2θ	hkl
18.9	$02\bar{2}$	27.8	$20\bar{4}$	39.7	$33\bar{2}$	21.0	$\bar{2}01$
21.8	$\bar{2}02$	28.3	220	40.8	$\bar{2}44$	26.8	$220/\bar{2}20$
22.6	$1\bar{1}2$	29.4	$13\bar{2}$	42.1	$24\bar{2}$	27.1	$\bar{2}02$
23.4	$13\bar{0}$	30.2	$04\bar{2}$	43.1	$13\bar{5}$	29.8	$131/1\bar{3}1$
24.5	130	30.4	$02\bar{4}$	49.4	$40\bar{6}$	32.3	$1\bar{3}2/\bar{1}32$
25.7	$11\bar{4}$	31.6	132	49.6	400	34.7	$24\bar{1}/\bar{2}41$
26.4	$\bar{1}14$	33.7	$31\bar{2}$	51.8	$20\bar{8}$	41.6	060
27.2	$22\bar{0}$	35.4	$\bar{2}42$			50.8	$\bar{2}04$

proportions and were analyzed by X-ray diffractometry. The sanidine was separated from a coarse-grained porphyry from Port Cygnet, Tasmania. Its composition is $(K_{0.82}\ Na_{0.13}\ Ca_{0.04})\ Al\ Si_3\ O_8$ (sample CY13 of Ford, 1983). The plagioclase $[(Ca_{0.93}\ Na_{0.07})\ Al_2\ Si_2\ O_8]$ was separated from a dredged basaltic lava from the north Tonga ridge (sample No.D3 - 52 of Falloon, in prep). For a mixture of the above sanidine (5%) and plagioclase (95%), the $(\bar{2}01)$ peak of sanidine and other peaks were sometimes shown and sometimes not clearly shown in the XRD charts for repetitive XRD analyses. For a mixture of 10% sanidine and 90% plagioclase, the $(\bar{2}01)$ and other sanidine peaks are clearly shown in the chart. As a result, 5% is loosely defined as the detection limit of this technique. This limit is important when two feldspars are present in a run product and when determination of the position of the solvus is concerned. The results of the XRD analysis are given in Table 2.4.

2.4.3 SEM observation

A polished microprobe mount of run products was observed under a Philips 505 Scanning Electron Microscope (SEM). Phases present in the run products could not be detected because of small differences in mean atomic number between these phases. To avoid this problem, a sample was etched with HF acid (1 wt% HF solution) at room temperature for about 1 minute. Acid-etching gave marked surface relief [plate 2.1 (a)], with glass being the most easily dissolved by the HF-solution, highlighting the remaining etch-resistant surfaces of crystals. However, in samples without glass etching may have occurred along the boundaries between crystals, leading to very irregular boundaries of these crystals. Any interpretation of plate 2.1 (a) is thus equivolcal; it may infer that the charge contains at least two phases,

but whether one is glass or both are crystals is not certain, since individual crystals can not be identified. Furthermore, when the sample was analyzed by electron microprobe after etching, analyses were always poor. The total oxide weight percent was less than 80% and the cation sum per 8 oxygen, as high as 7.000. The etching technique was therefore not useful.

Another technique was adopted in order to determine the phases present in run products. This was the "broken surface" technique. After each experiment the run product was crushed and some small chips were picked up, coated with gold, and observed under the SEM. The broken surface morphology of the chips could esily be seen [plate 2.1(b)]. A back scattered electron image of the same run product as that shown in plate 2.1(a) is given in plate 2.1(b). (All other electron micrographs shown later are taken in the back scattered electron mode). Although the sample is the original run product and was not etched, there are many holes between the obvious crystals. Such an image is considered to show typical subsolidus features, which means that there are only feldspar crystals present in this run product. It is clear that all the crystals are indeed very small, only about 5 micrometers long and 2 - 3 micrometers wide. For supersolidus (above solidus) runs, both crystals and glass are present. The crystals, with regular shapes, stand out because they are harder than glass. Sometimes regular voids are left on surfaces when the crystals were knocked out during crushing (plate 2.2). Occasionally, a kind of "step-like" feature within a crystal can be seen (plate 2.3). The "steps" are probably cleavages. On the other hand, glass always appears smooth, sometimes showing conchoidal fracture (plate 2.4).

For runs very close to the solidus, traces of melt are very difficult to recognize from SEM images. In such cases, identification of glass was made

by electron microprobe analysis of run products.

2.4.4 Electron microprobe analysis

Microprobe analyses were carried out using a JEOL - 50A electron probe microanalyzer with an energy - dispersive system. Normal beam current was 7.0×10^{-10} A on a Cu metal standard, with an accelerating voltage of 15 Kv.

Theoretically, if a starting composition "X" is run at T_1 temperature (Fig 2.4), two kinds of crystals should crystallize, with compositions "a" and "b" respectively. The two compositions "a" and "b" can be determined by electron microprobe analysis. The analysis may give a series of compositions (because the analysis area may overlap the two kinds of crystals) but should not be beyond the limits of "a" and "b", because all the phases present in the run product should have compositions within the "a" -- "b" limit. This is also applicable to the melt-plus-crystal field; i.e. the run products of a suitable starting composition run at temperature T_2 (Fig 2.4) should have phases having their compositions within the "c" -- "d" limit. In the one-crystal-only field, only one phase is present and it should have only one composition, its starting composition. The same is true in the melt-only field. By applying the above considerations to the present study of the system anorthite -- K-feldspar, it was hoped that a phase diagram could be readily constructed, simply by using the electron microprobe analysis method. There are, however, several complications. Microprobe analyses of the run products are shown in Fig 2.9 (selected as discussed later referring to Fig 2.10). Different numbers denote different starting compositions. Lines between the same numbers at a given temperature indicate the compositional ranges of the run products. As is evident from Fig 2.9, the ranges at each temperature are not limited in the regular way that was

expected. For example, at 1300°C the compositional ranges of run products for starting compositions Kf_{30}, Kf_{40}, and Kf_{50} are very different, although they are expected to lie within the melt-plus-crystal field. These compositional ranges do not show any common limit, which whould otherwise give the compositions of coexisting melt and crystals. In the subsolidus field where two feldspars (anorthite with K-feldspar solid solution and K-feldspar with anorthite solid solution) should be present, K-feldspar was not detected. This is probably due to the small quantity of this phase present in the run products.

The majority of the microprobe analyses are not ideal, often with both bad weight totals and cation sums. This is perhaps caused by the small size of the feldspar crytals synthesized. SEM observations showed that these crystals are only slightly larger than the diameter of the focused electron beam of the microprobe. During random analysis, the beam positions were not accurately known (because the phase being analyzed could not be observed). Most analytical areas probably extended beyond the margins of a single crystal. These analyses are thus a combination of different phases (including voids between the phases). In order to evaluate the analyses, a Si-Ca-K diagram was constructed. Accepted analyses should not only have good weight total (100 +/- 1%) and cation sum (5.00 +/- 0.01 per 8 oxygen) but also lie on the tie-line connecting anorthite and K-feldspar in the Si-Ca-K diagram. An example is given in Fig 2.10, where the accepted analyses at 1200°C and 1300°C are shown. These selected data are also shown in Fig 2.9 and are used to define the phase relations in the binary system anorthite -- K-feldspar at 10 Kbar (Fig 2. 11). Fig 2.11 is also consistent with and defined by the XRD data and SEM observations (Table 2.4).

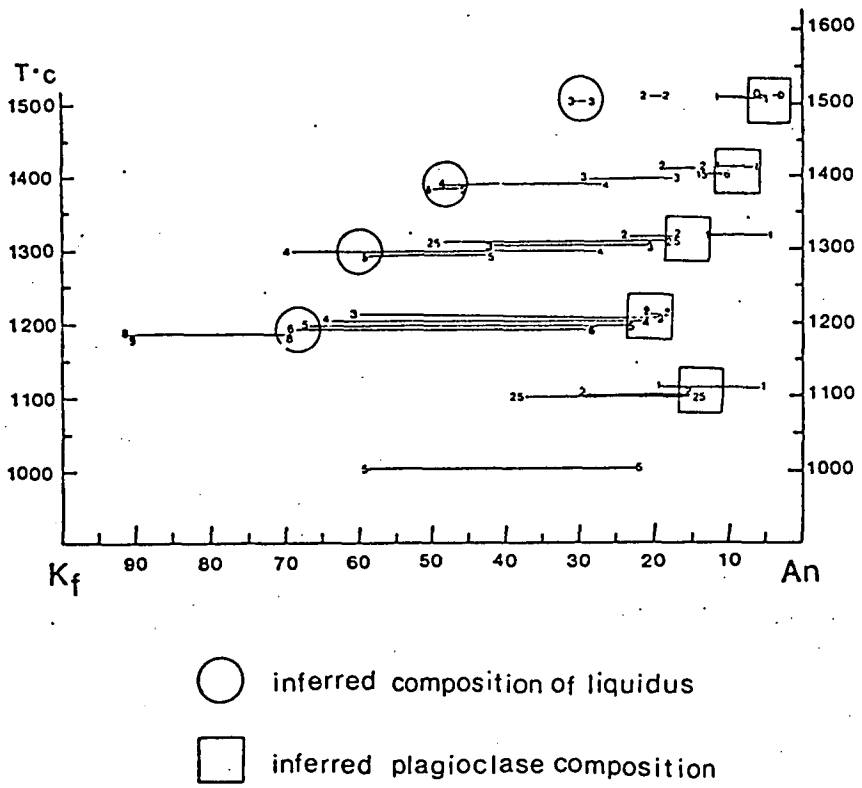

Fig 2.9 Electron Microprobe Analysis Results of Run Products (Lines are compositional ranges, bracketed by the numbers that denote starting compositions:

Number	0	1	15	2	25	3	4	5	6	7	8	9
Kf#	5	10	15	20	25	30	40	50	60	70	80	90).

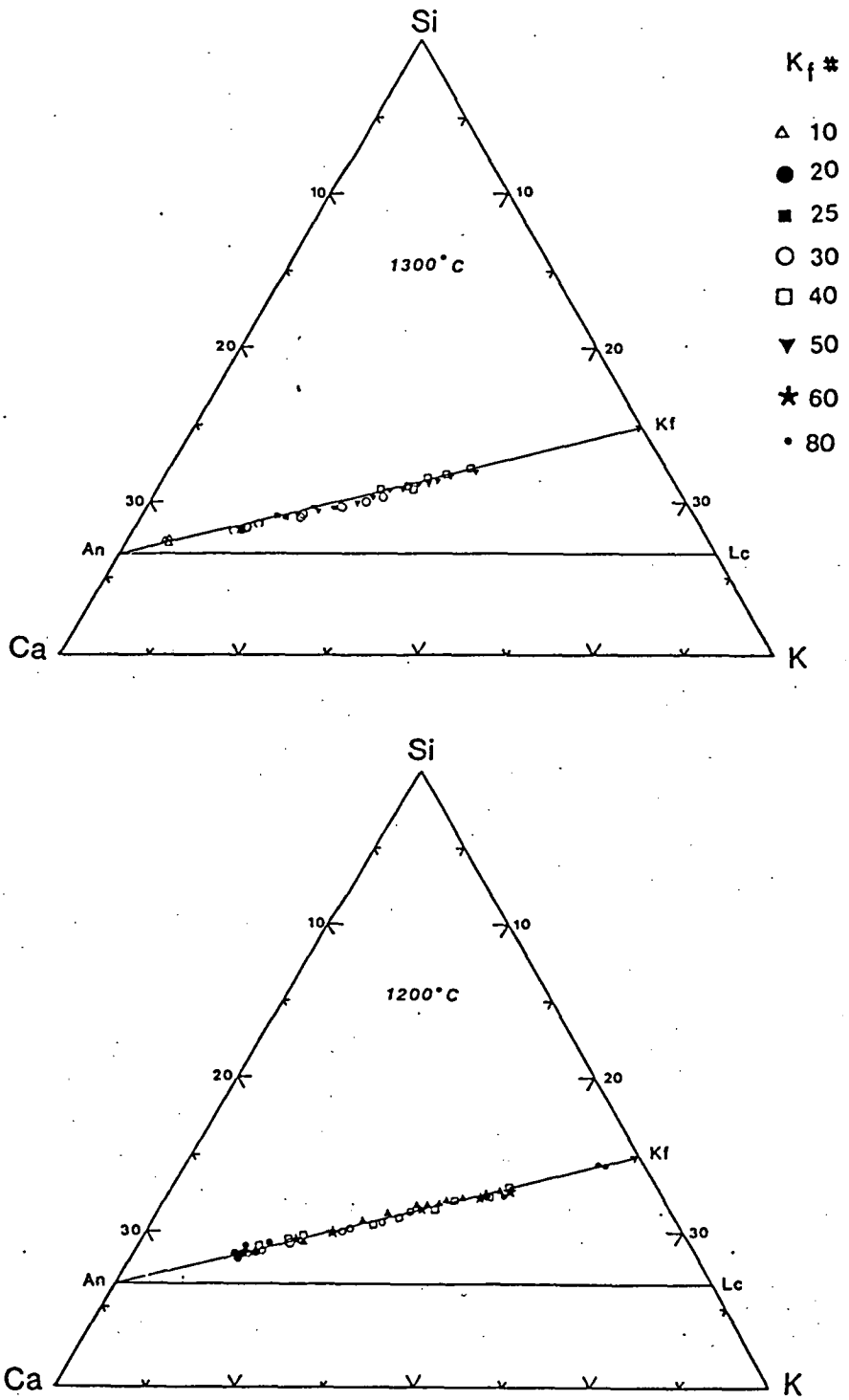

Fig 2.10 The Si -- Ca -- K Diagram to Evaluate the Quality of Feldspar Microprobe Analyses.

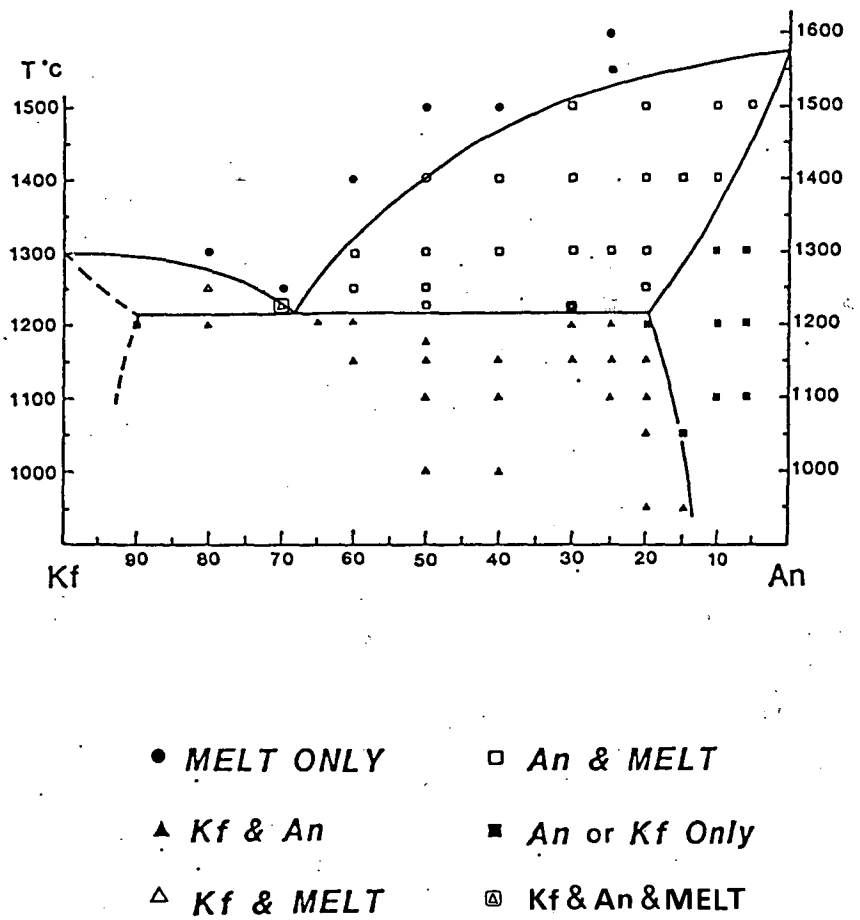

Fig 2.11 Phase Relations in the Binary System Anorthite -- K-feldspar at 10 Kbar.

Table 2.4 Experimental Results

run No.	starting composition	temper-ature	run duration	results XRD	results SEM
T-2080	25	1600	0.5 hr	no peak	no crystal
T-2130	25	1550	1 hr 35 min	no peak	no crystal
T-2127	50	1500	2 hr	no peak	no crystal
T-2127	40	1500	2 hr	no peak	no crystal
T-2062	30	1500	2 hr	An peaks	more melt than
T-2057	20	1500	1 hr	An peaks	crystals
T-2057	10	1500	1 hr	An peaks	melt + crystals
T-2060	10	1500	3 hr	An peaks	melt + crystals
T-2070	5	1500	2 hr	An peaks	crystal (+ melt?)
T-2125	60	1400	3 hr 40 min	no peak	no crystal
T-2061	50	1400	3 hr	An peaks	melt + crystals
T-1996	40	1400	5 hr 10 min	An peaks	melt + crystals
T-1996	30	1400	5 hr 10 min	An peaks	melt + crystals
T-2017	30	1400	5 hr	An peaks	melt + crystals
T-1996	20	1400	5 hr 10 min	An peaks	crystals + melt
T-2073	15	1400	3 hr	An peaks	crystals + melt
T-1996	10	1400	5 hr 10 min	An peaks	crystals (+ melt?)
T-2134	80#	1300	6 hr 40 min	no peak	no crystal
T-2134	60	1300	6 hr 40 min	An peaks	melt (+ crystals?)
T-1984"	50	1300	2 days		melt (+ crystals?)
T-1984"	40	1300	2 days		melt + crystals
T-1984"	30	1300	2 days		crystals + melt
T-2064	30(+c)	1300	6 days 1 hr	An peaks	crystals + melt
T-2090"	30	1600-1300	8 days	An peaks	crystals + melt
T-2071	25	1300	8 hr	An peaks	crystals + melt
T-1984"	20	1300	2 days	An peaks	crystals (+ melt?)
T-1736	9.5′	1300	2 days	An peaks	
T-1736	5.6′	1300	2 days	An peaks	
T-1736	1.9′	1300	2 days	An peaks	
T-2148	80	1250	2 days	Kf (+An?) peaks	melt + crystals
T-2213	70	1250	10 days	weak An peaks	melt + crystals
T-2213	60	1250	10 days	An peaks only	melt + crystals
T-2172	50	1250	10 days	An peaks only	melt + crystals
T-2172	25	1250	10 days	An peaks only	crystals + melt
T-2122	25	1250	2 days	An peaks only	crystals + melt
T-2193	50(+KCl)	1225	10 days	An peaks only	
T-2160	70	1225	6 days 1 hr	An + Kf peaks	melt + crystals
T-2135	30	1225	3 days 22.5 hr	An peaks only	crystals + melt
T-2186	65	1220-1185	11 days	An + Kf peaks	
T-2186	60	1220-1185	11 days	An + Kf peaks	

Table 2.4 Experimental Results (con't)

run No.	starting composition	temperature	run duration	results XRD	results SEM
T-2152	90	1200	7 days	Kf peaks only	crystals
T-2152	80	1200	7 days	Kf + An peaks	crystals + melt
T-1933"	60	1200	10 days 18 hr	(not enough	melt + crystals
T-1933"	50	1200	10 days 18 hr	samples)	melt + crystals
T-1933"	40	1200	10 days 18 hr		melt + crystals
T-1933"	30	1200	10 days 18 hr		crystals + melt
T-2030	30	1200	6 days 23 hr	An (+ Kf?) peaks	crystals + melt
T-2131	25	1200	3 hr	An (+ Kf?) peaks	crystals + melt
T-2151	25	1200	11 days 12 hr	An + Kf peaks	crystals + melt?
T-2155	25	1200	11 days 18 hr	An + Kf peaks	crystals + melt?
T-2155	20	1200	11 days 18 hr	An peaks only	crystals (+ melt?)
T-1887"	20	1200	10 days	An peaks only	crystals (+ melt?)
T-1887"	9.5'	1200	10 days	(not enough	
T-1765"	9.5'	1200	6 days 22 hr	samples)	
T-1740	9.5'	1200	7 days		
T-1887"	5.6'	1200	10 days		crystals only
T-1765"	1.9'	1200	6 days 22 hr		
T-1749	1.9'	1200	7 days		
T-2105	50	1175	13 days	Kf + An peaks	
T-1987"	60	1150	7 days	An + Kf peaks	crystals only
T-1987"	50	1150	7 days	An + Kf peaks	crystals only
T-1987"	40	1150	7 days	An + Kf peaks	crystals only
T-1987"	30	1150	7 days	An + Kf peaks	
T-2142"	25	1150	7 days 22.5 hr	An + Kf peaks	
T-2149	25	1150	3 days 15 min	An + Kf peaks	
T-2156	25	1150	8 days	An + Kf peaks	
T-2118	20	1150	2 days 3 hr	An peaks only	
T-2035"	50(+Cl)	1100	6 days 23 hr	An + Kf peaks	crystals only
T-2084"	40(+V)	1100	3 days 4 hr		V203 + ?
T-2153	25	1100	1 day 12 hr	An + Kf peaks	
T-2147	20	1100	14 days 16 hr	An + Kf peaks	
T-1792"	9.5'	1100	11 days 3 hr		
T-1839"	9.5'	1100	13 days		crystals only
T-1852"	9.5'	1100	10 days 23 hr	An peaks only	
T-1852"	5.6'	1100	10 days 23 hr		
T-1830"	5.6'	1100	13 days		
T-1792"	5.6'	1100	11 days 3 hr		
T-1792"	1.9'	1100	11 days 3 hr		
T-1839"	1.9'	1100	13 days		
T-1852"	1.9'	1100	10 days 23 hr	An peaks only	
T-2158	20	1050	20 days	An + Kf peaks	
T-2158	15	1050	20 days	An peaks only	

Table 2.4 Experimental Results (con't)

run No.	starting composition	temper-ature	run duration	results XRD
T-2067	50(+c)	1000	20 days	An + Kf peaks
T-2066	50(+c)	1000	4 hr	An + Kf peaks
T-2102	40(+V)	1000	2 days	An + Kf peaks (not obvious)
T-2154	20	950	11 days	An + Kf peaks (not obvious)
T-2154	15	950	11 days	An + Kf peaks
reversal runs:				
T-2264	20 (T-2155)	1050	15 days	An + Kf peaks
T-2285	20 (crystalline)	1200	20 days	An peaks only
T-2202$	50	1300	4 days 25 min	An + Kf peaks

1) Pressures for all the runs except the last are 10 Kbar and temperatures are in ^{o}C.

2) " indicates salt/pyrex assembly;
the rest are talc/pyrex assembly.

3) Starting composition is given by Kf# [=100 * Kf/(Kf + An)].
The starting material for all the runs is glass except:

´) anorthite - seeded starting material;

#) oxide mix starting material;

+c) carbonates ($CaCO_3$ + K_2CO_3) fluxed;

+Cl) chlorides ($CaCl_2$ + KCl) fluxed:

+V) V_2O_3 fluxed.

It is clear from Fig 2.11 that this is a binary eutectic-type system. The eutectic point occurs at 1215° +/- 15°C, Kf_{69} +/- 5%. The melting temperatures of pure anorthite and pure K-feldspar at 10 Kbar are 1575°C (Goldsmith, 1980) and 1300°C (Lindsley, 1966) respectively. The maximum solubility of K-feldspar in anorthite is 20 +/- 5% and that of anorthite in K-feldspar, 10 +/- 5%. They occur at the eutectic temperature.

2.5 Problems and Further Work

2.5.1 Equilibrium

In melting experiments in the Ab -- An -- H_2O and the Qz -- Ab -- An -- H_2O systems at 5 Kbar water pressure, Johannes (1978) observed that reaction rates are extremely dependent upon temperature: a change in temperature of 100°C causes a change in the reaction rate of several orders of magnitude. At 1000°C in the Ab -- An -- H_2O system, equilibrium is believed to be reached in 1 hour, while at 800°C Johannes considered the reaction to be too slow to reach equilibrium. In the Qz -- Ab -- An -- H_2O system, plagioclase approached equilibrium compositions very slowly and it was extrapolated that at 730°C about 100,000 years are needed to achieve equilibrium.

In an experimental study of the ternary feldspar system, Johannes (1979) used synthetic feldspar starting material and found that equilibrium was reached after 10 days at 800°C and 20 days at 650°C, at 1 Kbar water pressure. This was orders of magnitude faster than the reactions that had occurred in his previous melting experiments (Johannes, 1978).

The reactions in the melting experiments (Johannes, 1978) were supersolidus, and those in the ternary feldspar experiments (Johannes, 1979) subsolidus. It is generally believed that supersolidus reactions should be

faster than subsolidus reactions because melt is involved in the supersolidus reactions and ions move faster in melt than in solid. However, the reaction rates noted above in the melting and the ternary feldspar experiments are opposite to those predicted. This problem was acknowledged by Johannes (1979), although he could offer no simple explanation. It was also observed that the rate of a reaction leading to a more An-rich plagioclase is much faster than a reaction producing a more Ab-rich plagioclase. This was suggested to be due to the obstacle effect of albite, which blocks the spaces for transportation of reactants (Johannes, 1979). If this is true, then reactions in the pure anorthite -- K-feldspar system should reach equilibrium more easily than those in systems containing albite.

Talc/pyrex assemblies were used in most of the experiments. It is very likely that H_2 was generated during experiments through OH breakdown from talc at high pressures and high temperatures. The presence of H_2 has the effect of promoting Al -- Si interdiffusion (Goldsmith, 1986), and thus can help to achieve equlibrium in the anorthite -- K-feldspar reaction during the experiments.

Reversal experiments are necessary to confirm the phase relations shown in Fig 2.11. The focus of the study was on the maximum K-feldspar solubility in anorthite, which occurs at the eutectic temperature. Two types of reversal experiments were performed in order to bracket the solvus; one was an exsolution experiment using anorthite with the maximum K-feldspar solid solution, and the other was a synthesis experiment of such anorthite from pure crystalline anorthite and K-feldspar starting material. For the first experiment (T-2264), the temperature was chosen at 1050°C in order to have the temperature high enough to reach equilibrium during the short run time

and to produce sufficient K-feldspar to be detected by the XRD method. The starting material was the run product of T-2155, believed to contain only the anorthite with the maximum K-feldspar solid solution (20%) at 10 Kbar. The run time was 15 days, long enough for K-feldspar to exsolve from the anorthite host. Shown in Fig 2.12(a) is part of the XRD pattern of the starting material. It shows that the $(\bar{2}01)$ peak of K-feldspar is not present (it should appear close to 21°), suggesting that no K-feldspar is present in the starting material (other K-feldspar peaks are also absent from the XRD chart). An obvious peak at 20.8° (2θ) occurred in the XRD pattern of the run product of T-2264 [Fig 2.12(b)], clearly indicating the presence of K-feldspar together with anorthite in the run product. This means that the high temperature anorthite (with 20% K-feldspar solid solution) decomposed into two phases at lower temperature: an anorthite phase with less K-feldspar solid solution and a K-feldspar phase that also contains anorthite solid solution.

The starting material for the second reversal experiment was a mixture of synthetic anorthite (80%) and K-feldspar (20%). Anorthite was synthesized at 1050°C and 10 Kbar for 10 hours in a Ag_{50} Pd_{50} capsule from an oxide mix of CaO, Al_2O_3, and SiO_2. About 7 wt% water was added to the oxide mix in order to help crystallization. K-feldspar was synthesized at 1100°C and 25 Kbar for 22 hours from an oxide mix of K_2O, Al_2O_3, and SiO_2 in a graphite capsule (K_2O was obtained from the decomposition of K_2CO_3). No flux was added. The purity of the synthetic anorthite and K-feldspar were checked by the XRD method. No other phases except anorthite and K-feldspar were found. The synthetic anorthite (80%) and K-feldspar (20%) were mechanically mixed in an agate mortar for more than 20 minutes. The mix was kept in

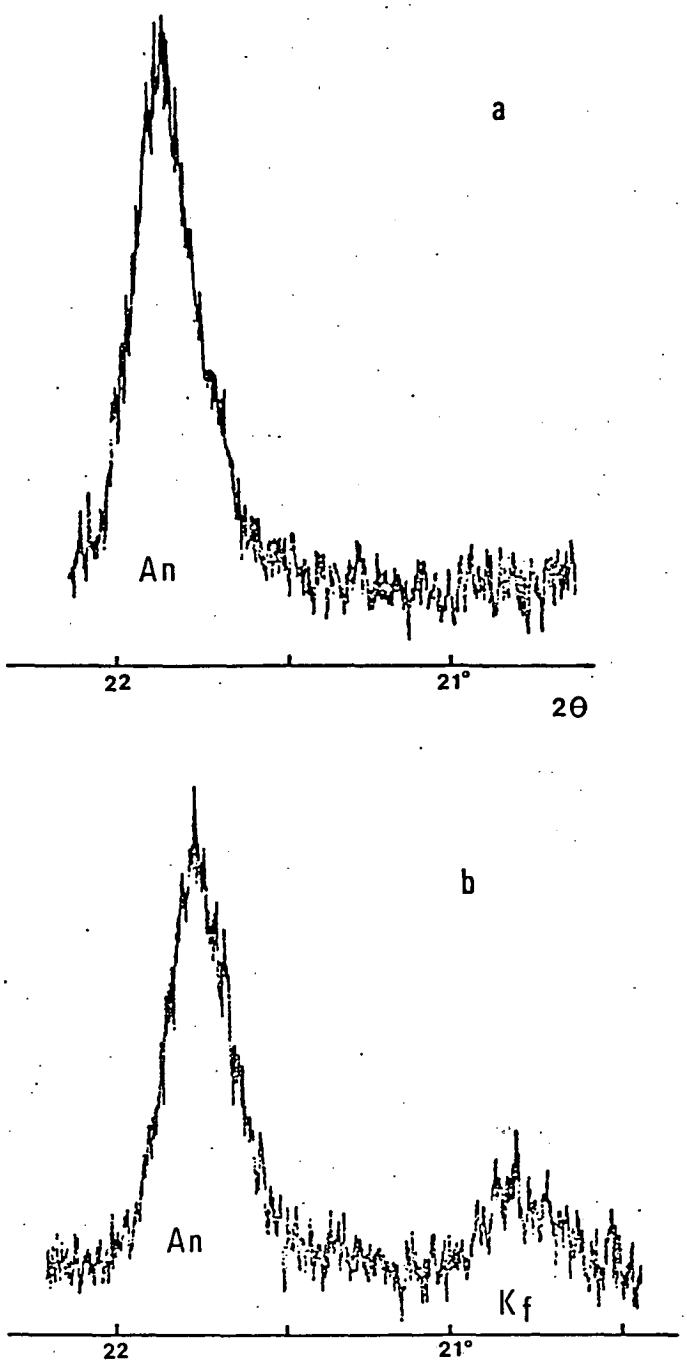

Fig 2.12 Part of the XRD Patterns of (a) the Starting Material & (b) the Run Product of a Reversal Run T-2264 at 1050°C.

an oven at 120°C overnight, and then heated at 1200°C and 10 Kbar for 20 days in a platinum capsule (run T-2285). The XRD patterns of the mechanical mix (the starting material) and the run product are shown in Fig 2.13. The pattern of the starting material [Fig 2.13(a)] clearly shows the presence of both anorthite and K-feldspar, while that of the run product [Fig 2.13(b)] demonstrates that only anorthite is present (the 20% K-feldspar has been dissolved by anorthite). The results of the two reversal experiments strongly suggest that only one phase is present at 1200°C and 10 Kbar for the composition Kf_{20} An_{80}. In a similar way, the other part (the K-feldspar-rich part) of this binary system can also be checked. Such work, however, was beyond the purpose of this study (to demonstrate experimentally the exsolution origin of the unusual feldspar intergrowths found in the Antarctic dykes).

2.5.2 Attempts to increase the crystal size of the synthetic feldspars

Since the synthetic feldspar crystals were too small to be accurately analyzed by electron microprobe, several methods were tried to produce larger feldspar crytals. Although unsuccessful, these methods will be briefly discussed here, as they are considered as useful information for future studies.

a) Seed method:

For the first few experiments with starting composition K-feldspar equal or less than 10%, about 5% anorthite [synthesized at 1300°C and 10 Kbar for 16 hours and 15 minutes in a graphite capsule] crystals were added to the glass starting material. The crystals obtained did not seem to be larger (plate 2.5), therefore this method was not used in later experiments.

b) Melting - crystallization method:

It was thought that the presence of melt would assist crystallization.

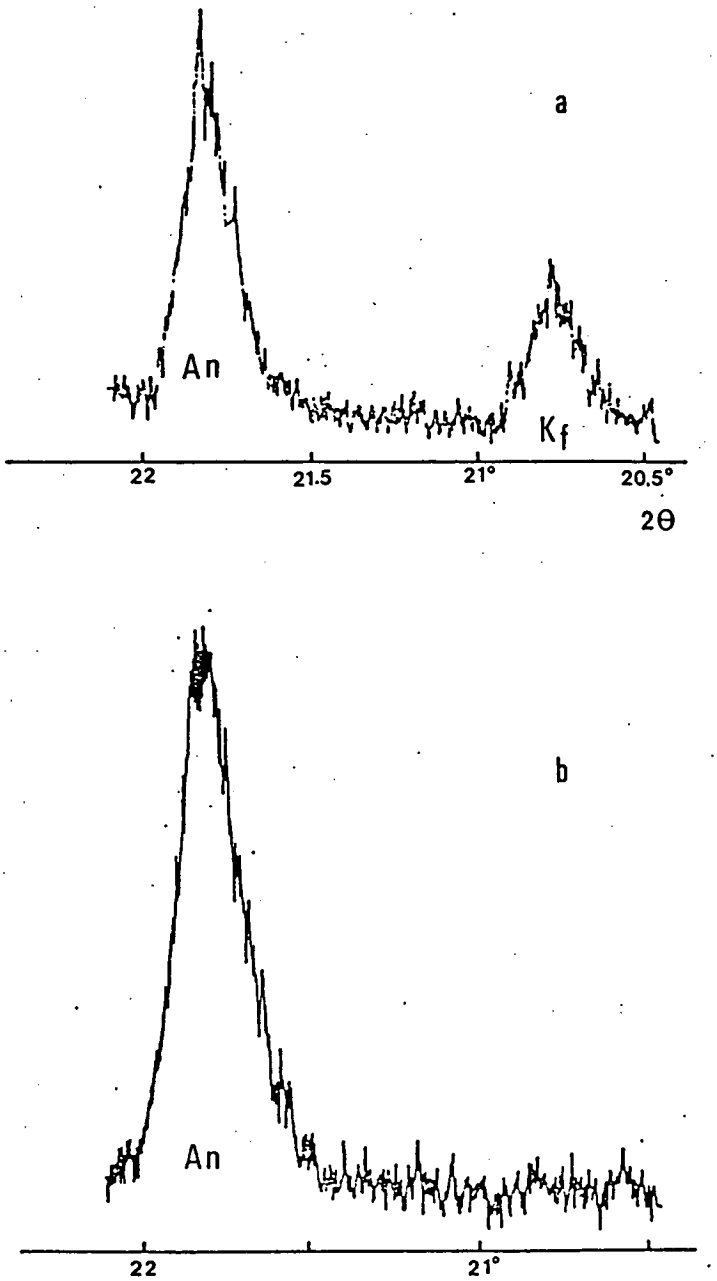

Fig 2.13 Part of the XRD Patterns of

(a) Mechanical Mix of 80% Anorthite + 20% K-feldspar

(b) the Run Product of T-2285 at 1200°C.

A run was done to confirm this idea, with starting composition Kf_{30} (glass). The temperature was first raised to 1600°C, at which the glass should become melt, and held at 1600°C for 5 minutes to ensure complete melting, then temperature was decreased to 1550°C for 5 minutes, 1500°C for 5 minutes, 1450°C for 5 minutes, 1400°C for 10 minutes, 1350°C for 20 minutes, and at last the temperature was fixed at 1300°C for 8 days. The result was far from encouraging: feldspars seemed to be even smaller. Perhaps crystallization from melt in the feldspar system is slower than subsolidus reactions, as mentioned earlier in relation to Johannes' (1979) study.

c) Flux method:

This is a conventional method for accelerating reactions. The addition of suitable components into a system will make reactions occur more quickly without affecting the equilibrium itself. In many experimental studies, fluid phases are used to flux subsolidus reactions. H_2O and CO_2 are the two commonly used fluid phases. For the experiments performed in this study, H_2O was unsuitable because of its pronounced effect on the solidus temperatures of feldspars. CO_2 has a low solubility in silicate melt at low pressures (<20 Kbar) and might possibly be useful. To test this, silver oxalate and K_2CO_3 + $CaCO_3$ (1:1 wt ratio) mix were used seperately. The run with silver oxalate produced similar result to the anorthite seeded run (plate 2.6): feldspar crystals are not larger. In the runs with carbonate mix, feldspar crystals were even smaller (plate 2.7). Sometimes a CO_2- and K-rich phase was present in the run product. Obviously a CO_2 fluid is not useful in producing larger crystals.

The chloride mix KCl + $CaCl_2$ (1:1 wt ratio) was tried in the same way as the carbonates, again with poor result (plate 2.8).

Vanadium pentoxide was successfully used as a flux in aiding growth of pyroxenes and olivine in the CMAS ($CaO - MgO - Al_2O_3 - SiO_2$) system (Carlson, 1986). It was hoped that it might work in the feldspar system as well. Initially V_2O_5 was mixed with prepared glass starting material and the mix was directly run at high pressure. No feldspar crystals could be found in the run product using SEM; instead, large euhedral V_2O_3 crystals are present (plate 2.9). This was thought to be caused by the intrinsically reduced conditions in the sample chamber during the experiment, in which V_2O_5 was reduced to V_2O_3. Following this, V_2O_5 was mixed with oxides of anorthite + K-feldspar composition and heated at 980°C for 5 days in a one-atmosphere furnace. This time, no feldspar was synthesized at all and some unknown minerals were present in the run product, as revealed by XRD analysis.

2.5.3 Further work

Because of the specific purpose of this study, experiments in the K-feldspar-rich part of the anorthite -- K-feldspar system were not sufficient to determine the positions of solidus and solvus in this part of the binary diagram. One or two runs at temperatures below 1200°C should be sufficient to locate the solvus. At present, the solvus and solidus are approximately indicated.

More work can be done using the XRD powder analysis results of the run products in order to understand the crystallography of these new feldspars. Cell parameters, for example, should be easy to calculate by using a special computer programme and will be useful for development of thermodynamic models in feldspar systems. Since such a programme is not readily available, the calculation has not been undertaken.

Finally, it is worth emphasizing that methods for synthesizing larger feldspar crystals (large enough for electron microprobe analysis) are needed in order to understand the exact relations among temperature, pressure and feldspar compositions in synthetic systems.

2.6 Conclusions

The experimental study of phase relations in the anorthite -- K-feldspar binary system at 10 Kbar pressure has confirmed the eutectic character of this system. At 10 kbar the eutectic point is located at 1215°C, Kf (69 +/- 5%) . The mutual solubilities between anorthite and K-feldspar are increased relative to those at atmospheric pressure (from K-feldspar 5% at 1 atm to 20% at 10 Kbar in anorthite, anorthite 3% to 10% in K-feldspar). Such an increase is probably a result of the combined effects of pressure and temperature. Pressure was thought to increase feldspar melting temperatures, but have little effect on their solid solutions. This may not be completely true, since a run at 25 Kbar and 1300°C with starting composition Kf_{50} An_{50} has yielded a result showing very extensive solid solutions between anorthite and K-feldspar, as implied by the peak positions in the XRD chart (Fig 2.14). Further work is needed to determine whether pressure really has an effect on the solvus position. It is hypothesized here that the solvus narrows greatly at temperatures greater than 1200°C (with increasing pressure). This is schematically illustrated in Fig 2.15.

The methods used in this study should be applicable to studies of the ternary feldspar system. It is pointed out that in experimental studies of feldspar systems, two main difficulties will be encountered: attainment of equilibrium and analysis of synthetic feldspar compositions. Equilibrium is

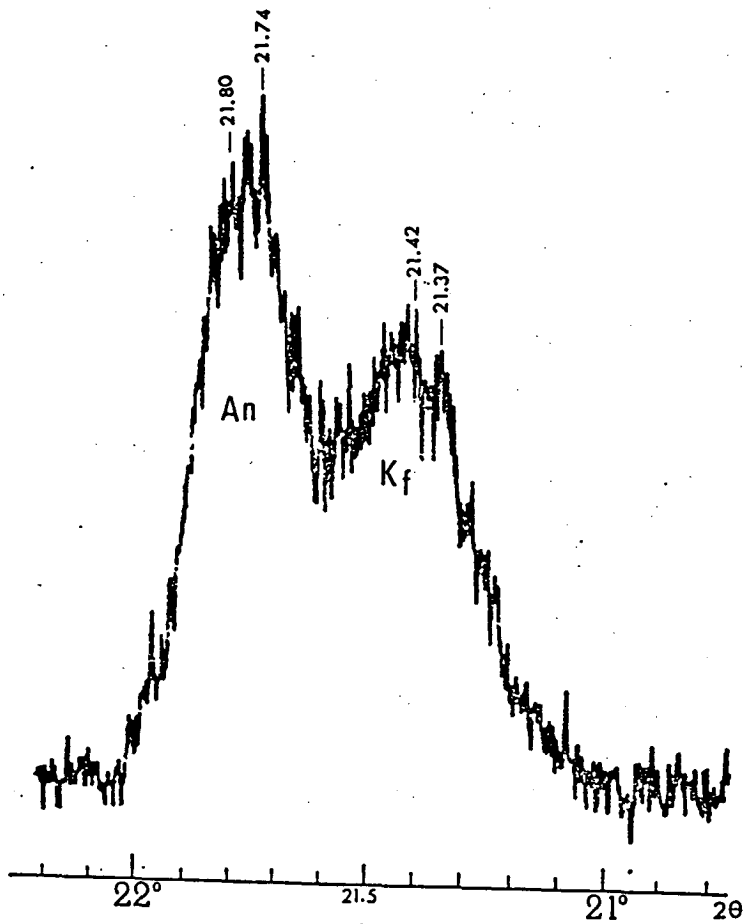

Fig 2.14 ($\bar{2}01$) Peak Positions of Coexisting Anorthite and K-feldspar in Run T - 2202 (1300°C, 25 Kbar, $Kf_{50}An_{50}$).

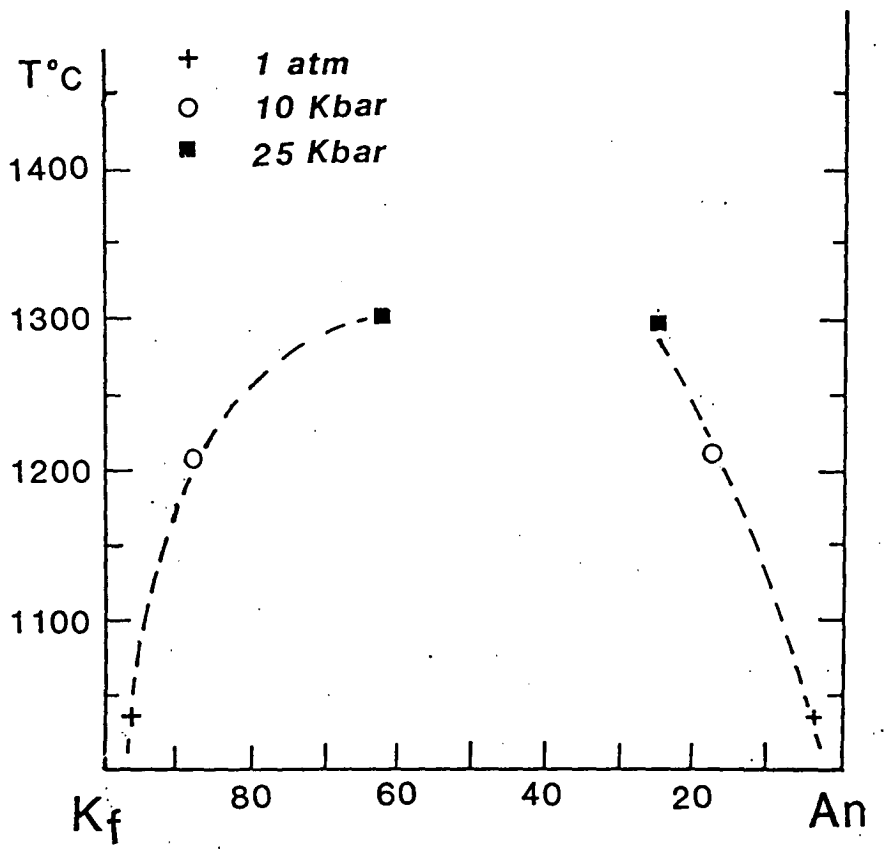

Fig 2.15 a Sketch Showing the Effect of Temperature and Pressure on the Solvus Position in the Binary System Anorthite -- K-feldspar.

believed to have been reached in this study, as discussed earlier on. The problem of accurately determining the compositions of the tiny feldspars produced has not been completely solved.

The increased K-feldspar solubility in anorthite suggests the likelihood that the unusual feldspar intergrowths from Departure Rocks can be exsolution product of previously homogeneous feldspars (K-feldspar-rich plagioclase). This study has demonstrated that as much as 20% K-feldspar can be dissolved by anorthite at 10 Kbar pressure. This matches the bulk compostition of the unusual feldspar intergrowths, when Na_2O content is neglected. Additional experimental studies in part of the ternary feldspar system have confirmed that a high temperature, homogeneous K-feldspar-rich plagioclase can exist at 10 Kbar and that it could well be the parental feldspar of those unusual feldspar intergrowths. These experimental studies are detailed in the next chapter.

(a)

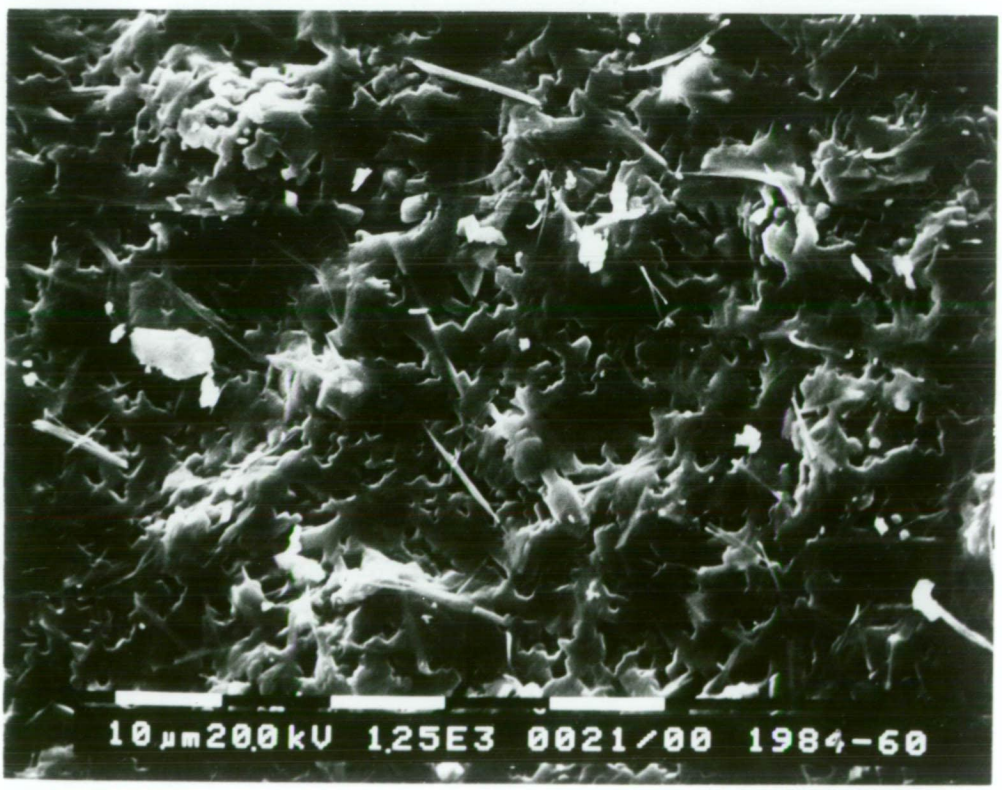

(b)

Plate 2.1 Back Scattered Electron (BSE) Image of Run T-1987 (1150°C, Kf_{60})

a) HF-etched; b) broken surface.

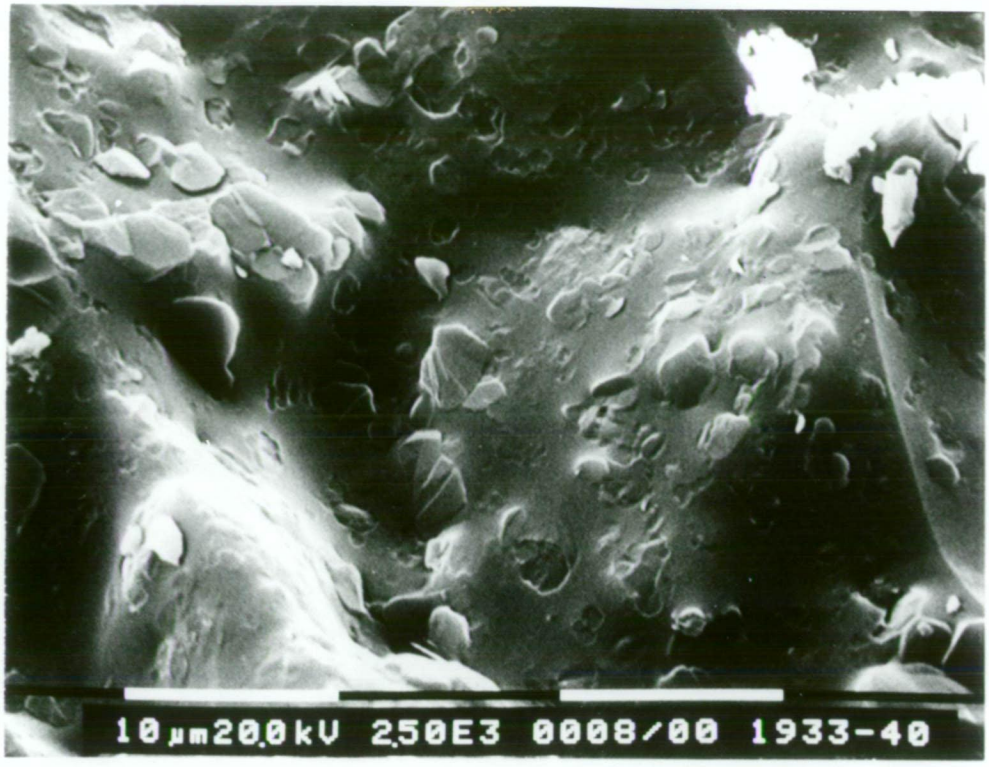

Plate 2.2 BSE Image of Run T-1933 (1200°C, Kf_{40}) Showing Coexisting Crystals and Melt on a Broken Surface (notice voids indicating crystal positions).

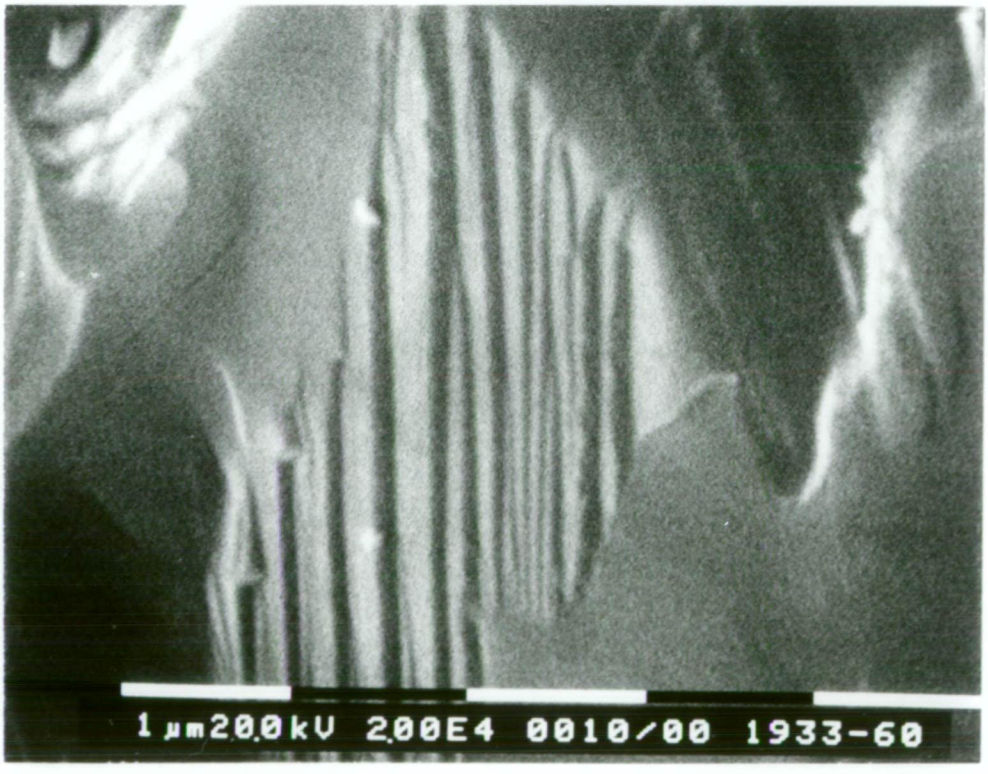

Plate 2.3 BSE Image of Run T-1933 (1200°C, Kf_{60}). Showing Cleavages in a Feldspar Crystal.

Plate 2.4 BSE Image of Run T-2080 (1600°C, Kf_{25}) Showing Conchoidal Fracture of Glass.

Plate 2.5 The Result of an Anorthite-seeded Run (T-1792 1100°C Kf_{10} + 5% An Seeds).

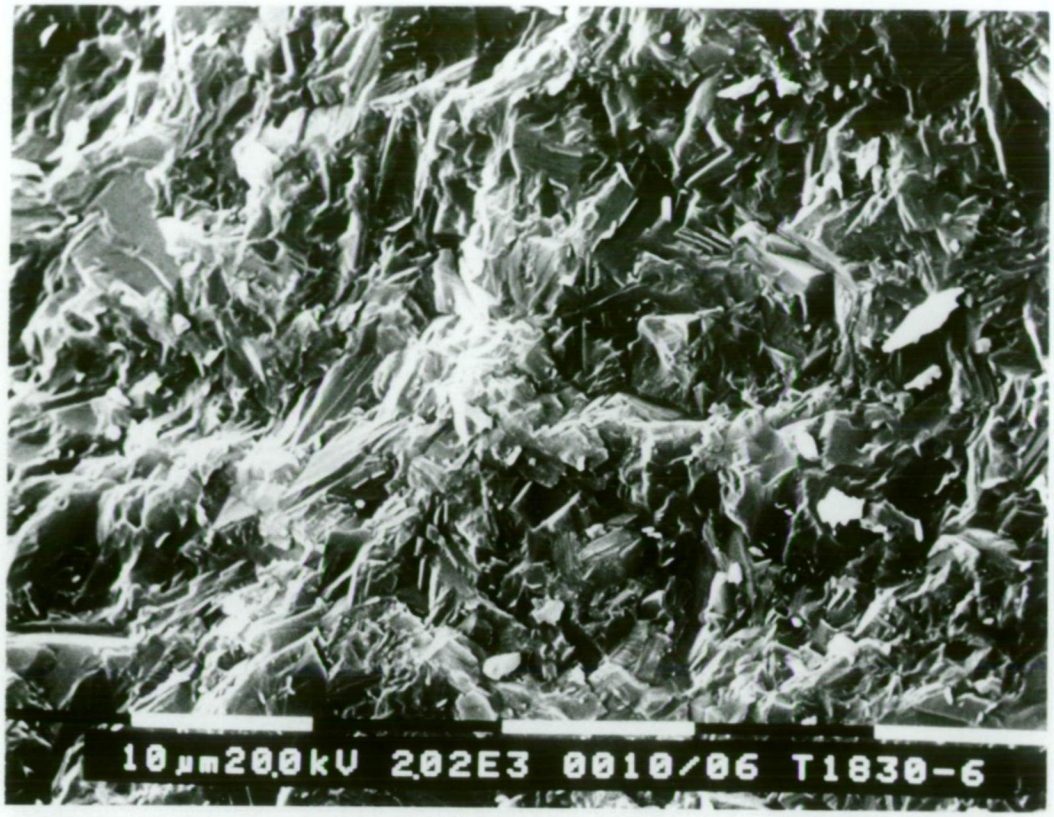

Plate 2.6 The Result of a Silver Oxalate-fluxed Run (T-1830 1100°C Kf_6).

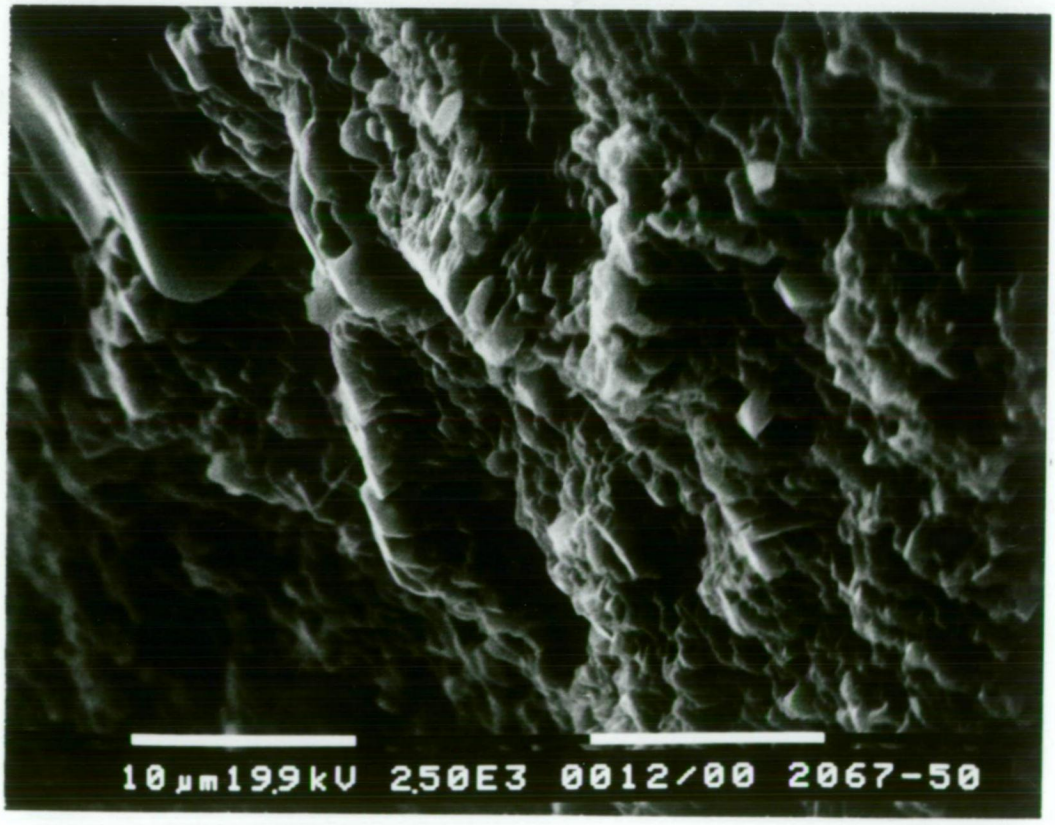

Plate 2.7 The Result of a Carbonate-fluxed Run (T-2067 1000°C Kf_{50} + 2 wt% $CaCO_3$ & K_2CO_3).

Plate 2.8 The Result of a Chlorides-fluxed Run

(T-2035 1100°C Kf_{50} + 5 wt% KCl & $CaCl_2$).

Plate 2.9 The Result of a V_2O_5-fluxed Run

(T-2084 1100°C Kf_{40} + 20 wt% V_2O_5).

CHAPTER THREE

AN EXPERIMENTAL STUDY IN THE TERNARY FELDSPAR SYSTEM, WITH IMPLICATIONS FOR THE ORIGIN OF THE UNUSUAL FELDSPAR INTERGROWTHS FROM DEPARTURE ROCKS, MACROBERTSON LAND

CONTENTS

CHAPTER THREE

AN EXPERIMENTAL STUDY IN THE TERNARY FELDSPAR SYSTEM, WITH IMPLICATIONS FOR THE ORIGIN OF THE UNUSUAL FELDSPAR INTERGROWTHS FROM DEPARTURE ROCKS, MACROBERTSON LAND

3.1 Introduction

Experiments done in the binary system anorthite -- K-feldspar have demonstrated that pure anorthite can dissolve as much as 20 +/- 5 mol% K-feldspar as solid solution at 10 Kbars pressure. The addition of albite to this system (to form the ternary feldspar system) should slightly increase the amount of K-feldspar solid solution in plagioclase formed under the same conditions, since the amounts of albite and K-feldspar dissolved in plagioclase are positively correlated (Fig 1.9). At these conditions plagioclase should be able to dissolve more than 20 +/- 5 mol% K-feldspar. Such a K-feldspar-rich plagioclase solid solution could be a suitable parental feldspar from which the unusual feldspar intergrowths described in the first chapter formed. This homogeneous parental feldspar should have a composition close to $Kf_{21}An_{65}Ab_{14}$, the estimated bulk composition of the intergrowths.

The existence of this parental K-feldspar-rich plagioclase has been tested by two types of experiments. First, the K-feldspar-rich plagioclase was synthesized in the laboratory and the conditions of its formation determined. Those conditions were then used to homogenize the natural feldspar intergrowths in the second series of experiments. The results of

these experimental studies show that the proposed parental feldspar can exist and the unusual feldspar intergrowths may well be an exsolution product.

It is suggested that the limit of ternary feldspar solid solution is pushed further towards the two-feldspar field at high pressures, so that the one-feldspar field is expanded. This permits the existence of many examples of single-phase feldspars outside the limit of solid solution that was previously suggested for the feldspar system at low pressures. The increase in solid solutions in the ternary feldspar system is mainly caused by the increase of melting temperatures of feldspars at high pressures.

3.2 Existence of the Parental Feldspar: Experimental Evidence

3.2.1 Experimental Methods

The methods used in the ternary feldspar system are essentially the same as those used in the binary system anorthite -- K-feldspar, described in chapter two. Platinum capsules and talc/pyrex (dry) sample assemblies were used for all experiments. Pressure was kept constant at 10 Kbar. Run time was set at about 10 days for each experiment and temperatures were in the range 1100°C to 1215°C. The run time chosen was considered long enough for equilibrium to be reached, on the basis of the previous experiments in the anorthite -- K-feldspar system.

Glasses of K-feldspar, albite, and anorthite compositions were mixed in an agate mortar in the required molar proportions. The glass mixes were used as starting material. The albite glass was obtained by heating a mix of Na_2CO_3, Al_2O_3, and SiO_2 at 400°C, 800°C, and 900°C for several hours.

Detailed procedures of glass preparation are given in chapter two. The platinum capsule was usually divided by 2 or 3 platinum discs into two halves, so that two different compositions could be run under identical conditions. This techique is efficient but the amount of sample that can be used is very limited. The high pressure assembly was heated in an oven at 120°C overnight before each experiment to ensure that runs were done in dry conditions.

3.2.2 Experimental Results

Four runs have been performed in the ternary feldspar system at 1100°C, 1150°C, 1200°C, and 1215°C and 10 Kbars. The albite content in all the starting mixes was fixed as 20 mol%; thus the results can be discussed in the albite-constant psudo-binary anorthite -- K-feldspar system. This has the advantage of direct comparison with the binary system anorthite -- K-feldspar.

The run products were checked by the XRD method to confirms that no other minerals except feldspars were present. The presence of plagioclase or/and alkali feldspar can be readily identified from the $(\bar{2}01)$ peak position in the XRD charts. In the run products of starting compositions $Kf_{40}An_{40}Ab_{20}$ and $Kf_{30}An_{50}Ab_{20}$ at 1150°C and 1100°C respectively, two coexisting feldspars were present. However, only plagioclase is shown in the run products of starting composition $Kf_{20}An_{60}Ab_{20}$ at both 1150°C and 1100°C (Fig 3.1). The existence of two feldspars clearly suggests that both runs were in subsolidus conditions. This was further confirmed by SEM observation, which showed no melt present in the run products. The $(\bar{2}01)$ peaks of plagioclase in the run products of starting composition $Kf_{20}An_{60}Ab_{20}$ at 1150°C and 1100°C are identical. This implies that plagioclases syn-

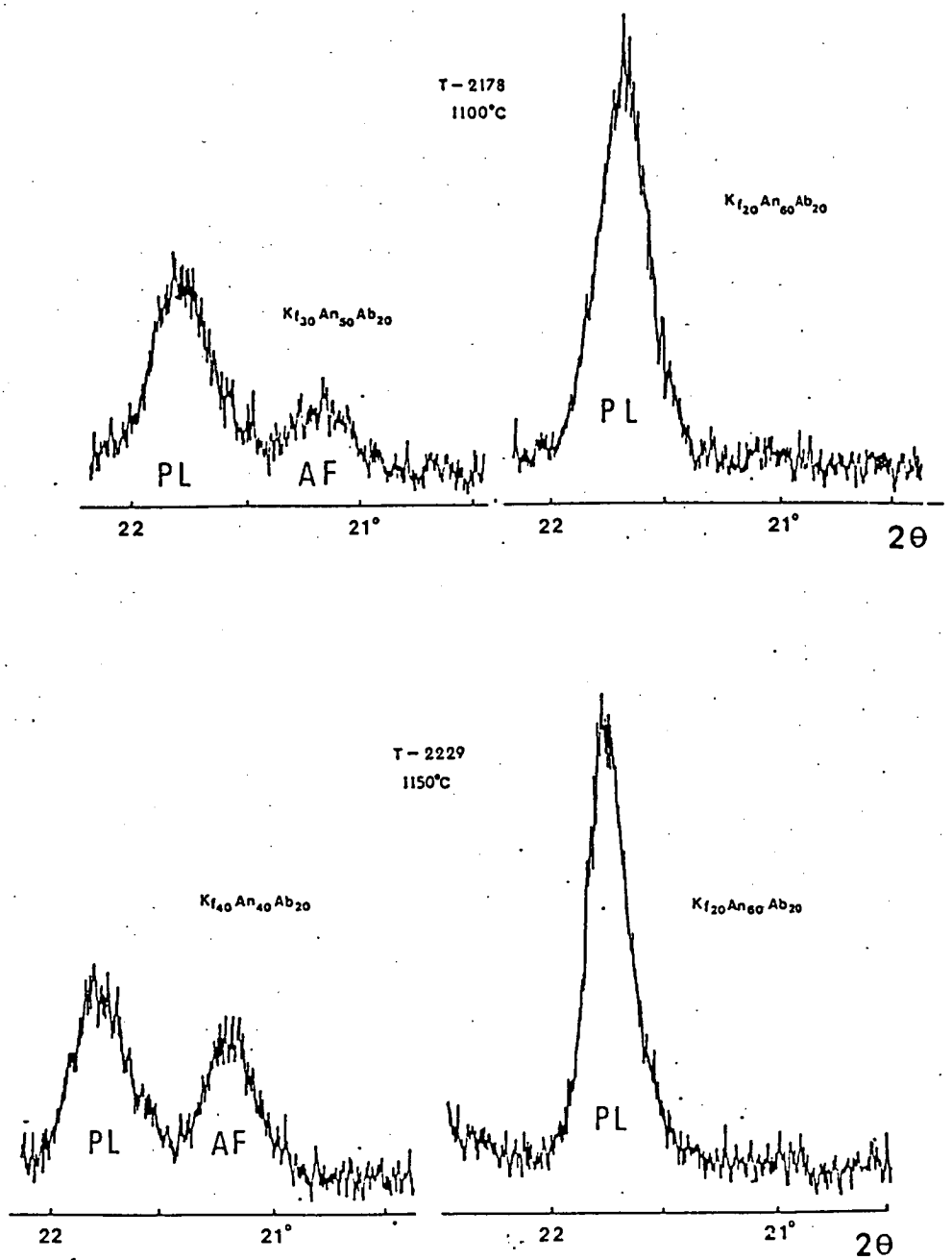

Fig 3.1 ($\bar{2}01$) Peak Positions of Plagioclase (PL) and/or Alkali Feldspar (AF) in Run Products at 1100°C and 1150°C. Notice the Identical Peak Positions of the Two Run Products.

thesized at both temperatures have the same composition. This would not be expected if equilibrium had not been achieved and there were other phases present together with the plagioclase. This also provides evidence to support the attainment of equilibrium during the experiments.

Microprobe analyses of run products indicate that there was less than 3 mol% K-feldspar loss from the original starting mixes (Fig 3.2). This is considered insignificant because it falls within the accuracy limit of 5 mol%. The plagioclases crystallized from the two runs should, therefore, have a composition $Kf_{20}An_{60}Ab_{20}$ (with an accuracy of 5 mol%). This homogeneous plagioclase does not contain the maximum K-feldspar solid solution, though, because it is within the plagioclase-only field. The other two compositions, $Kf_{40}An_{40}Ab_{20}$ at 1150°C and $Kf_{30}An_{50}Ab_{20}$ at 1100°C are in the (plagioclase + alkali feldspar) field. The plagioclases crystallized from these two compositions should have the maximum K-feldspar solid solution. Microprobe analyses of the run products give the probable K-feldspar solid solution in plagioclase of Ab_{20} at 1150°C to be 24 +/- 5 mol% and at 1100°C to be 21 +/- 5 mol% (Fig 3.3). The large uncertainty (5 mol%) is caused by the fine-grained nature of the run products. This problem has already been mentioned in the previous chapter.

The existence of the proposed parental feldspar (plagioclase) found in the unusual feldspar intergrowths from the two basalt dykes has been experimentally confirmed. This single, homogeneous plagioclase can be formed at 1150°C and 10 Kbar under dry conditions. The results of the other two runs at 1200°C and 1215°C are not as relevant, but do support the conclusions drawn above. These two temperatures are just above the solidus. The "eutectic temperature" in the albite-constant (20 mol%) pseudo-binary system

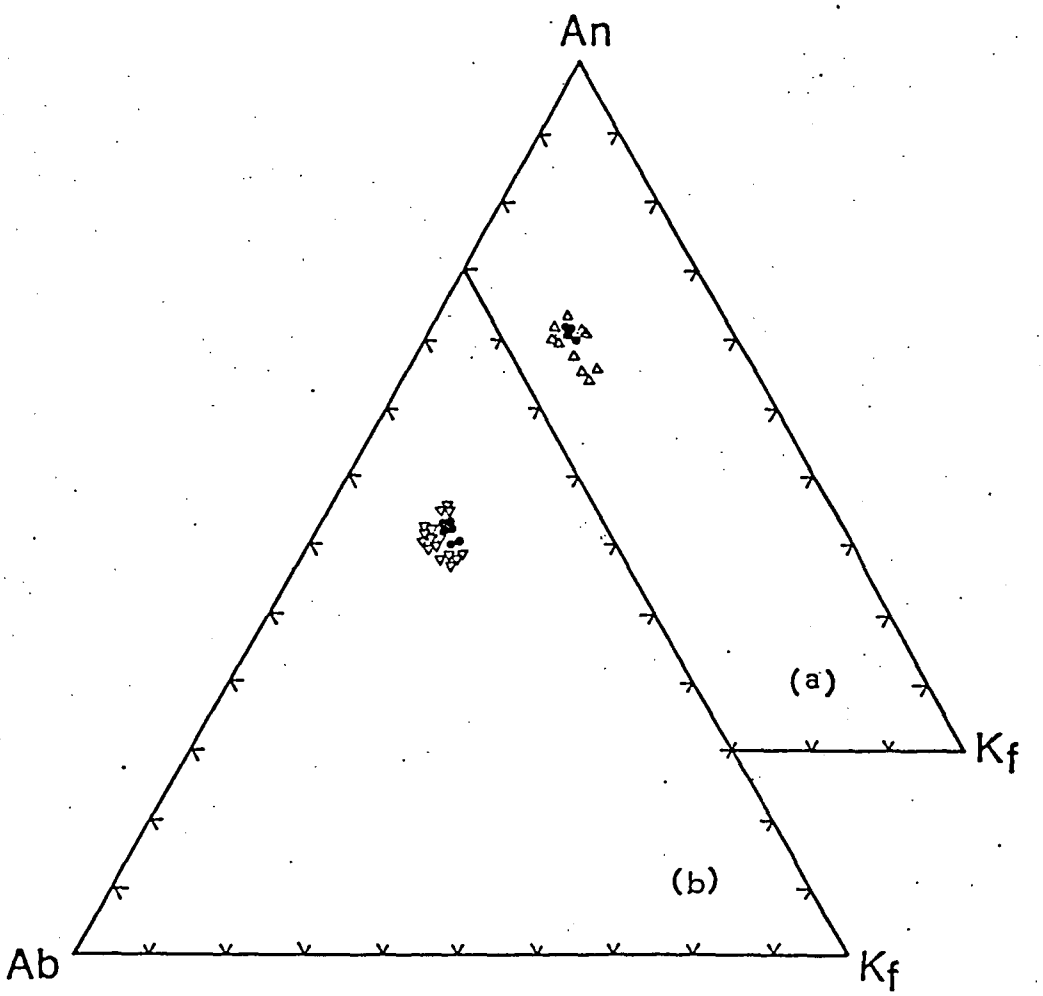

Fig 3.2 Electron Microprobe Analyses of Run Products of Starting Composition $Kf_{20}An_{60}Ab_{20}$ at 1100°C (b) and 1150°C (a).

Solid Dots: defocused-beam area scan analyses;

Open Triangles: spot-mode analyses.

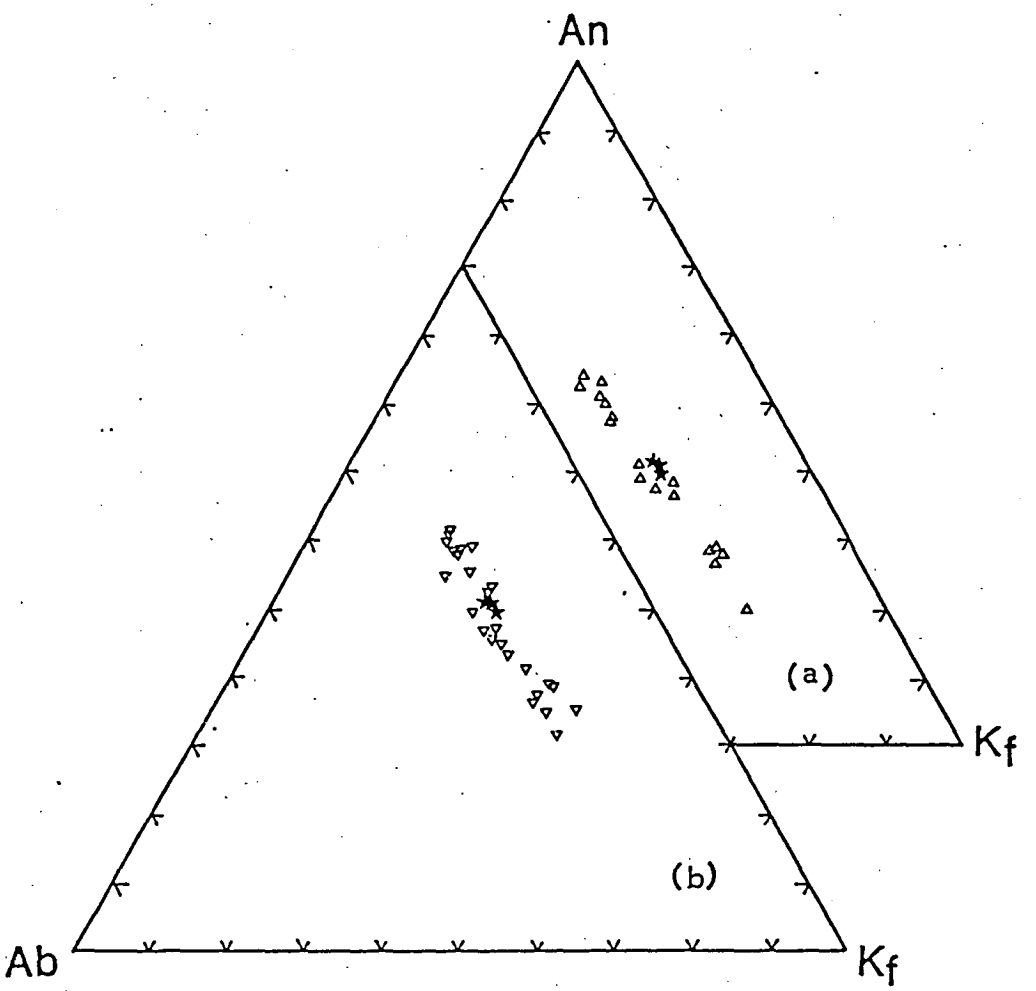

Fig 3.3. Electron Microprobe Analyses of Run Products of
(a) Starting Composition $Kf_{40}An_{40}Ab_{20}$ at 1150°C;
(b) Starting Composition $Kf_{30}An_{50}Ab_{20}$ at 1100°C.
Stars: defocused-beam area scan analyses;
Triangles: spot-mode analyses.

anorthite -- K-feldspar is found at 1180 +/- 15°C (Fig 3.4).

3.3 Homogenization of the Natural Feldspar Intergrowths

3.3.1 Starting Material

Natural feldspar intergrowths from dyke 65786 were chosen as the starting material for the homogenization experiment because they are large and abundant. First, the dyke sample was crushed and ground to millimeter size. The intergrowth feldspars were then hand-picked under a binocular microscope. The chosen feldspar crystals were ground and put though a magnetic separator so that traces of pyroxenes and iron-titanium oxides were separated. The purified feldspar pieces were finally ground into powder. A small amount of the powder was melted on an iridium strip heater and the glass was analyzed by electron microprobe to determine the bulk composition of the intergrowths. These analyses are fairly similar, with an average composition of $Kf_{21.5}An_{64}An_{14.5}$ (Fig 3.5 and Table 3.1). This composition is taken as the bulk composition of the intergrowths and agrees well with the estimated bulk composition $Kf_{21}An_{65}Ab_{14}$ (Chapter One). The rest of the powder was kept as the starting material.

3.3.2 Experimental Conditions

Experimental results in the binary system anorthite -- K-feldspar and in the ternary system albite -- anorthite -- K-feldspar have supported the existence of the high temperature homogeneous plagioclase, from which the unusual feldspar intergrowths may have originated. This homogeneous plagioclase (of composition $Kf_{21.5}An_{64}Ab_{14.5}$) could have formed at around 1150°C and 10 Kbar under dry conditions. If the intergrowths are really the exsolution product of this homogeneous feldspar, then they should become

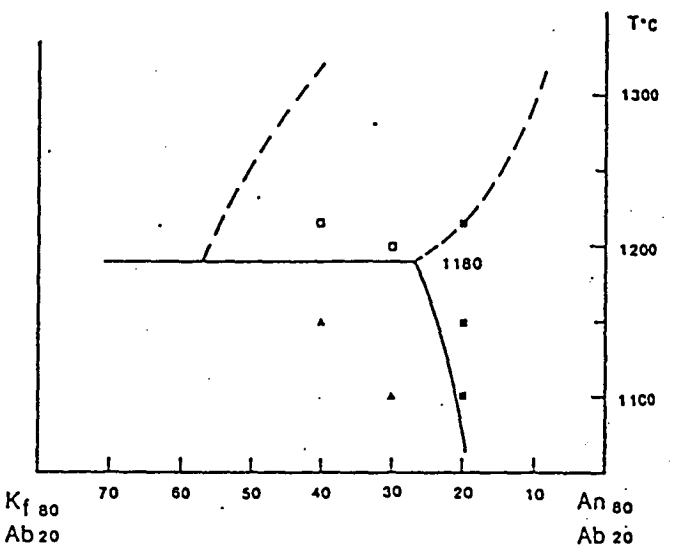

Fig 3.4 Anorthite End of the Albite-constant (20 mol%) Pseduo-binary System Anorthite -- K-feldspar at 10 Kbar.

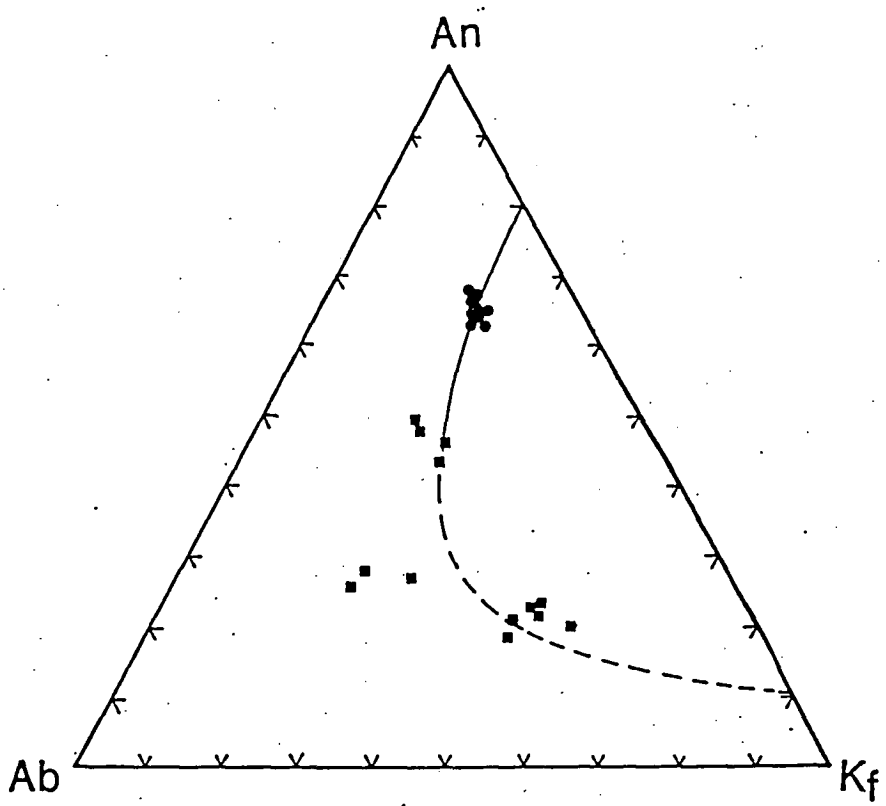

Fig 3.5 Defocused-beam Area Scan Analyses of Glass Melted from the Natural Feldspar Intergrowths from Dyke 65786 (Solid Circles). The proposed limit of ternary feldspar solid solution at 10 Kbar (Curve) and the area scan analyses of mesoperthites in Gt-Opx-bearing granulites from the Napier Complex, Enderby Land (Solid Squares; Harley, 1985, Fig 10) are also shown.

Table 3.1 Defocused-beam Area Scan Analyses of Glass Melted from Feldspar Intergrowths in Dyke 65786

	1		2		3		4	
	wt%	cat*	wt%	cat	wt%	cat	wt%	cat
SiO2	51.30	2.3434	51.88	2.3553	52.48	2.3606	52.74	2.3565
TiO2	0.17	0.0059	0.19	0.0063				
Al2O3	30.53	1.6438	30.47	1.6302	30.72	1.6284	31.10	1.6377
FeO	0.37	0.0140	0.40	0.0152	0.28	0.0106	0.23	0.0087
CaO	13.40	0.6557	13.02	0.6332	13.41	0.6463	13.49	0.6457
Na2O	1.55	0.1370	1.63	0.1434	1.67	0.1458	1.70	0.1469
K2O	3.34	0.1947	3.85	0.2227	3.70	0.2121	3.60	0.2052
Sum	100.66	4.9945	101.43	5.0062	102.26	5.0039	102.85	5.0007
Ca:Na:K	66.4	13.9 19.7	63.4	14.3 22.3	64.4	14.5 21.1	64.7	14.7 20.6
	5		6		7		8	
SiO2	51.35	2.3838	50.64	2.3408	50.94	2.3635	52.49	2.3708
Al2O3	29.38	1.6075	30.36	1.6540	29.86	1.6330	30.55	1.6259
FeO	0.27	0.0106	0.36	0.0138	0.37	0.0144		
CaO	12.63	0.6283	13.06	0.6467	12.55	0.6239	13.23	0.6403
Na2O	1.48	0.1331	1.60	0.1434	1.56	0.1408	1.63	0.1427
K2O	3.91	0.2314	3.57	0.2105	3.88	0.2294	3.75	0.2158
Sum	99.02	4.9946	99.60	5.0091	99.16	5.0050	101.65	4.9955
Ca:Na:K	63.3	13.4 23.3	64.6	14.3 21.0	62.8	14.2 23.1	64.1	14.3 21.6
	9		10		11		12	
SiO2	52.60	2.3751	51.70	2.3472	51.96	2.3618	52.67	2.3704
Al2O3	30.43	1.6193	30.65	1.6399	30.54	1.6360	30.49	1.6172
FeO	0.32	0.0119	0.39	0.0149	0.24	0.0091	0.32	0.0122
CaO	12.82	0.6202	13.48	0.6558	13.33	0.6490	13.42	0.6473
Na2O	1.75	0.1529	1.60	0.1411	1.53	0.1346	1.61	0.1409
K2O	3.90	0.2244	3.61	0.2090	3.35	0.1942	3.61	0.1070
Sum	101.81	5.0038	101.44	5.0078	100.94	4.9846	102.12	4.9949
Ca:Na:K	62.2	15.3 22.5	65.2	14.0 20.8	66.4	13.8 19.9	65.0	14.2 20.8

*) cations per 8 oxgens.

a homogeneous phase at 1150°C and 10 Kbar. Therefore the temperature and pressure conditions for the homogenization experiment are 1150°C and 10 Kbar.

3.3.3 Experimental Results

In the first homogenization exoeriment, the prepared powder was held in a Pt capsule and heated at 1150°C and 10 Kbar for 15 days. The sample was dried in an oven at 120°C before the run commenced. Direct comparison of the XRD pattern of the run product with that of the starting material clearly suggests that the intergrowths were homogenized (Fig 3.6). There are two feldspars (plagioclase and alkali feldspar) present in the starting material [Fig 3.6(a)], but there is only plagioclase present in the run product [Fig 3.6(b)]. All the alkali feldspar is, presumably, dissolved into the plagioclase. It is worth pointing out that the $(\bar{2}01)$ peak of the plagioclase in the run product is almost identical to that of the run T-2229 ($Kf_{20}An_{60}Ab_{20}$) at 1150°C, implying that the two plagioclases have similar composition and that equilibrium was attained in the homogenization experiment.

However, when the run product was analyzed by the EMP analysis method, a series of compositions ranging from $Kf_{5.3}An_{80}Ab_{14.7}$ to $Kf_{48.9}An_{34.1}Ab_{17}$ were found (Fig 3.7 & Table 3.2). It was suspected that a K-rich melt was present and thus this homogenization experiment had failed. However, in the Ab-constant (Ab20 mol%) ternary feldspar system, 1150°C is a subsolidus temperature. Melting should not happen until temperature exceeds 1180°C (Fig 3.1 & 3.4). It is possible that the intergrowths were in the homogenization process during the experiment but the short run time (relative to such process in nature) is not enough for them to achieve complete homogenization. The alkali feldspar lamellae have probably broken down

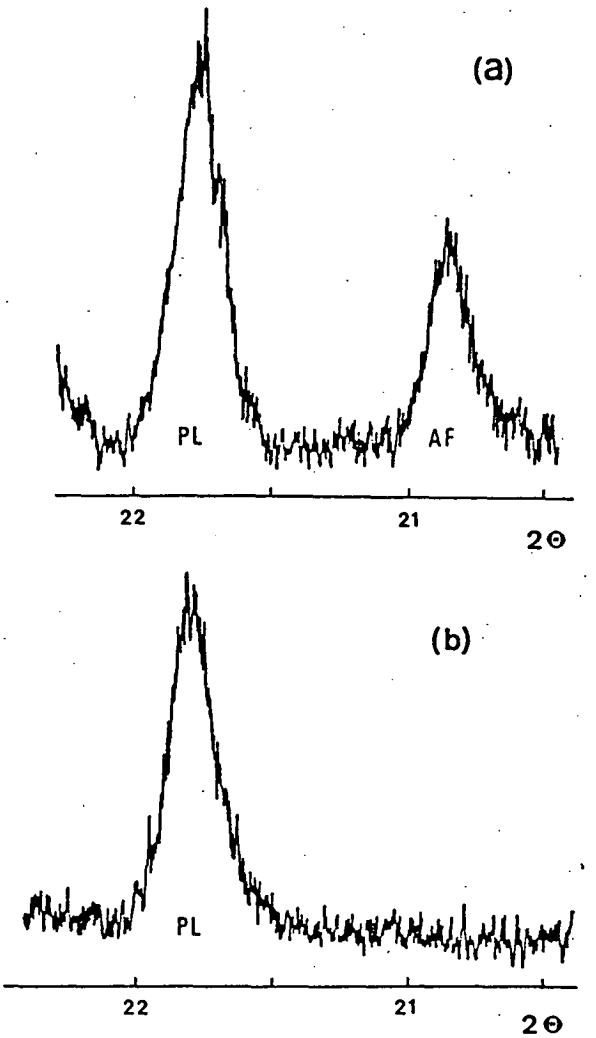

Fig 3.6 Part of the XRD patterns of (a) Starting Material (Natural Feldspar Intergrowths from Dyke 65786) for Homogenization Experiment T-2417; (b) Run Product of Homogenization Experiment T-2417. Note that both plagioclase (PL) and alkali feldspar (AF) are present in (a) but only plagioclase (PL) is present in (b), implying solution of the alkali feldspar into the palgiocalse.

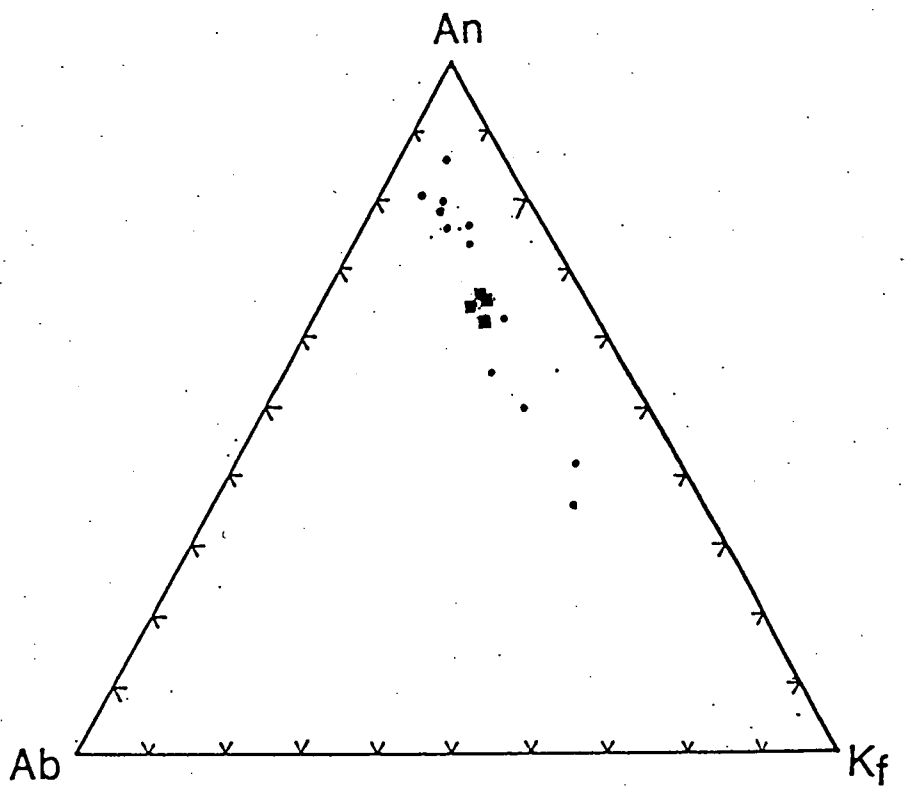

Fig 3.7 EMP Analyses of the Run Product in the Homogenization Experiment T-2417. Squares represent defocused-beam area scan analyses. Dots are spot analyses. Data are from Table 3.2. See text for explanation.

Table 3.2 EMP Analyses of Feldspar in the Homogenization Run T-2417

area scan	1		2		3		4	
	wt%	cat*	wt%	cat	wt%	cat	wt%	cat
SiO2	52.49	2.3672	52.70	2.3831	52.85	2.3790	53.43	2.3919
Al2O3	30.45	1.6183	30.19	1.6089	30.51	1.6185	30.39	1.6034
FeO	0.24	0.0092	0	0	0	0	0	0
CaO	13.43	0.6491	13.31	0.6450	13.34	0.6435	13.20	0.6330
Na2O	1.77	0.1552	1.64	0.1434	1.60	0.1392	1.66	0.1443
K2O	3.55	0.2045	3.60	0.2075	3.52	0.2020	3.71	0.2116
Sum	101.94	5.0034	101.44	4.9879	101.82	4.9823	102.39	4.9843
Ca:Na:K	64.3	15.4 20.3	64.8	14.4 20.8	65.4	14.1 20.5	64.0	14.6 21.4
spot	1		2		3		4	
SiO2	48.39	2.1720	48.24	2.1780	50.05	2.2319	50.46	2.2710
Al2O3	34.47	1.8230	34.38	1.8292	33.59	1.7655	32.60	1.7293
CaO	17.03	0.8188	17.19	0.8317	16.32	0.7798	15.29	0.7373
Na2O	1.73	0.1504	0.96	0.0843	1.45	0.1251	1.70	0.1479
K2O	0.95	0.0547	0.91	0.0524	1.61	0.0914	1.83	0.1053
Sum	102.57	5.0189	101.68	4.9757	103.02	4.9936	101.88	4.9909
Ca:Na:K	80.0	14.7 5.3	85.9	8.7 5.4	78.3	12.6 9.2	74.4	14.9 10.6
	5		6		7		8	
SiO2	50.06	2.2769	50.86	2.2856	53.31	2.4060	54.44	2.4614
Al2O3	32.12	1.7216	32.22	1.7062	29.87	1.5890	28.83	1.5362
CaO	15.00	0.7307	15.24	0.7337	12.77	0.6173	11.52	0.5578
Na2O	1.62	0.1427	1.37	0.1195	1.52	0.1328	1.92	0.1681
K2O	2.13	0.1236	2.65	0.1519	4.20	0.2417	4.55	0.2622
Sum	100.93	4.9954	102.34	4.9969	101.67	4.9867	101.25	4.9856
Ca:Na:K	73.3	14.3 12.4	73.0	11.9 15.1	62.2	13.4 24.4	56.5	17.0 26.5
	9		10		11		12	
SiO2	51.36	2.3124	56.74	2.5593	58.28	2.6656	58.76	2.7129
TiO2	0.19	0.0063	0.20	0.0068	0	0	0.17	0.0058
Al2O3	31.53	1.6728	26.79	1.4240	24.73	1.3332	23.58	1.2828
FeO	0	0	0.26	0.0099	0	0	0	0
CaO	14.63	0.7058	9.59	0.4632	7.74	0.3793	6.56	0.3246
Na2O	1.54	0.1348	1.84	0.1606	1.66	0.1476	1.81	0.1620
K2O	2.79	0.1603	6.21	0.3572	7.40	0.4315	7.91	0.4657
Sum	102.04	4.9924	101.63	4.9808	99.81	4.9573	98.78	4.9537
Ca:Na:K	70.5	13.5 16.0	47.2	16.4 36.4	39.6	15.4 45.0	34.1	17.0 48.9

*) cations per 8 oxgens.

in structure (as revealed by the XRD pattern) but the new, homogeneous K-rich plagioclase has not yet been completely formed. Therefore, a compositional range would be expected.

3.4 Origin of the Unusual Feldspar Intergrowths

Chapter one presented strong evidence for an exsolution origin of the unusual feldspar intergrowths, based on petrographic observation and electron microprobe analysis. It is suggested that they were exsolved from a homogeneous plagioclase of $Kf_{21}An_{65}Ab_{14}$. This homogeneous parental feldspar has been synthesized at 1150°C and 10 Kbar under dry conditions. The natural feldspar intergrowths were also homogenized under the same conditions to form one homogeneous feldspar, which not only confirms the existence of the homogeneous parental feldspar but also indicates the attainment of equilibrium during these experiments. There is now little doubt about the exsolution origin of the unusual feldspar intergrowths found in the basalt dykes from Antarctica.

There is much work left to be done in order to find out exactly how the homogeneous K-feldspar-rich plagioclase exsolved to form the complex intergrowths observed in the dykes. Transmission electron microscope study should yield a lot of useful information towards solution of this problem. For the time being a general outline is given below to describe (or speculate on) the evolutionary history of these intergrowths.

At the end of the Proterozoic, East Antarctica was in a tectonically active zone, perhaps similar to the situation of the Himalayas in a doubly--thickened crust environment (Kuehner, 1986; Ellis, 1987). Mawson charnockite in MacRobertson Land was forming, probably by essentially anhydrous,

deep crustal melting with very high temperatures due to underplating by mantle diapirism, leading to basaltic magma emplacement in the base of the crust. At high pressures and temperatures, and dry conditions near the base of the Proterozoic crust, the K-rich plagioclases crystallized directly from a (K-rich?) basaltic magma. A regional upper greenschist- to amphibolite-facies metamorphism took place after emplacement of the dykes and caused the exsolution of K-rich alkali feldspar from the original homogeneous Kf-rich plagioclase. These K-rich alkali feldspar exsolution lamellae are the regular lamellae decribed in the first chapter. They were exsolved in three directions, probably parallel to the minimum interfacial energy orientation, through (coherent) spinodal decomposition. The regular lamellae were coarsened during the long cooling history of the stable east Antarctic continent, resulting in the development of the more complex lamellae. There are basically two ways of thickening the K-rich alkali feldspar lamellae. One is the gradual addition of K-feldspar component to some lamellae from the surrounding host and neighbouring lamellae. This causes the formation of some thick lamellae standing in the thinner lamellae. The other way that coarsening may occur is in the junction where two regular lamellae cross cut each other and are cut by a cleavage. This happens because the junction has the minimum strain energy and therefore is the preferred place for lamellae growth. This mechanism produces the other type of irregular lamellae, which is much thicker and shorter. These coarsening processes are very slow, since they are solid-state diffusional processes. Thus all the different types of lamellae can still be observed.

3.5 Further studies

Although the presence of the parental plagioclase has been experimentally proven, the detailed processes that produced the observed intergrowths are not entirely clear. TEM study of the natural feldspar intergrowths and the synthetic feldspars should be very helpful in this respect. The TEM method has already been used to reveal details of the complicated exsolution and coarsening processes in cryptoperthite (e.g. Brown & Parsons, 1984). Besides, it may be very useful for investigation of kinetic problems during crystal growth and subsolidus mineral reations. For example, the problem of reaction depth and kinetics in the ternary feldspar system has been tackled by Johannes (1979), using scanning electron microscope and electron probe microanalysis techniques. His interesting conclusions can be improved by using TEM techniques.

The experimental results of this study have demonstrated that ternary feldspar solid solution is substantially increased at high pressures. At 10 Kbar, the limit of ternary feldspar solid solution appears similar to that shown in Fig 3.5, although more experiments are needed to confirm the exact position of this curve. The significance of this curve is that it allows the existence of some homogeneous feldspars that have very extensive ternary feldspar compositions, outside the limit of the ternary feldspar solid solution suggested for low pressure feldspars (e.g. those in Fig 1.9). For example, Harley (1985) found a group of feldspar intergrowths in garnet - orthopyroxene-bearing granulites from the Napier Complex of Enderby Land with bulk compositions (suggested by defocused-beam area scan analyses) in the two-feldspar field, well beyond the limit of ternary feldspar solid solution at low pressures. However, they lie very close to the limit sug-

gested for the ternary feldspar system at 10 Kbar (Fig 3.5). An exsolution origin for these intergrowths was predicted. Experimental results in the ternary feldspar system at high pressures should be very useful in clearifying details of mixing/unmixing processes in this system. The feldspar thermometer can be improved on such a basis. Further experimental work in the ternary feldspar system at high pressures should, therefore, be very rewarding. However, microprobe analysis of experimental results is still a very critical problem because of the small size of synthetic feldspar crystals.

CHAPTER FOUR

CRYSTALLIZATION OF PLAGIOCLASES FROM BASALTIC MAGMAS: ORIGIN OF THE PROPOSED PARENTAL PLAGIOCLASE

CONTENTS

CHAPTER FOUR

CRYSTALLIZATION OF PLAGIOCLASES FROM BASALTIC MAGMAS: ORIGIN OF THE PROPOSED PARENTAL PLAGIOCLASE

4.1 Introduction

The existence of the proposed parental plagioclase for the unusual feldspar intergrowths has been proven by the three sets of experiments in simple (feldspar) systems discussed in previous chapters. It is concluded that this K-rich plagioclase can be formed at 1150°C and 10 kbar. In this chapter, discussion is focused on the plagioclase crystallization from basaltic magmas and the generation of the K-rich plagioclase in complex (rock) systems.

Petrographic observation suggests phenocryst origin of the unusual feldspar intergrowths in dykes 65786 & 65787. Considering the fact that the intergrowths are the only phase which contains potassium in the two dykes and that the K-partition coefficient between melt and plagioclase is very large, it is most unlikely that the K-rich plagioclase crystallized directly from the K-poor dyke magma (K_2O = 0.80 wt% and 0.56 wt% in dykes 65786 & 65787 respectively).

From the K partition relation between melt and plagioclase, it is reasonable to suggest that K-rich plagioclase can only crystallize from a K-rich magma. The host charnockite is a possible candidate that might generate the K-rich plagioclase. But the low Ba contents in the K-rich alkali feldspars in the charnockite and the high Ba contents in the K-rich lamellae of the unusual feldspar intergrowths in the dyke strongly argue

against the possibility of the intergrowths being xenocrystal or modified xenocrystal alkali feldspar from the host charnockite (Chapter one, Table 1.3). It is thus possible that the K-rich plagioclase is not formed out of either the original dyke magma or the charnockitic magma, but is formed in a local contamination environment resulting from interaction of the two magmas.

To initiate the investigation of the generation of the K-rich plagioclase, a composition similar to that of dyke 65786 was tried. There were two purposes in doing this preliminary experiment. One was to see whether liquidus plagioclase can be formed at all. The other was to find out how much K is in the liquidus plagioclase and to estimate the K partition relation between the bulk rock composition and the plagioclase crystallized from that composition. This relation was then used to roughly predict the amount of K in the bulk rock necessary to generate the required K-rich plagioclase.

4.2 Experimental Details

4.2.1 Starting Material

The starting material for this set of experiments was sintered oxide mix plus synthetic fayalite. A mixture of oxides (for Ti, Al, Fe^{3+}, Mn, Mg, and part of Si), carbonates (for Ba, K, Na, and part of Ca), and $Ca_2P_2O_7$ was sintered at 950°C prior to addition of synthetic fayalite. The sintered mix and fayalite were then ground under acetone and the whole mix was heated at 450°C for 1 hour in an argon atmorsphere to release acetone from the starting mix. The low temperature and short heating time ensured the stable existence of Fe_2O_3. The added fayalite was synthesized at 1000°C for 4 days

Table 4.1 EMP Area Scan Analyses of the Run Products

	65786 (XRF)	T-2432 (5)*	(3)	T-2459 (5)	T-2487 (11)
SiO2	52.27	52.85	53.16	52.65	56.38
TiO2	2.10	2.08	2.15	2.17	1.55
Al2O3	15.97	16.31	16.67	16.42	16.36
FeO**	11.47	10.82	12.50	11.00	7.67
MnO	0.29	0.30	0.24	0.38	0.23
MgO	4.98	5.17	4.40	4.81	3.36
CaO	9.45	9.80	9.71	9.91	7.44
BaO	0.07	NA	NA	NA	NA
Na2O	0.68	0.62	0.80	0.88	0.76
K2O	0.80	1.30	1.54	1.42	5.91
P2O5	0.36	0.47	0.44	0.42	0.29
Sum	98.44	99.72	101.61	100.06	99.95
Mg#	47.7	46.0	38.6	43.8	43.9
Ca(a	39.90	38.52	37.95	39.34	41.10
Mg	28.89	28.28	23.92	26.57	25.83
Fe	31.71	33.20	38.13	34.09	33.07
Ca(b	81.27	78.59	74.74	75.11	46.93
Na	10.57	9.00	11.14	12.07	8.68
K	8.16	12.41	14.11	12.82	44.39
Run(c T(°C)			1150	1150	1140
Condition Time(hour)			6	5	5
Run(d Results			Px+Pl+ Mt+M	Px+Pl+ Qz+Mt+M	Cpx+Pl+Af+ Sp+Qz+M

*). Composition of the glass melted from the sintered oxide mix that was used as the starting material for run T-2432; Numbers in the brackets are the number of analyses averaged to obtain the given results.
**). Total iron as FeO;
(a). Atomic ratioes among Ca, Mg, Fe;
(b). Atomic ratioes among Ca, Na, K;
(c). All runs were carried out at 10 kbar pressure;
(d). Mineral abbreviations: Px--Ca-poor pyroxene, Cpx--clinopyroxene, Pl--plagioclase, Mt--magnetite, Af--alkali-feldspar, Sp--spinel, Qz--quartz, M--melt.

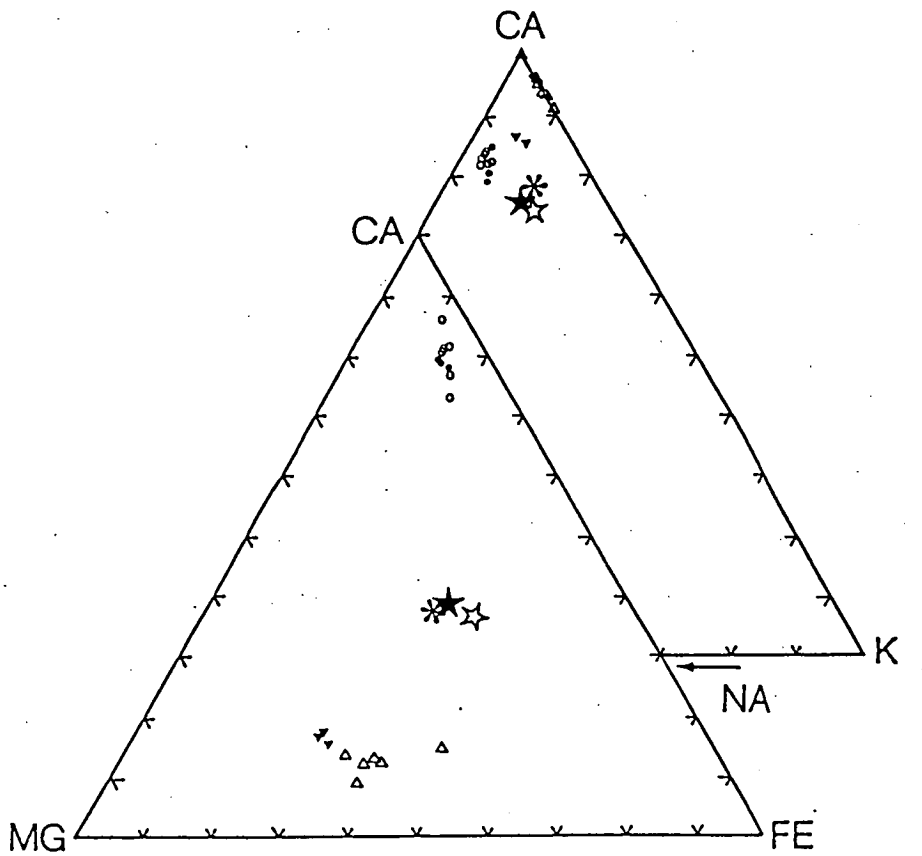

Fig 4.1 Ca-Na-K and Ca-Mg-Fe Diagrams (in atomic ratio) for Evaluation of the EMP Analyses of Pyroxene (triangles) and Plagioclase (circles) in T-2432 (empty symbols) & T-2459 (solid symbols). Stars are the average EMP area scan analyses of the two charges. Asterisk represents the glass melted from the starting material for the two runs.

by heating quartz plus magnetite in an evacuated silica tube.

All the compositions are given in Table 4.1 with the numbers T-2432, T-2459, and T-2487 being the run numbers of the three experiments on the two compositions prepared. For the direct comparison, the natural rock analysis of dyke 65786 (XRF analysis by Dr. Kuehner, Fe_2O_3 is converted to FeO) is given in the first column. Numbers in brackets following the run numbers are the number of analyses made to obtain the compositions shown. All of them are area scan analyses of the run products except the left column under T-2432 (the second column in the table), which is the average area scan analysis of the glass melted from the starting material for runs T-2432 & T-2459. Approximately 0.06 wt% BaO was added in the starting mixes but was not analyzed.

The starting compositions for runs T-2432 and T-2459 are identical. The composition difference shown in Table 4.1 is mainly caused by the difference in capsule type. A Fe capsule was used for T-2432 and a Pt capsule, for T-2459. Fe loss from the starting mix into the Pt capsule is a severe problem in doing high-P experiments reported by many experimentalists (Kuehner, 1987; and references therein). It is believed that Fe capsule can reduce the problem although no systematic study has yet been undertaken. Obvious Fe addition in run T-2432 caused considerable composition shift (especially Fe, Mg ratios; Table 4.1 and Fig 4.1). A Pt capsule was thus used for the next run (T-2459). In this experiment Fe loss is not a problem. The bulk compositions of the run product (under T-2459 in Table 4.1) and of the glass melted from the starting mix (left column under T-2432 in Table 4.1) are in fact very similar. Therefore, Pt capsule is a better capsule type and was used for the next run (T-2487).

The starting composition of run T-2487 is a mixture of the starting mix for T-2432 & T-2459 (73%) and sintered $K_2O \cdot Al_2O_3 \cdot 6SiO_2$ oxides (27%). The whole mix was prepared by grinding the mixture in an agate mortar for 1 hour without water or acetone. The mix was then kept in an oven at 120°C for 4 hours. Thus thorough dryness of the starting material was confidently ensured.

4.2.2 Experimental Conditions

All runs were carried out in a solid-media piston-cylinder apparatus hosted in Geology Department (University of Tasmania). Pressures were fixed at 10 kbar for all runs. Temperatures were checked with a Pt/Pt(90%)Rh(10%) thermocouple and kept within an accuracy of +/- 10°C. The first two runs were done at 1150°C and the third (T-2487), at 1140°C. Run durations were 5 - 6 hours (Table 4.1).

4.3 Experimental Results

4.3.1 Mineralogy

Phases present in the run products can be identified under optical microscope with the exception of distinction between feldspars and between feldspars and quartz (Table 4.1). Ca-poor pyroxene, plagioclase, and magnetite are the major crystalline phases in the first two runs (T-2432 & T-2459). Clinopyroxene, spinel, plagioclase, and alkali feldspar are the dominant phases in T-2487. All runs have relatively low degree of crystallization (< 20% for the first two runs, ca 25% for T-2487), indicating P, T conditions close to the liquidi. Quartz was found in T-2459 and T-2487, but not in T-2432, probably implying the difference in oxygen fugacity between runs in Pt capsules (T-2459 & T-2487) and the run in a Fe capsule

Table 4.2 EMP Analyses of Ca-poor Pyroxenes in T-2432 & T-2459

Pyroxenes in T-2432 (Fe capsule):									
analy No	(1)			(2)			(3)		
	wt%	cat*	wt%	wt%	cat	wt%	wt%	cat	wt%
SiO2	53.07	1.9322	51.96	53.47	1.9414	52.31	52.86	1.9097	51.39
TiO2	0.97	0.0265	0.95	1.04	0.0283	1.01	1.19	0.0323	1.16
Al2O3	4.39	0.1882	4.29	5.56	0.0283	5.43	7.31	0.3113	7.11
FeO	18.96	0.5773	18.56	19.69	0.5980	19.26	19.93	0.6022	19.38
MnO	0.55	0.0169	0.54	0.38	0.0118	0.38	0.46	0.0141	0.45
MgO	17.43	0.9460	17.07	15.87	0.8589	15.53	14.75	0.7944	14.34
CaO	6.51	0.2541	6.38	5.82	0.2263	5.69	5.86	0.2268	5.70
K2O	0.25	0.0117	0.25	0.40	0.0184	0.39	0.50	0.0230	0.49
Sum	102.13	3.9530	100	102.23	3.9207	100	102.86	3.9138	100
Ca:Mg:Fe	14.3	53.2	32.5	13.4	51.0	35.5	14.0	48.9	37.1
Ca:Na:K	95.6	0	4.4	92.5	0	7.5	90.8	0	9.2

	(4)			(5)		
SiO2	51.32	1.9312	51.14	51.17	1.8487	50.45
TiO2	0.65	0.0184	0.65	1.29	0.0350	1.27
Al2O3	2.49	0.1104	2.48	5.86	0.2495	5.78
FeO	22.59	0.7108	22.51	21.15	0.6547	20.86
MnO	0.54	0.0172	0.54	0.56	0.0171	0.55
MgO	18.35	1.0294	18.29	15.07	0.8116	14.86
CaO	4.41	0.1777	4.39	5.92	0.2291	5.84
K2O	0	0	0	0.39	0.0179	0.39
Sum	100.35	3.9951	100	101.42	3.9484	100
Ca:Mg:Fe	9.3	53.7	37.1	13.6	48.3	38.0
Ca:Na:K	100.0	0	0	92.8	0	7.2

Pyroxenes in T-2459 (Pt capsule):									
	(1)			(2)			(3)		
SiO2	52.70	1.9124	52.03	54.78	1.9270	52.73	55.36	1.9160	52.89
TiO2	0.76	0.0208	0.75	1.14	0.0302	1.10	0.92	0.0240	0.88
Al2O3	5.75	0.2459	5.68	6.93	0.2874	6.67	8.93	0.3641	8.53
FeO	15.61	0.4738	15.42	15.99	0.4704	15.39	14.68	0.4250	14.03
MnO	0.66	0.0203	0.65	0.53	0.0159	0.51	0.50	0.0145	0.47
MgO	17.83	0.9644	17.60	17.17	0.9003	16.53	16.66	0.8595	15.92
CaO	7.74	0.3010	7.64	6.54	0.2467	6.30	6.84	0.2538	6.54
K2O	0.23	0.0104	0.22	0.52	0.0234	0.50	0.45	0.0200	0.43
Na2O	0	0	0	0.28	0.0191	0.27	0.33	0.0220	0.31
Sum	101.29	3.9491	100	103.89	3.9203	100	104.67	3.8989	100
Ca:Mg:Fe	17.3	55.4	27.2	15.3	55.7	29.1	16.5	55.9	27.6
Ca:Na:K	96.7	0	3.3	85.3	6.6	8.1	85.8	7.4	6.8

*). cations per 6 oxygens.

Table 4.3 EMP Analyses of Plagioclases in T-2432 & T-2459

Plagioclases in T-2432 (Fe capsule):									
analy No	(1)			(2)			(3)		
	wt%	cat*	wt%	wt%	cat	wt%	wt%	cat	wt%
SiO2	49.07	2.2306	48.12	49.93	2.3175	49.95	49.49	2.2299	47.97
TiO2	0.44	0.0149	0.43	0.57	0.0200	0.57	0.49	0.0167	0.48
Al2O3	31.27	1.6754	30.67	28.12	1.5384	28.14	31.18	1.6556	30.22
FeO	2.48	0.0943	2.43	3.31	0.1284	3.31	3.46	0.1304	3.35
MgO	0.49	0.0332	0.48	0.73	0.0507	0.73	0.82	0.0551	0.80
CaO	16.12	0.7849	15.80	15.23	0.7573	15.23	15.67	0.7562	15.18
K2O	0.62	0.0360	0.61	0.77	0.0458	0.77	0.59	0.0339	0.57
Na2O	1.48	0.1308	1.46	1.29	0.1157	1.29	1.48	0.1294	1.44
Sum	101.96	5.0002	100	99.95	4.9739	100	103.18	5.0072	100
Ca:Mg:Fe	86.5	3.6	10.3	80.9	5.4	13.7	80.3	5.9	13.8
Ca:Na:K	82.5	13.7	3.8	82.4	12.6	5.0	82.2	14.1	3.7
	(4)			(5)			(6)		
SiO2	50.01	2.2810	48.83	48.05	2.2000	47.03	49.03	2.2301	47.92
TiO2	0.85	0.0291	0.83	0.64	0.0220	0.63	0.57	0.0194	0.55
Al2O3	28.72	1.5438	28.04	30.67	1.6551	30.02	30.79	1.6506	30.10
FeO	4.58	0.1747	4.47	4.38	0.1677	4.29	3.55	0.1349	3.47
MgO	1.06	0.0717	1.03	0.98	0.0671	0.96	0.63	0.0428	0.62
CaO	14.99	0.7327	14.64	15.58	0.7641	15.25	15.85	0.7727	15.50
K2O	0.84	0.0489	0.82	0.55	0.0321	0.54	0.58	0.0337	0.57
Na2O	1.37	0.1209	1.33	1.32	0.1168	1.29	1.31	0.1154	1.28
Sum	102.41	5.0028	100	102.17	5.0248	100	102.30	4.9996	100
Ca:Mg:Fe	74.8	7.3	17.8	76.5	6.7	16.8	81.3	4.5	14.2
Ca:Na:K	81.2	13.4	5.4	83.7	12.8	3.5	83.8	12.5	3.7
Plagioclases in T-2459 (Pt capsule):									
analy No	(1)			(2)			(3)		
	wt%	cat*	wt%	wt%	cat	wt%	wt%	cat	wt%
SiO2	49.95	2.3305	50.20	49.95	2.3044	49.54	48.93	2.2539	48.23
TiO2	0.67	0.0235	0.67	0.63	0.0218	0.62	0.68	0.0235	0.67
Al2O3	27.72	1.5243	27.86	28.63	1.5567	28.39	29.24	1.5874	28.82
FeO	3.31	0.1291	3.33	3.41	0.1315	3.38	4.03	0.1552	3.97
MgO	0.82	0.0570	0.82	0.88	0.0605	0.87	0.95	0.0652	0.94
CaO	14.79	0.7393	14.86	14.88	0.7355	14.76	15.82	0.7807	15.59
K2O	0.86	0.0777	0.86	0.83	0.0742	0.82	0.62	0.0553	0.61
Na2O	1.38	0.0821	1.39	1.62	0.0953	1.61	1.19	0.0699	1.17
Sum	99.50	4.9638	100	100.83	4.9802	100	101.46	4.9915	100
Ca:Mg:Fe	79.9	6.2	13.9	79.3	6.5	14.2	78.0	6.5	15.5
Ca:Na:K	80.7	13.7	5.6	79.1	15.6	5.3	84.6	11.5	3.9

*). cations per 8 oxygens.

(T-2432). The compositions of pyroxene and plagioclase in T-2432 & T-2459 are similar (Table 4.2 & 4.3; Fig 4.1) because the two runs have identical starting compositions. There is a small difference in pyroxene composition between the two runs. Pyroxene analyses in T-2432 are generally richer in Fe than in T-2459, which can be readily explained by addition of Fe from the Fe capsule into the starting mix, as shown by the marked decrease in Mg# compared with the glass melted from the starting material for both runs (Table 4.1).

It was thought that addition of alkalies (K in this case) into the starting composition for the first two runs should lower the liquidus. Thus the run temperature for T-2487 was decreased into 1140°C. The 10°C temperature difference between the first two runs and T-2487 should not make much difference in the run product, as later confirmed by the experiment (T-2487). The crystallization of alkali feldspar and spinel in T-2487 is considered to be a result of the very different bulk composition, which also caused the difference in compositions of pyroxene and plagioclase between the first two runs and T-2487.

The compositions of clinopyroxene, spinel, plagioclase, and alkali feldspar are shown in Table 4.4, 4.5 & 4.6 respectively. Because most of the crystalline phases are very small, the given EMP analyses may not be the exact composition of the phases present in the run product. Ca-Na-K and Ca-Mg-Fe diagrams (in atomic ratio) are constructed in order to evaluate these analyses (Fig 4.1 & 4.2). Mafic minerals should contain minimum alkalies and feldspars should contain minimum mafic components. In fact, spinel should not contain any K, Na or Ca. The given analyses do, however, show the presence of small amount of K & Ca in the spinel

Table 4.4 EMP Analyses of Clinopyroxene in T-2487

analy No	(1)			(2)			(3)		
	wt%	cat*	wt%	wt%	cat	wt%	wt%	cat	wt%
SiO2	50.02	1.8578	50.16	52.95	1.9129	51.97	52.61	1.9084	51.86
TiO2	1.48	0.0414	1.49	1.60	0.0435	1.57	1.33	0.0362	1.31
Al2O3	8.95	0.3919	8.98	9.69	0.4127	9.51	9.94	0.3992	9.21
FeO	9.10	0.2827	9.13	10.07	0.3041	9.88	9.71	0.2945	9.57
MnO	0.39	0.0121	0.39	0.35	0.0107	0.34	0.35	0.0109	0.35
MgO	10.53	0.5832	10.56	9.37	0.5044	9.19	9.98	0.5398	9.84
CaO	17.21	0.6829	17.21	14.82	0.5738	14.55	15.53	0.6035	15.31
K2O	1.83	0.0865	1.83	2.61	0.1202	2.56	2.31	0.1070	2.28
Na2O	0.26	0.0190	0.26	0.43	0.0300	0.42	0.28	0.0194	0.27
Sum	99.73	3.9575	100	101.88	3.9123	100	101.43	3.9189	100
Ca:Mg:Fe	44.1	37.7	18.3	41.5	36.5	22.0	42.0	37.5	20.5
Ca:Na:K	86.6	2.4	11.0	79.3	4.1	16.6	82.7	2.7	14.7

	(4)			(5)			(6)		
SiO2	52.49	1.9282	52.53	51.07	1.8325	49.17	53.31	1.9312	52.67
TiO2	1.54	0.0425	1.54	1.36	0.0367	1.31	1.26	0.0345	1.25
Al2O3	9.98	0.4321	9.99	7.92	0.3350	7.63	8.83	0.3771	8.73
FeO	9.81	0.3012	9.81	10.78	0.3234	10.38	10.11	0.3063	9.99
MnO	0.25	0.0077	0.25	0.45	0.0138	0.44	0	0	0
MgO	8.45	0.4624	8.45	12.93	0.6914	12.45	10.42	0.5624	10.29
CaO	14.27	0.5617	14.28	18.25	0.7016	17.57	14.75	0.5726	14.58
K2O	2.81	0.1319	2.82	0.83	0.0379	0.80	2.26	0.1043	2.23
Na2O	0.32	0.0230	0.32	0.28	0.0198	0.27	0.27	0.0192	0.27
Sum	99.92	3.8907	100	103.87	3.9920	100	101.21	3.9075	100
Ca:Mg:Fe	42.4	34.9	22.7	40.9	40.3	18.8	39.7	39.0	21.3
Ca:Na:K	78.4	3.2	18.4	92.4	2.6	5.0	82.3	2.8	15.0

	(7)			(8)			(9)		
SiO2	51.27	1.8968	51.20	51.21	1.9150	52.04	50.35	1.8829	50.64
TiO2	1.24	0.0345	1.24	1.04	0.0294	1.06	1.13	0.0316	1.13
Al2O3	7.41	0.3229	7.40	7.98	0.3518	8.11	6.02	0.2653	6.05
FeO	10.72	0.3318	10.71	9.38	0.2933	9.53	10.34	0.3235	10.40
MnO	0.27	0.0085	0.27	0.29	0.0091	0.29	0.27	0.0084	0.27
MgO	11.60	0.6398	11.59	10.86	0.6057	11.04	12.57	0.7005	12.64
CaO	15.81	0.6266	15.79	15.51	0.6215	15.76	18.08	0.7244	18.18
K2O	1.55	0.0731	1.55	1.84	0.0879	1.87	0.68	0.0323	0.68
Na2O	0.27	0.0194	0.27	0.28	0.0201	0.28	0	0	0
Sum	100.15	3.9535	100	98.40	3.9337	100	99.433	3.9689	100
Ca:Mg:Fe	39.2	40.0	20.8	40.9	39.8	19.3	41.4	40.1	18.5
Ca:Na:K	87.1	2.7	10.2	85.2	2.8	12.0	95.7	0	4.3

*). cations per 6 oxygens.

Table 4.5 EMP Analyses of Spinel in T-2487

analy No	(1)			(2)			(3)		
	wt%	cat*	wt%	wt%	cat	wt%	wt%	cat	wt%
SiO2	11.49	0.3391	12.59	12.77	0.3394	12.77	5.50	0.1477	5.44
TiO2	0.80	0.0177	0.87	0.62	0.0124	0.62	0.54	0.0110	0.54
Al2O3	41.26	1.3445	45.18	47.40	1.4846	47.38	52.65	1.6668	52.13
FeO	23.97	0.5914	26.25	24.99	0.5554	24.98	27.65	0.6211	27.37
MnO	0.41	0.0102	0.45	0	0	0	0.26	0.0060	0.26
MgO	9.42	0.4142	10.32	10.27	0.4070	10.27	12.63	0.5058	12.51
CaO	3.45	0.1090	3.78	3.43	0.0977	3.43	1.65	0.0474	1.63
K2O	0.52	0.0195	0.57	0.55	0.0185	0.55	0.12	0.0042	0.12
Sum	91.32	2.9356	100	100.04	2.9150	100	101.00	3.0099	100
Ca:Mg:Fe	9.8	37.2	53.1	9.2	38.4	52.4	4.0	43.1	52.9
Ca:Na:K	84.8	0	15.2	84.1	0	15.9	91.9	0	8.1

	(4)			(5)			(6)		
SiO2	6.68	0.1806	6.69	8.67	0.2355	8.77	10.54	0.2931	10.89
TiO2	0.48	0.0098	0.48	0.56	0.0114	0.56	0.69	0.0145	0.72
Al2O3	51.53	1.6417	51.61	49.51	1.5854	50.10	45.58	1.4935	47.10
FeO	26.61	0.6015	26.65	25.53	0.5800	25.83	25.19	0.5857	26.03
MnO	0.24	0.0056	0.24	0.28	0.0065	0.28	0.24	0.0058	0.25
MgO	12.17	0.4903	12.19	11.32	0.4583	11.45	10.58	0.4384	10.93
CaO	1.93	0.0560	1.94	2.73	0.0794	2.76	3.71	0.1104	3.83
K2O	0.19	0.0067	2.20	0.23	0.0081	0.24	0.24	0.0084	0.25
Sum	99.83	2.9921	100	98.82	2.9644	100	96.77	2.9450	100
Ca:Mg:Fe	4.9	42.7	52.4	7.1	41.0	51.9	9.7	38.6	51.6
Ca:Na:K	89.3	0	10.7	90.8	0	9.2	92.9	0	7.1

*). cations per 4 oxygens.

Table 4.6 EMP Analyses of Feldspars in T-2487

Plagioclases in T-2487:									
analy No	(1)			(2)			(3)		
	wt%	cat*	wt%	wt%	cat	wt%	wt%	cat	wt%
SiO2	51.23	2.3910	51.27	50.34	2.3477	50.29	51.87	2.4166	51.48
TiO2	0.60	0.0210	0.60	0.58	0.0204	0.58	1.03	0.0361	1.02
Al2O3	26.74	1.4708	26.76	27.71	1.5231	27.68	25.27	1.3877	25.08
FeO	3.87	0.1512	3.88	4.24	0.1652	4.23	5.20	0.2027	5.16
MgO	1.14	0.0791	1.14	0.87	0.0605	0.87	1.16	0.0805	1.15
CaO	11.55	0.5774	11.55	12.41	0.6200	12.40	11.33	0.5657	11.25
K2O	3.56	0.2121	3.56	2.93	0.1742	2.93	3.70	0.2200	3.67
Na2O	1.24	0.1122	1.24	1.02	0.0926	1.02	1.20	0.1081	1.19
Sum	99.92	5.0147	100	100.1	5.0037	100	100.77	5.0174	100
Ca:Mg:Fe	71.5	9.8	18.7	73.3	7.1	19.5	66.6	9.5	23.9
Ca:Na:K	64.0	12.4	23.5	69.9	10.4	19.6	63.3	12.1	24.6
alkali-feldspars in T-2487:									
	(1)			(2)			(3)		
SiO2	62.05	2.8605	61.46	60.33	2.8219	60.65	55.29	2.7431	59.19
TiO2	1.08	0.0375	1.07	0.87	0.0305	0.87	0.56	0.0210	0.60
Al2O3	17.79	0.9667	17.62	19.36	1.0670	19.46	20.37	1.1908	21.80
FeO	4.11	0.1583	4.07	2.28	0.0893	2.29	1.19	0.0494	1.27
MgO	1.08	0.0740	1.07	0.65	0.0454	0.65	0.40	0.0298	0.43
CaO	3.63	0.1791	3.59	3.45	0.1730	3.47	4.44	0.2359	4.75
K2O	10.43	0.6136	10.33	11.71	0.6986	11.77	10.13	0.6411	10.84
Na2O	0.80	0.0714	0.79	0.83	0.0753	0.83	1.04	0.0998	1.11
Sum	100.97	4.9611	100	99.48	5.0010	100	93.42	5.0109	100
Ca:Mg:Fe	43.5	18.0	38.5	56.2	14.8	29.0	74.9	9.5	15.7
Ca:Na:K	20.7	8.3	71.0	18.3	8.0	73.8	24.2	10.2	65.6

*). cations per 8 oxygens.

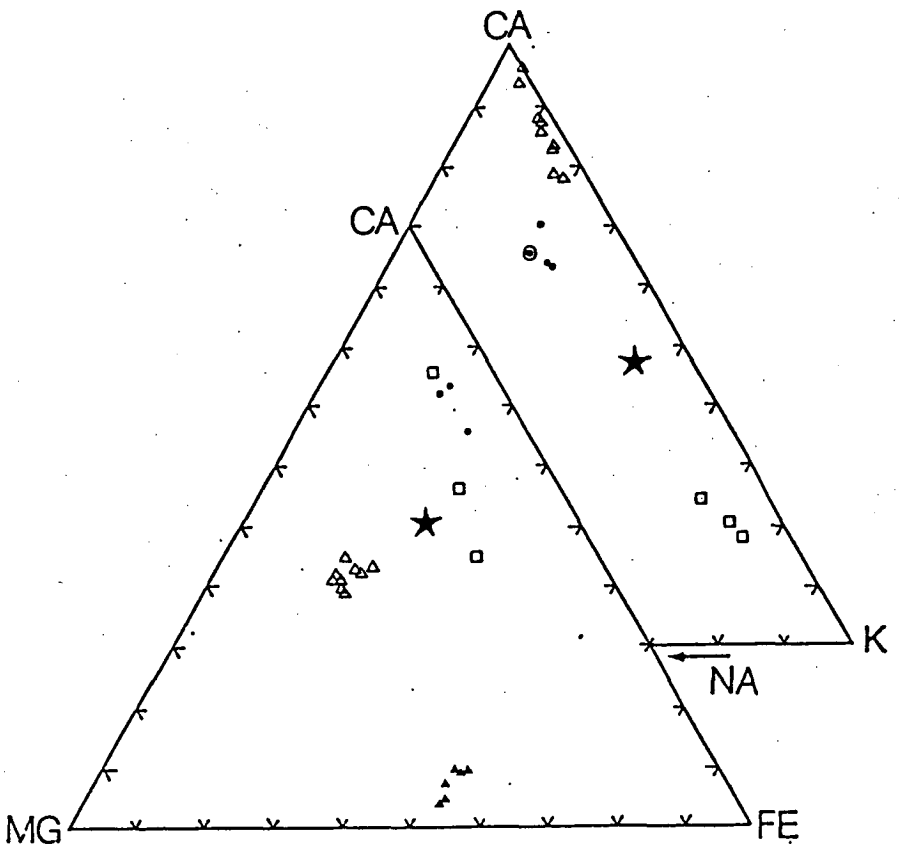

Fig 4.2 Ca-Na-K and Ca-Mg-Fe Diagrams (in atomic ratio) for Evaluation of the EMP Analyses of the Run Products in T-2487. Empty triangles represent clinopyroxene analyses; solid triangles represent spinel analyses; soild dots are plagioclase analyses; empty squares are alkali feldspar analyses. Star indicates the average EMP area scan analysis of the whole charge. Data are from the corresponding tables. (For comparison, the proposed parental plagioclase for the unusual feldspar intergrowths is indicated by the asterisk within a circle).

(Table 4.5, solid triangles in Fig 4.2). This is strong evidence suggesting "contamination" of these analyses. Therefore, all analyses should be evaluated carefully. Because the phases other than feldspars are not quite relevant to this study, only feldspar analyses will be discussed in detail. It should be noted that whereas the near liquidus pyroxene of the low-K melt in the first two runs is pigeonite (low-Ca pyroxene), the near liquidus pyroxene of the K-rich melt in T-2487 is a high-Ca pyroxene.

4.3.2 Feldspar Compositions in the Run Products

All feldspar analyses show the presence of Fe and Mg. It can not be ascertained if these contents reflect contamination by other phases (e.g. melt, pyroxene, or/and spinel) nearby. Several lines of evidence support the presence of most of the Fe & Mg in the feldspars analyzed. Firstly, there are not enough cations to match 8 oxygens when the analyses are calculated to ideal feldspar molecule and no Fe & Mg are included. The amount of Al^{3+} is always less than required. Secondly, it is observed that natural (both terrestrial and lunar) plagioclases often contain Fe & Mg (Longhi et al., 1976). $Ca(Fe,Mg)Si_3O_8$ component is suggested to be the main substition form. Thirdly, the natural feldspars in the two dykes contain small amount of Fe (Table 1.5 & 3.1).

Using the distribution coefficients for Fe & Mg between plagioclase and basaltic liquids suggested by Longhi et al. (1976, Table 5), it is estimated that ca 2 - 6 wt% of FeO, 0.4 - 0.6 wt% of MgO can be present in plagioclases crystallized from T-2432 & T-2459; and ca 1.5 - 4 wt% of FeO, 0.4 wt% of MgO can substitute into plagioclases crystallized from T-2487. Therefore, some of the analyses given in Table 4.3 & 4.6 can be acceptable, but most of them seem to be contaminated by more mafic phases.

The analyses in Table 4.3 & 4.6 show a positive correlation between the amount of K and those of Fe & Mg in the plagioclase. This is believed to be a combined result of contamination and Fe^{3+} substitution into plagioclase. The study of Longhi et al. (1976) suggests that Fe^{3+} is more readily substituted into plagioclase than Mg, and Mg, more readily than Fe^{2+}. To minimize the amount of contamination it is suggested that plagioclase analyses with minimum Mg & Fe are closest to the true composition. The plagioclase with 0.49 wt% MgO contains 3.8 Kf component [= 100*K/(Ca+Na+K)] in T-2432, and that with 0.82 wt% MgO contains 5.6 Kf component in T-2459. In T-2487 both plagioclase and alkali feldspar are present. The plagioclase should thus have maximum Kf solid solution for these P, T conditions. This increased Kf solid solution may increase the Fe & Mg in the plagioclase, as implied by the positive correlation between K and Fe & Mg in the plagioclase analyses. The plagioclase with minimum MgO (0.87 wt%) has 19.6 Kf solid solution, which approaches quite closely the composition of the proposed parental plagioclase ($Kf_{21.5}$ An_{64} $Ab_{14.5}$) suggested for the unusual feldspar intergrowths in the two dykes (Fig 4.2). The coexisting alkali feldspar contains 18.3 An component, further supporting the suggested limit of ternary feldspar solid solution at 10 kbar (Fig 3.5).

4.4 Origin of the K-rich Magma

The above experimental results have demonstrated that plagioclase with high-Kf solid solution can be generated in K-rich magmas. Ordinary basaltic magmas are very poor in potassium and thus can only produce plagioclases with little Kf solid solutions.

The bulk composition of run T-2487, in which the K-rich plagioclase

($Kf_{19.6}$ An_{70} $Ab_{10.4}$) crystallized, is very K-rich compared with both the basalt dykes and the charnockite in Departure Rocks (Table 4.1 & 1.2). However, such K-rich magma may be formed through interaction between the dyke magma and charnockitic magma. In fact, a very K-rich sample (191) has been found near the intersection area between dyke 65787, the Opx-bearing gneiss, and the charnockite in West Rock (Fig 1.3 & Table 1.2). This sample is very rich in K (K_2O = 5.43 wt%) but poor in Ca (CaO = 1.07 wt%). It is probably a result of partial melting of the Opx-bearing gneiss induced by the charnockite emplacement. Interaction between such K-rich melt and the dyke magma may further locally enrich K in the dyke magma and may also deplete Na from the dyke magma into the more siliceous melt (the partial melt or/and charnockitic magma). This type of selective diffusion between contrasted melt structures (basaltic and granitic melts) is suggested by the experiments of Watson & Jurewicz (1984). In the interaction area, the K-rich melt that can produce the K-rich plagioclase may be generated. This possibility remains to be tested by combination of detailed examination of the field occurrence in the light of the experimental study and further geochemical and experimental studies.

The study reported in this thesis has proven the existence of plagioclases with high Kf solid solutions. The Kf-rich plagioclases can be formed at high temperatures and high pressures under anhydrous conditions. The conclusions reached in this study on the conditions of formation of the feldspar phenocrysts and interaction between the mafic and charnockitic magmas argue ~~This shows~~ that the later Proterozoic mafic dykes in Departure Rocks were emplaced almost contemporaneously with the charnockitic magma and that the conditions of emplacement were at high crustal level (ca 10 kbar) and high temperature in a remarkably anhydrous environment.

Appendix I Representative Compositions of Mineral Pairs Used for Estimation of Temperatures and Pressures

1). Orthopyroxene - Clinopyroxene Pairs

	microprobe analysis result				Fe3+ recalculation (Robinson 1982)			
65786-1	Opx		Cpx		Opx		Cpx	
	wt%	cat	wt%	cat	wt%	cat	wt%	cat
SiO2	51.47	1.945	49.00	1.910	51.47	1.934	49.00	1.896
TiO2			0.22	0.006			0.22	0.006
Al2O3	1.41	0.063	2.79	0.128	1.41	0.062	2.79	0.127
Cr2O3			0.26	0.008			0.26	0.008
Fe2O3					2.52	0.071	2.87	0.084
FeO	27.76	0.877	11.03	0.369	25.51	0.802	8.45	0.273
MnO	1.08	0.035	0.43	0.014	1.08	0.034	0.43	0.014
MgO	19.06	1.074	12.23	0.710	19.06	1.067	12.23	0.706
CaO	0.75	0.030	20.78	0.868	0.75	0.030	20.78	0.862
Na2O			0.32	0.024			0.32	0.024
Sum	101.53	4.024	97.06	4.028	101.78	4.000	97.35	4.000
Mg#	55.0		66.4		57.1		72.1	
Ca:Mg:Fe	1.5	54.2 44.3	43.9	37.2 18.8	1.7	56.2 42.2	43.8	40.5 15.7
Ln(a)EN					-1.242		-3.131	
65786-3	Opx		Cpx		Opx		Cpx	
	wt%	cat	wt%	cat	wt%	cat	wt%	cat
SiO2	50.95	1.9267	53.35	1.9711	49.91	1.913	53.35	1.971
TiO2	0.23	0.0065			0.23	0.006		
Al2O3	1.72	0.0768	1.29	0.0561	1.68	0.076	1.29	0.056
Fe2O3					2.96	0.085	0.08	0.002
FeO	28.32	0.8956	10.36	0.3202	25.08	0.804	10.29	0.318
MnO	0.99	0.0316	0.38	0.0118	0.97	0.031	0.38	0.012
MgO	18.83	1.0612	13.14	0.7237	18.44	1.061	13.14	0.724
CaO	0.75	0.0302	23.18	0.9178	0.73	0.030	23.18	0.917
Sum	101.78	4.0284	101.70	4.0008	100.00	4.000	101.71	4.000
Mg#	54.2		69.3		56.7		69.5	
Ca:Mg:Fe	1.5	53.4 45.1	46.8	36.9 16.3	1.7	55.8 42.5	46.0	37.5 16.5
Ln(a)EN					-1.336		-3.409	

	microprobe analysis result				Fe3+ recalculation (Robinson 1982)			
65786-4	Opx		Cpx		Opx		Cpx	
	wt%	cat	wt%	cat	wt%	cat	wt%	cat
SiO2	52.44	1.9573	52.83	1.9610	50.71	1.945	51.96	1.957
Al2O3	0.84	0.0370	1.44	0.0628	0.81	0.037	1.42	0.063
Fe2O3					2.52	0.073	0.80	0.023
FeO	29.04	0.9065	11.31	0.3512	25.82	0.828	10.41	0.328
MnO	1.10	0.0347	0.38	0.0119	1.06	0.035	0.37	0.012
MgO	19.18	1.0669	13.08	0.7238	18.55	1.061	12.87	0.722
CaO	0.55	0.0219	22.55	0.8968	0.53	0.022	22.20	0.895
Sum	103.14	4.0242	101.59	4.0076	100.00	4.000	100.00	4.000
Mg#	54.1		67.3		56.2		68.8	
Ca:Mg:Fe	1.1	53.5 45.4	45.5	36.7 17.8	1.2	55.5 43.3	44.8	38.0 17.2
Ln(a)EN					-1.308		-3.179	
65786-6	Opx		Cpx		Opx		Cpx	
	wt%	cat	wt%	cat	wt%	cat	wt%	cat
SiO2	51.22	1.9466	52.72	1.9577	51.03	1.945	52.00	1.956
Al2O3	1.13	0.0506	1.78	0.0777	1.38	0.062	1.76	0.078
Fe2O3					1.69	0.049	0.37	0.010
FeO	27.42	0.8714	11.14	0.3461	25.25	0.805	10.66	0.335
MnO	0.92	0.0297	0.37	0.0117	1.00	0.032	0.36	0.012
MgO	19.55	1.1072	13.13	0.7267	19.09	1.085	12.95	0.726
CaO	0.55	0.0224	22.21	0.8834	0.57	0.023	21.91	0.883
Sum	100.79	4.0280	101.35	4.0034	100.00	4.000	100.00	4.000
Mg#	56.0		67.7		57.4		68.4	
Ca:Mg:Fe	1.1	55.3 43.5	45.2	37.1 17.7	1.2	56.7 42.1	44.1	38.2 17.6
Ln(a)EN					-1.250		-3.058	
65786-8	Opx		Cpx		Opx		Cpx	
	wt%	cat	wt%	cat	wt%	cat	wt%	cat
SiO2	52.00	1.9633	52.72	1.9539	52.00	1.955	52.72	1.950
Al2O3	0.88	0.0391	1.76	0.0768	0.88	0.039	1.76	0.077
Fe2O3					1.81	0.051	0.83	0.023
FeO	28.04	0.8854	11.15	0.3456	26.42	0.831	10.41	0.322
MnO	0.99	0.0317	0.45	0.0140	0.99	0.032	0.45	0.014
MgO	19.17	1.0788	12.92	0.7139	19.17	1.074	12.92	0.712
CaO	0.46	0.0187	22.75	0.9034	0.46	0.019	22.75	0.902
Sum	101.55	4.0171	101.75	4.0077	101.72	4.000	101.83	4.000
Mg#	54.9		67.4		56.4		68.9	
Ca:Mg:Fe	0.9	54.4 44.7	46.0	36.4 17.6	1.0	55.8 43.2	45.2	37.0 17.1
Ln(a)EN					-1.270		-3.283	

	microprobe analysis result				Fe3+ recalculation (Robinson 1982)			
65787-1	Opx		Cpx		Opx		Cpx	
	wt%	cat	wt%	cat	wt%	cat	wt%	cat
SiO2	52.52	1.9576	52.29	1.9399	50.98	1.947	51.33	1.934
Al2O3	0.92	0.0403	2.19	0.0956	0.89	0.040	2.15	0.095
Fe2O3					2.32	0.067	1.31	0.037
FeO	28.22	0.8796	11.93	0.3701	25.31	0.808	10.53	0.332
MnO	0.87	0.0273	0.27	0.0086	0.84	0.027	0.27	0.008
MgO	19.75	1.0975	13.20	0.7296	19.17	1.091	12.96	0.728
CaO	0.50	0.0200	21.85	0.8685	0.49	0.020	21.45	0.866
Sum	102.78	4.0223	101.73	4.0123	100.00	4.000	100.00	4.000
Mg#	55.5		66.3		57.5		68.7	
Ca:Mg:Fe	1.0	55.0 44.0	44.1	37.1 18.8	1.1	56.8 42.1	43.0	39.1 17.8
Ln(a)EN					-1.247		-2.913	
65787-2	Opx		Cpx		Opx		Cpx	
	wt%	cat	wt%	cat	wt%	cat	wt%	cat
SiO2	50.74	1.9583	51.70	1.9386	50.74	1.950	51.70	1.934
TiO2			0.36	0.0102			0.36	0.010
Al2O3	1.06	0.0483	1.86	0.0823	1.06	0.048	1.86	0.082
Fe2O3					1.81	0.052	1.08	0.030
FeO	27.35	0.8828	11.45	0.3590	25.72	0.827	10.48	0.328
MnO	0.87	0.0286			0.87	0.028		
MgO	18.73	1.0775	13.05	0.7295	18.73	1.073	13.05	0.729
CaO	0.53	0.0220	22.17	0.8905	0.53	0.022	22.17	0.888
Sum	99.28	4.0175	100.59	4.0101	99.46	4.000	100.70	4.000
Mg#	55.0		67.0		56.5		68.9	
Ca:Mg:Fe	1.1	54.4 44.5	45.0	36.9 18.1	1.1	55.8 43.0	44.0	38.6 17.4
Ln(a)EN					-1.273		-3.022	
65787-3	Opx		Cpx		Opx		Cpx	
	wt%	cat	wt%	cat	wt%	cat	wt%	cat
SiO2	52.14	1.963	53.18	1.961	52.14	1.960	53.18	1.960
TiO2			0.23	0.006			0.23	0.006
Al2O3	1.34	0.059	1.96	0.085	1.34	0.059	1.96	0.085
Fe2O3					0.76	0.021	0.09	0.002
FeO	27.67	0.871	11.06	0.341	26.99	0.848	10.98	0.338
MnO	0.87	0.028	0.35	0.011	0.87	0.028	0.35	0.011
MgO	18.88	1.060	12.98	0.713	18.88	1.058	12.98	0.713
CaO	0.64	0.026	21.84	0.863	0.64	0.026	21.84	0.862
Na2O			0.29	0.021			0.29	0.021
Sum	101.54	4.007	101.89	4.001	101.62	4.000	101.90	4.000
Mg#	54.9		67.7		55.5		67.8	
Ca:Mg:Fe	1.3	54.1 44.5	44.0	37.9 18.1	1.4	54.7 43.9	44.0	38.0 18.0
Ln(a)EN					-1.285		-3.075	

	microprobe analysis result				Fe3+ recalculation (Robinson 1982)			
65789-5	Opx		Cpx		Opx		Cpx	
	wt%	cat	wt%	cat	wt%	cat	wt%	cat
SiO2	50.86	1.9593	51.62	1.9747	50.86	1.953	51.62	1.975
TiO2	0.22	0.0064			0.22	0.006		
Al2O3	1.17	0.0532	1.34	0.0605	1.17	0.053	1.34	0.060
Cr2O3			0.27	0.0082			0.27	0.008
Fe2O3					1.31	0.038		
FeO	26.54	0.8550	10.74	0.3437	25.36	0.814	10.74	0.344
MnO	0.55	0.0180			0.55	0.018		
MgO	18.35	1.0539	12.54	0.7151	18.35	1.050	12.54	0.715
CaO	1.43	0.0591	21.68	0.8887	1.43	0.059	21.68	0.889
Na2O	0.12	0.0057			0.12	0.009		
Sum	99.25	4.0106	98.20	3.9909	99.37	4.000	98.19	3.991
Mg#	55.2		67.5		56.3		67.5	
Ca:Mg:Fe	3.0	53.5 43.4	45.6	36.7 17.6	3.1	54.6 42.3	44.4	37.6 18.0
Ln(a)EN					-1.311		-3.019	
65789-6	Opx		Cpx		Opx		Cpx	
	wt%	cat	wt%	cat	wt%	cat	wt%	cat
SiO2	51.44	1.9759	51.61	1.9667	51.44	1.972	51.61	1.966
Al2O3	0.72	0.0326	1.87	0.0840	0.72	0.033	1.87	0.084
Fe2O3					0.80	0.023		
FeO	27.49	0.8832	9.92	0.3160	26.77	0.858	9.92	0.316
MnO	0.66	0.0216	0.24	0.0077	0.66	0.021	0.24	0.008
MgO	18.68	1.0697	13.10	0.7437	18.68	1.068	13.10	0.744
CaO	0.60	0.0247	21.39	0.8733	0.60	0.025	21.39	0.873
Sum	99.60	4.0078	98.13	3.9913	99.67	4.000	98.13	3.992
Mg#	54.8		70.2		55.4		70.2	
Ca:Mg:Fe	1.2	54.1 44.7	45.2	38.5 16.3	1.3	54.7 44.0	43.7	39.5 16.8
Ln(a)EN					-1.267		-2.879	
65791-1	Opx		Cpx		Opx		Cpx	
	wt%	cat	wt%	cat	wt%	cat	wt%	cat
SiO2	53.26	1.9126	50.33	1.8418	53.26	1.9096	50.33	1.8380
TiO2			1.19	0.0329			1.19	0.0329
Al2O3	3.83	0.1622	6.45	0.2780	3.83	0.1620	6.45	0.2775
Cr2O3			0.32	0.0091			0.32	0.0091
Fe2O3					0.70	0.0188	0.88	0.0243
FeO	12.32	0.3701	4.87	0.1492	11.70	0.3507	4.08	0.1246
MgO	28.96	1.5501	13.85	0.7552	28.96	1.5477	13.85	0.7536
CaO	0.29	0.0112	22.68	0.8892	0.29	0.0112	22.68	0.8874
Na2O			0.74	0.0527			0.74	0.0526
Sum	98.66	4.0063	100.43	4.0081	98.73	4.000	100.52	4.0000
Mg#	80.7		83.5		81.5		85.8	
Ca:Mg:Fe	0.6	80.3 19.2	49.6	42.1 8.3	0.6	81.0 18.4	46.2	46.2 7.6
Ln(a)EN					-0.525		-3.345	

Appendix I Representative Compositions of Mineral Pairs Used for Estimation of Temperatures and Pressures (con't)

2). Magnetite - Ilmenite Pairs

	65786-1				65786-2			
	magnetite		ilmenite		magnetite		ilmenite	
	wt%	cat	wt%	cat	wt%	cat	wt%	cat
SiO2	0.26	0.0099			1.43	0.0536		
TiO2	0.95	0.0272	44.96	0.8520	0.73	0.0205	46.15	0.8550
Al2O3	1.01	0.0454	0.20	0.0060	0.80	0.0354	0.21	0.0060
Cr2O3	0.47	0.0142			0.36	0.0107		
Fe2O3	65.02	1.8661	15.29	0.2900	63.94	1.8055	15.34	0.2845
FeO	31.96	1.0195	37.84	0.7975	32.57	1.0220	38.75	0.7980
MnO			0.69	0.0145			0.74	0.0155
MgO	0.31	0.0176	1.06	0.0400	0.94	0.0525	1.21	0.0410
Sum	99.98	3.0000	100.04	2.0000	100.76	3.0002	102.32	2.0000
	X(Usp)=0.02872		X(Ilm)=0.8504		X(Usp)=0.02167		X(Ilm)=0.85308	

	65786-3				65786-4			
	wt%	cat	wt%	cat	wt%	cat	wt%	cat
SiO2	0.99	0.0373			0.99	0.0373	0.51	0.0125
TiO2	3.29	0.0931	48.79	0.8755	3.29	0.0931	46.28	0.8680
Al2O3	0.83	0.0368			0.83	0.0368	0.22	0.0065
Cr2O3	0.39	0.0116			0.39	0.0116		
Fe2O3	59.69	1.6908	13.87	0.2490	59.69	1.6908	12.38	0.2325
FeO	34.23	1.0774	40.71	0.8125	34.23	1.0774	39.34	0.8205
MnO			0.64	0.0130			0.63	0.0135
MgO	0.60	0.0337	1.41	0.0500	0.60	0.0337	1.26	0.0470
CaO	0.48	0.0194			0.48	0.0194		
Sum	100.50	3.0000	105.42	2.0000	100.50	3.0000	100.62	2.0000
	X(Usp)=0.09744		X(Ilm)=0.87137		X(Usp)=0.09744		X(Ilm)=0.87892	

	65786-5				65786-6			
	wt%	cat	wt%	cat	wt%	cat	wt%	cat
SiO2	1.54	0.0570	0.18	0.0045	0.48	0.0177		
TiO2	0.32	0.0089	47.75	0.8880	0.20	0.0056	45.95	0.8615
Al2O3	1.47	0.0641			1.18	0.0514		
Cr2O3	0.35	0.0102			0.43	0.0126		
Fe2O3	64.38	1.7937	11.53	0.2145	67.95	1.8895	14.76	0.2770
FeO	32.91	1.0190	40.19	0.8315	32.67	1.0095	38.83	0.8095
MnO			0.57	0.0120			0.75	0.0160
MgO	0.85	0.0469	1.19	0.0440	0.25	0.0138	0.97	0.0360
CaO			0.21	0.0055				
Sum	101.82	3.0000	101.62	2.0000	103.16	3.0000	101.26	2.0000
	X(Usp)=0.00978		X(Ilm)=0.88903		X(Usp)=0.00601		X(Ilm)=0.85774	

	65786-13				65786-14			
	magnetite		ilmenite		magnetite		ilmenite	
	wt%	cat	wt%	cat	wt%	cat	wt%	cat
TiO2	0.21	0.0060	48.90	0.8565	0.25	0.0037	48.29	0.9025
Al2O3	0.58	0.0259			0.35	0.0160		
Cr2O3	0.40	0.0120			0.36	0.0110		
Fe2O3	66.49	1.8988	6.62	0.1270	39.67	2.0282	10.40	0.1945
FeO	32.71	1.0381	41.13	0.8760	28.98	0.9376	40.47	0.8415
MnO			0.64	0.0140			1.03	0.0215
MgO	0.34	0.0192	1.32	0.0465			1.07	0.0395
Sum	100.72	3.0000	98.52	2.0000	99.61	3.0000	101.26	2.0000
	X(Usp)=0.02659		X(Ilm)=0.93169		X(Usp)=0.00368		X(Ilm)=0.89960	

	65787-1				65787-2			
	wt%	cat	wt%	cat	wt%	cat	wt%	cat
SiO2	0.23	0.0094			0.83	0.0322		
TiO2	0.18	0.0055	46.30	0.8570	0.20	0.0055	35.53	0.6925
Al2O3	0.73	0.0350			2.91	0.1332	0.26	0.0080
Cr2O3	0.50	0.0161			0.56	0.0172	0.22	0.0045
Fe2O3	62.70	1.9192	15.47	0.2865	60.69	1.7735	30.70	0.6020
FeO	29.60	1.0070	38.62	0.7950	30.64	0.9952	29.68	0.6470
MnO			0.67	0.0140			0.53	0.0115
MgO			1.31	0.0480	0.64	0.0371	0.88	0.0340
CaO	0.18	0.0078			0.14	0.0058		
Sum	94.12	3.0000	102.37	2.0000	96.61	3.0000	97.63	2.0000
	X(Usp)=0.00581		X(Ilm)=0.85211		X(Usp)=0.00641		X(Ilm)=0.68980	

	65787-3				65787-4			
	wt%	cat	wt%	cat	wt%	cat	wt%	cat
SiO2					0.32	0.0124		
TiO2	0.20	0.0056	46.66	0.8615	0.69	0.0201	44.80	0.8535
Al2O3	0.49	0.0216			1.29	0.0588	1.56	0.0465
Cr2O3	0.49	0.0145			0.40	0.0122		
Fe2O3	69.34	1.9526	15.00	0.2770	64.10	1.8642	12.92	0.2465
FeO	32.13	1.0056	39.41	0.8090	31.35	1.0134	37.42	0.7930
MnO			0.63	0.0130			0.59	0.0125
MgO			1.07	0.0390	0.33	0.0190	1.27	0.0480
Sum	102.65	3.0000	102.77	2.0000	98.48	3.0000	98.56	2.0000
	X(Usp)=0.00581		X(Ilm)=0.85770		X(Usp)=0.02150		X(Ilm)=0.86970	

Appendix I Representative Compositions of Mineral Pairs Used for Estimation of Temperatures and Pressures (con't)

3). Clinopyroxene - Plagioclase Pairs

65786-1	Cpx				Plag		
	microprobe analysis		Fe3+ recalculation				
	wt%	cat	wt%	cat		wt%	cat
SiO2	49.00	1.910	49.00	1.896	SiO2	48.39	2.2297
TiO2	0.22	0.006	0.22	0.006	Al2O3	32.42	1.7607
Al2O3	2.79	0.128	2.79	0.127	CaO	15.80	0.7799
Cr2O3	0.26	0.008	0.26	0.008	Na2O	1.57	0.1402
Fe2O3			2.87	0.084	K2O	1.68	0.0988
FeO	11.03	0.369	8.45	0.273			
MnO	0.43	0.014	0.43	0.014			
MgO	12.23	0.710	12.23	0.706			
CaO	20.78	0.868	20.78	0.862			
Na2O	0.32	0.024	0.32	0.024			
Sum	97.06	4.028	97.35	4.000	Sum	99.87	5.0094
CaTs			0.0315		Ca:Na:K	76.5	13.8 9.7

65786-2	Cpx				Plag		
	wt%	cat	wt%	cat		wt%	cat
SiO2	50.61	1.922	50.61	1.900	SiO2	46.34	2.1576
TiO2	0.33	0.009	0.33	0.009	Al2O3	33.29	1.8266
Al2O3	2.65	0.119	2.65	0.117	FeO	0.42	0.0165
Cr2O3	0.21	0.006	0.21	0.006	CaO	16.99	0.8478
Fe2O3			4.77	0.135	Na2O	1.78	0.1608
FeO	11.89	0.378	7.60	0.239			
MnO	0.45	0.014	0.45	0.014			
MgO	11.88	0.673	11.88	0.665			
CaO	20.78	0.846	20.78	0.836			
Na2O	1.07	0.079	1.07	0.078			
Sum	99.87	4.045	100.35	4.000	Sum	98.82	5.0094
CaTs			0.024		Ca:Na:K	84.1	15.9 0

65786-3	Cpx				Plag		
	microprobe analysis		Fe3+ recalculation				
	wt%	cat	wt%	cat		wt%	cat
SiO2	53.35	1.9711	52.45	1.971	SiO2	45.60	2.1220
Al2O3	1.29	0.0561	1.27	0.056	Al2O3	34.05	1.8676
Fe2O3			0.08	0.002	CaO	17.67	0.8809
FeO	10.36	0.3202	10.12	0.318	Na2O	1.37	0.1236
MnO	0.38	0.0118	0.37	0.012			
MgO	13.14	0.7237	12.92	0.724			
CaO	23.18	0.9178	22.79	0.917			
Sum	101.70	4.0008	100.00	4.000	Sum	98.98	5.0059
CaTs			0.027		Ca:Na:K	87.7	12.3 0

65786-4	Cpx				Plag		
	wt%	cat	wt%	cat		wt%	cat
SiO2	52.83	1.9610	51.96	1.957	SiO2	47.27	2.1633
Al2O3	1.44	0.0628	1.42	0.063	Al2O3	33.86	1.8265
Fe2O3			0.80	0.023	CaO	17.43	0.8549
FeO	11.31	0.3512	10.41	0.328	Na2O	1.77	0.1574
MnO	0.38	0.0119	0.37	0.012			
MgO	13.08	0.7238	12.87	0.722			
CaO	22.55	0.8968	22.20	0.895			
Sum	101.59	4.0076	100.00	4.000	Sum	100.34	5.0021
CaTs			0.020		Ca:Na:K	84.4	15.6 0

65786-5	Cpx				Plag		
	wt%	cat	wt%	cat		wt%	cat
SiO2	52.72	1.9577	52.00	1.956	SiO2	46.70	2.1469
Al2O3	1.78	0.0777	1.76	0.078	Al2O3	34.01	1.8428
Fe2O3			0.37	0.010	FeO	0.24	0.0093
FeO	11.14	0.3461	10.66	0.335	CaO	17.35	0.8543
MnO	0.37	0.0117	0.36	0.012	Na2O	1.76	0.1566
MgO	13.13	0.7267	12.95	0.726			
CaO	22.21	0.8834	21.91	0.883			
Sum	101.35	4.0034	100.00	4.000	Sum	100.06	5.0099
CaTs			0.034		Ca:Na:K	84.5	15.5 0

65787-2	Cpx				Plag	
	micrprobe analysis		Fe3+ recalculation			
	wt%	cat	wt%	cat	wt%	cat
SiO2	51.70	1.9386	51.70	1.934	SiO2 46.46	2.1680
TiO2	0.36	0.0102	0.36	0.010	Al2O3 33.20	1.8259
Al2O3	1.86	0.0823	1.86	0.082	CaO 16.88	0.8438
Fe2O3			1.08	0.030	Na2O 1.80	0.1626
FeO	11.45	0.3590	10.48	0.328		
MgO	13.05	0.7295	13.05	0.729		
CaO	22.17	0.8905	22.17	0.888		
Sum	100.60	4.0101	100.70	4.000	Sum 98.34	5.0003
CaTs			0.016		Ca:Na:K 83.8	16.2 0

65787-3	Cpx				Plag	
	wt%	cat	wt%	cat	wt%	cat
SiO2	53.18	1.961	53.18	1.960	SiO2 45.94	2.1304
TiO2	0.23	0.006	0.23	0.006	Al2O3 34.02	1.8594
Al2O3	1.96	0.085	1.96	0.085	FeO 0.30	0.0015
Fe2O3			0.09	0.002	CaO 17.59	0.8741
FeO	11.06	0.341	10.98	0.338	Na2O 1.43	0.1288
MnO	0.35	0.011	0.35	0.011		
MgO	12.98	0.713	12.98	0.713		
CaO	21.84	0.863	21.84	0.862		
Na2O	0.29	0.021	0.29	0.021		
Sum	101.89	4.001	101.90	4.000	Sum 99.29	5.0042
CaTs			0.046		Ca:Na:K 87.2	12.8 0

65787-4	Cpx				Plag	
	wt%	cat	wt%	cat	wt%	cat
SiO2	52.09	1.937	52.09	1.925	SiO2 46.80	2.1587
TiO2	0.25	0.007	0.25	0.007	Al2O3 33.65	1.8295
Al2O3	1.97	0.086	1.97	0.086	CaO 17.50	0.8650
Cr2O3	0.23	0.007	0.23	0.007	Na2O 1.64	0.1468
Fe2O3			2.72	0.076		
FeO	11.18	0.348	8.73	0.270		
MnO	0.42	0.013	0.42	0.013		
MgO	13.01	0.721	13.01	0.717		
CaO	21.95	0.874	21.95	0.869		
Na2O	0.44	0.032	0.44	0.032		
Sum	101.54	4.025	101.81	4.000	Sum 99.59	4.9999
CaTs			0.0175		Ca:Na:K 85.4	14.6 0

65791-1	Cpx				Plag		
	microprobe analysis		Fe3+ recalculation				
	wt%	cat	wt%	cat		wt%	cat
SiO2	49.46	1.8364	49.46	1.830	SiO2	53.97	2.4458
TiO2	1.31	0.0367	1.31	0.036	Al2O3	29.06	1.5521
Al2O3	6.38	0.2791	6.38	0.279	FeO	0.33	0.0126
Cr2O3	0.29	0.0086	0.29	0.008	CaO	11.50	0.5585
Fe2O3			1.43	0.040	Na2O	4.62	0.4060
FeO	5.12	0.1591	3.83	0.119	K2O	0.22	0.0125
MgO	13.77	0.7620	13.77	0.760			
CaO	21.89	0.8710	21.89	0.868			
Na2O	0.84	0.0606	0.84	0.060			
Sum	99.07	4.0134	99.20	4.000	Sum	99.71	4.9873
CaTs			0.1175		Ca:Na:K	57.2	41.6 1.3

65791-2	Cpx				Plag		
	wt%	cat	wt%	cat		wt%	cat
SiO2	53.69	1.9641	53.69	1.961	SiO2	60.82	2.7180
Al2O3	2.12	0.0915	2.12	0.091	Al2O3	24.55	1.2934
Fe2O3			0.60	0.017	CaO	6.08	0.2910
FeO	3.89	0.1191	3.35	0.102	Na2O	7.23	0.6265
MgO	16.10	0.8777	16.10	0.877	K2O	0.65	0.0371
CaO	23.54	0.9225	23.54	0.921			
Na2O	0.43	0.0306	0.43	0.030			
Sum	99.76	4.0055	99.83	4.000	Sum	99.33	4.9665
CaTs			0.052		Ca:Na:K	30.5	65.6 3.9

65791-3	Cpx				Plag		
	wt%	cat	wt%	cat		wt%	cat
SiO2	50.31	1.8343	50.31	1.8294	SiO2	55.35	2.4442
TiO2	1.33	0.0364	1.33	0.0363	Al2O3	29.92	1.5572
Al2O3	6.52	0.2803	6.52	0.2796	CaO	12.01	0.5682
Cr2O3	0.40	0.0116	0.40	0.0116	Na2O	4.66	0.3990
Fe2O3			1.18	0.0322	K2O	0.28	0.0159
FeO	4.82	0.1471	3.77	0.1145			
MgO	13.96	0.7587	13.96	0.7567			
CaO	22.72	0.8875	22.72	0.8851			
Na2O	0.78	0.0549	0.78	0.0547			
Sum	100.84	4.0108	100.96	4.0000	Sum	102.22	4.9846
CaTs			0.12055		Ca:Na:K	57.8	40.6 1.6

Appenix II Formulae of the Geothermometers and Barometer Used for Estimation of Temperatures and Pressures

1. Two-pyroxene thermometers

(1) Wells (1977)

$$T\ (^{o}K) = \frac{7341}{3.355 + 2.44 * X^{opx} - \mathrm{Ln}\ K}\ ;$$

$$X^{opx} = \frac{Fe^{2+}}{Fe^{2+} + Mg}\ ; \qquad K = (a_{en}^{cpx}) / (a_{en}^{opx})\ ;$$

$$a_{en} = \left(\frac{Mg}{(Fe^{2+} + Ca + Mg + Mn + Na)}\right)^{M2} * \left(\frac{Mg}{(Fe^{2+} + Mg + Fe^{3+} + Al + Cr + Ti)}\right)^{M1}$$

(2) Kretz (1982)

(a) Ca-transfer thermometer

$T > 1080^{o}C$:

$$T\ (^{o}K) = \frac{1000}{0.468 + 0.608 + [Fe]^{cpx} - 0.123 * \mathrm{Ln}(1-2*[Ca]^{cpx})}\ ;$$

$T < 1080^{o}C$:

$$T\ (^{o}K) = \frac{1000}{0.054 + 0.608 * [Fe]^{cpx} - 0.304 * \mathrm{Ln}(1-2*[Ca]^{cpx})}\ ;$$

$$[Fe]^{cpx} = \left(\frac{Fe^{2+}}{(Fe^{2+} + Mg)}\right)^{cpx}\ ; \qquad [Ca]^{cpx} = \left(\frac{Ca}{(Ca + Fe^{2+} + Mg)}\right)^{cpx}$$

(b) Fe - Mg exchange thermometer

$$T\,(^{o}K) = \frac{1130}{0.505 + \mathrm{Ln}\ K_D}\ ;$$

$$K_D = \frac{[Fe]^{opx}*(1 - [Fe]^{cpx})}{[Fe]^{cpx}*(1 - [Fe]^{opx})}\ ; \qquad [Fe] = \frac{Fe^{2+}}{Fe^{2+} + Mg}$$

(3) Bertrand & Mercier (1985)

$$T\,(^{o}K) = \frac{36273 + 399*P\ (bar)}{19.31 - 12.15*([Ca]^{cpx})^2 - 8.314*\mathrm{Ln}\ K'}\ ;$$

$$[Ca]^{cpx} = \frac{[Ca]^{M2}}{1 - [Na]^{M2}} + (-0.77 + 0.001*T)*\left(\frac{Fe}{Fe + Mg}\right)\ ;$$

$$[Ca]^{opx} = \frac{[Ca]^{M2}}{1 - [Na]^{M2}}\ ; \qquad K' = \frac{1 - [Ca]^{cpx}}{1 - [Ca]^{opx}}$$

2. Fe - Ti oxide thermometer

(a) Solution model (Spencer & Lindsley, 1981)

$$T(^{o}K) = \frac{-A_1*W_H^{usp} - A_2*W_H^{Mt} + A_3*W_H^{ilm} + A_4*W_H^{Hm} + \det(H^o)_{exch}}{-A_1*W_s^{usp} - A_2*W_s^{Mt} + A_3*W_s^{ilm} + A_4*W_s^{Hm} + \det(S^o)_{exch} - R*\mathrm{Ln}\ K_{exch}}$$

$$A_1 = -3*(X_{usp})^2 + 4*(X_{usp}) - 1; \qquad A_2 = 3*(X_{usp})^2 - 2*(X_{usp});$$

$$A_3 = -3*(X_{ilm})^2 + 4*(X_{ilm}) - 1; \qquad A_4 = 3*(X_{ilm})^2 - 2*(X_{ilm});$$

$\det(H^o)_{exch}$ = 27799 Joul/mol; $\det(S^o)_{exch}$ = 4.1920 Joul/mol*^{o}K;

$\det(H^o)_{usp}$ = -3073.1 Joul/mol; $\det(S^o)_{usp}$ = 10.724 Joul/mol*^{o}K;

Solution Parameters (in Joul)

	usp	Mt	ilm	Hm
W_H	64835	20798	102374	36818
W_s	60.296	19.652	71.095	7.7714

(b) Mole fractions of individual components (Stormer, 1983)

$$X_{ilm} = \frac{([Fe^{2+}] * [Ti])^{0.5}}{(0.5*[Fe^{3+}] + ([Fe^{2+}]*[Ti])^{0.5}} ;$$

$$X_{usp} = \frac{[Ti]*[Fe^{2+}]^{S2+}}{(0.5*[Fe^{3+}])*[Fe^{3+}]^{S3+} + [Ti]*[Fe^{2+}]^{S2+}} ;$$

$$[Fe^{2+}]^{S2+} = \frac{Fe^{2+}}{Fe^{2+} + Mg + Mn + Ca} ;$$

$$[Fe^{3+}]^{S3+} = \frac{Fe^{3+}}{Fe^{3+} + Cr + Al}$$

3. Cpx - Plag barometer

(a) Solution model (Ellis, 1980)

$$P_{(bar)} = 2.8653 * \{5360 + T*(2.9876 + 1.9872*LnK) + 12864*X_{CaTs}*(1 - X_{CaTs})$$
$$-26885*[X_{CaTs}*(1 - X_{CaTs})^2 - X_{Ab}*X_{An}*[967 + 715*(X_{Ab} - X_{An})]\}$$

T in ^oK; $\qquad K = \frac{(X_{CaTs})^{cpx}}{(X_{An})^{plag}}$

(b) Estimation of Ca-Tschermaks molecule in Cpx (Kushiro, 1962)

i) estimate Fe^{3+} from the electron microprobe data;

ii) add all K to Na; Mn to Fe^{2+}; Cr to Al;

iii) use the cations to make the individual components of clinopyroxene in the following order:

$NaFe^{3+}Si_2O_6$

$CaTiAl_2O_6$

$CaFe^{3+}AlSiO_6$

$CaAl_2SiO_6$ #

$(CaFe^{3+}_2SiO_6)$

$CaSiO_3$

$MgSiO_3$

$Fe^{2+}SiO_3$

iv) X_{CaTs} is equal to the amount of Ca or half of the amount of Al in the Ca-Tschermaks molecule (with #).

Appendix III Diffraction Types of Plagioclases

Primitive anorthite, which has the lowest structural symmetry among plagioclases, shows four types of X-ray diffraction patterns:

a	(h + k)	even	(l)	even
b	(h + k)	odd	(l)	odd
c	(h + k)	even	(l)	odd
d	(h + k)	odd	(l)	even

The "a" diffractions are common to all feldspars. The "b" diffractions indicatie Al_2Si_2 ordering of anorthite type and are absent in albite. The "c" diffractions imply that the Ca atoms move to one side with associated deformation of the aluminosilicate framework. The "d" diffractions mean the same thing as the "c" diffractions, but are weaker than the "c" diffractions. Two additional diffraction types have been found in natural plagioclases (with 20 to 70% An content) which have been annealed under plutonic or regional metamorphic conditions:

e	(h + k)	odd	(l)	odd
f	(h + k)	even	(l)	even

They occur in pairs around the "b" and "a" diffraction positions like satellites, corresponding to the first and second order diffractions of a kind of "antiphase irrational centered" superstructure, which is in a unit-cell scale. All the plagioclases with "e" and "f" type diffractions are called "e"-type plagioclase. (Smith, 1974; 1984).

REFERENCES

Barth TFW (1969) Feldspars. Interscience, John Wiley & Sons, Inc.

Bertrand P & Mercier J-CC (1985) The mutual solubility of coexisting ortho- and clinopyroxene: toward an absolute geothermometer for the natural system? Earth Planet Sci Lett 76: 109 - 122.

Black LP, Harley SL, Sun SS & McCulloch MT (1987) The Rayner Complex of east Antarctica: complex isotopic systematics within a Proterozoic mobile belt. J Metam Geol 5: 1 - 26.

Black LP, James PR & Harley SL (1983) The geochronology, structure and metamorphism of early Archaean rocks at Fyfe Hills, Enderby Land, Antarctica. Precambrian Research 21: 197 - 222.

Bowen NL (1913) The melting phenomena of the plagioclase feldspars. Am J Sci 35: 577 - 599.

Brooks CK (1976) The Fe_2O_3/FeO ratio of basalt analyses: an appeal for a standardised procedure. Bull Geol Soc Denmark 25: 117 - 120.

Brown WL & Parsons I (1981) Towards a more practical two-feldspar geothermometer. Contrib Mineral Petrol 76: 369 - 377.

Brown WL & Parsons I (1984) Exsolution and coarsening mechanisms and kinetics in an ordered cryptoperthite series. Contrib Mineral Petrol 86: 3 - 18.

Brown WL & Parsons I (1985) Calorimetric and phase-diagram approaches to two-feldspar geothermometry: a critique. Am Mineral 70: 356 - 361.

Buddington AF & Lindsley DH (1964) Iron-titanium oxide minerals and synthetic equivalents. J Petrol 5: 310 - 357.

Cahn JW (1968) Spinodal decomposition. Trans Metall Soc AIME 242: 166 - 180.

Carlson WD (1986) Vanadium pentoxide as a high-temperature solvent for phase equilibrium studies in CaO - MgO - Al_2O_3 - SiO_2. Contrib Mineral Petrol 92: 89 - 92.

Carmichael ISE, Turner FJ & Verhoogen J (1974) Igneous Petrology. New York, McGraw-Hill Book Company.

Carswell DA & Gibb FHF (1987) Evaluation of mineral thermometers and barometers applicable to garnet lherzolite assemblages. Contrib Mineral Petrol 95: 499 - 511.

Crohn PW (1959) A contribution to the geology and glaciology of the western part of Australian Antarctic Teritory. BMR Bull 52; Canberra ACT.

Ellis DJ (1980) Osumilite-sapphirine-quartz-granulites from Enderby Land, Antarctica: P - T conditions of metamorphism, implications for garnet-cordierite equilibria and the evolution of the deep crust. Contrib Mineral Petrol 74: 201 - 210.

Ellis DJ (1987) Origin and evolution of granulites in normal and thickened crusts. Geology 15: 167 - 170.

Fonarev VI & Graphchikov AA (1982) Experimental study of Fe-, Mg- and Ca-distribution between coexisting ortho- and clinopyroxenes. Contrib Mineral Petrol 79: 311 - 318.

Ford RJ (1983) The alkali rocks of Port Cygnet, Tasmania. Unpublished Ph.D Dissertation. University of Tasmania.

Goldsmith JR (1980) The melting and breakdown reactions of anorthite at high pressures and temperatures. Am Mineral 65: 272 - 284.

Goldsmith JR (1986) The role of hydrogen in promoting Al - Si interdiffusion in albite ($NaAlSi_3O_8$) at high pressure. Earth Planet Sci Lett 80: 135 - 138.

Hamilton DL (1969) Solid solution of anorthite in alkali feldspars at 700°C

and 900°C. Progress in Experimental Petrology. NERC publication First Report: 51 - 52.

Harley SL (1985) Garnet-orthopyroxene bearing granulites from Enderby Land, Antarctica: metamorphic pressure-temperature-time evolution of the Archaean Napier Complex. J Petrol 26: 819 - 856.

Hillard JE (1970) Spinodal decomposition. In: Phase Transformations. Am Soc Metals: Ohio. pp 498 - 560.

Johannes W (1978) Melting of plagioclase in the system Ab - An - H_2O and Qz - Ab - An - H_2O at $P(H_2O)$ = 5 Kbars, an equilibrium problem. Contrib Mineral Petrol 66: 295 - 303.

Johannes W (1979) Ternary feldspars: kinetics and possible equilibria at 800°C. Contrib Mineral Petrol 68: 221 - 230.

Kay SM (1977) The origin of antiperthites in anorthosites. Am Mineral 62: 905 - 912.

Kretz R (1982) Transfer and exchange equilibria in a portion of the pyroxene quadrilateral as deduced from natural and experimental data. Geochim Cosmochim Acta 46: 411 -421.

Kuehner SM (1986) Mafic dykes of the East Antarctic shield: experimental, geochemical and petrological studies focusing on the Proterozoic evolution of the crust and mantle. Unpulish Ph.D Dissertation. University of Tasmania.

Kushiro I (1962) Clinopyroxene solid solutions. Part I the $CaAl_2SiO_6$ component. Japanese J Geol Geograph 33: 213 - 220.

Langer JS (1973) Statistical methods in the theory of spinodal decomposition. Acta Metall 21: 1649 - 1659.

Laves F & Soldatos K (1963) Die albit/mikroklin -- orienteirungs -- beziehungen in mikroklin perthiten und deren genetische deutung. Z Kris-

tallogr 118: 69 - 102.

Lindsley DH (1966) Melting relations of $KAlSi_3O_8$: effect of pressure up to 40 kilobars. Am Mineral 51: 1793 - 1799.

Lindsley DH (1968) Melting relations of plagiocalse at high pressures. New York State Museum and Sci Service Memoir 18: 39 - 46.

Lindsley DH (1983) Pyroxene thermometry. Am Mineral 68: 477 - 493.

Lindsley DH & Dixon SA (1976) Diopside - enstatite equilibria at 850°C to 1400°C, 5 to 35 Kb. Am J Sci 276: 1285 - 1301.

Longhi J, Walker D & Hays JF (1976) Fe and Mg in plagioclase. Proc Lunar Sci Conf 7th: 1281 - 1300.

McLeod IR, Trail DS, Cook PJ & Wallis GR (1966) Geological work in Antarctica, January to March, 1965. BMR Record 9 (Unpublished).

Norris GH (1972) Experimental studies on ternary feldspars. Progress in Experimental Petrology. NERC publication series D, No 2: 15 - 19.

Parsons I (1978) Feldspars and fluids in cooling plutons. Mineral Mag 42: 1 - 18.

Parsons I & Brown WL (1983) A TEM and microprobe study of a two-perthite alkali gabbro: implications for the ternary feldspar system. Contrib Mineral Petrol 82: 1 - 12.

Powell R (1978) The thermodynamics of pyroxene geotherms. Phil Trans Roy Soc London A 288: 457 - 469.

Ribbe PH (1983) Exsolution textures in ternary and plagioclase feldspars; interference colors. In: PH Ribbe (ed) Feldspar Mineralogy. Review in Mineralogy Vol 2 (2nd ed). Mineral Soc Am. pp 241 - 270.

Ried H & Korekawa M (1978) Twinning and exolution in an antiperthite. Phys Chem Minerals 3: 263 - 270.

Robinson P (1982) The composition space of terrestrial pyroxene -- internal

and external limits. In: CT Prewitt (ed) Pyroxenes. Reviews in Mineralogy. Vol 7, Mineral Soc Am. pp 419 - 494.

Ross M & Huebner JS (1975) A pyroxene geothermometer based on composition-temperature relationships of naturally occurring orthopyroxene, pigeonite, and augite. Extended Abstr, International Conference on Geothermometry and Barometry, Pennsylvania State University.

Schairer JF & Bowen NL (1947) The system anorthite - leucite - silica. Geol Soc Finland Bull 20: 67 - 87.

Seck HA (1971) Koexistierende alkalifeldspate und plagioklase im system $NaAlSi_3O_8$ - $KAlSi_3O_8$ - $CaAl_2Si_2O_8$ - H_2O bei temperaturen von 650°C bis 900°C. N Jb Miner Abh 115 (3): 315 - 345.

Sen SK (1959) Potassium content of natural plagioclases and the origin of antiperthites. J Geol 67: 479 - 495.

Sheraton JW (1982) Origin of charnockitic rocks of MacRobertson Land. In: C Craddock (ed) Antarctic Geoscience, University of Wisconsin Press. pp 489 - 497.

Sheraton JW & Black LP (1981) Geochemistry and geochronology of Proterozoic tholeiitic dykes of East Antarctica: evidence for mantle metasomatism. Contrib Mineral Petrol 78: 305 - 317.

Sheraton JW & Black LP (1983) Geochemistry of Precambrian gneisses: relevance for the evolution of the east Antarctic shield. Lithos 16: 273 - 296.

Sheraton JW, Offe LA, Tingey RJ & Ellis DJ (1980) Enderby Land, Antarctica -- an unusual Precambrian high-grade metamorphic terrain. J Geol Soc Australia 27: 1 - 18.

Smith JV (1974) Feldspar Minerals. Vol I Crystal structure and physical properties. Springer-Verlag: New York.

Smith JV (1974) Feldspar Minerals. Vol II Chemical and Textural Properties. Spinger-Verlag: New York.

Smith JV (1983) Phase equilibria of plagioclase. In: PH Ribbe (ed) Feldspar Mineralogy. Reviews in Mineralogy Vol 2 (2nd ed), Mineral Soc Am. pp 223 - 240.

Smith JV (1984) Phase relations of plagioclase feldspars. In: WL Brown (ed) Feldspars and Feldspathoids. D.Reidel Publishing Company. pp 55 - 94.

Smith P (1978) The effect of anorthite on the alkali feldspar solvus at P(water) = 1 Kb. Progress Experimental Petrology. NERC publication series D: 247 - 248.

Spencer KJ & Lindsley DH (1981) A solution model for coexisting iron-titanium oxides. Am Mineral 66: 1189 - 1201.

Stephenson NCN (1984) Two-pyroxene thermometry of Precambrian granulites from Cape Riche, Albany - Fraser Province, Western Australia. J Metam Geol 2: 297 - 314.

Stormer JC Jr. (1983) The effect of recalculation on estimates of temperature and oxygen fugacity from analyses of multicomponent iron - titanium oxides. Am Mineral 268: 586 - 594.

Tingey RJ (1985) Uplift in Antarctica. Z Geomorph N F 54: 85 - 99.

Trail DS (1970) ANARE 1961 geological traverses on the MacRobertson Land and Kemp Land coast. BMR Report No 135. BMR Canberra, A C T.

Tuttle OF & Bowen NL (1958) Origin of granite in the light of experimental studies in the system $NaAlSi_3O_8$ - $KAlSi_3O_8$ - SiO_2 - H_2O. Geol Soc Am Memoir 74.

Viswanathan K (1971) A new X-ray method to determine the anorthite content and structual state of plagioclases. Contrib Mineral Petrol 30: 332 - 335.

Vogt JHL (1926) The physical chemistry of the magmatic differentiation of igneous rocks. II. On the feldspar diagram Or:Ab:An. Skrifter Utgitt av Det Norske Videns Kaps - Akademi I Oslo. I Mat. Naturvid Klasse, No.4.

Watson EB & Jurewicz SR (1984) Behavior of alkalies during diffusive interaction of granite xenoliths with basaltic magma. J Geol 92: 121 - 131.

Wells PRA (1977) Pyroxene thermometry in simple and complex systems. Contrib Mineral Petrol 62: 129 - 139.

Wood BJ (1978) Reactions involving anorthite and $CaAl_2SiO_6$ pyroxene at high pressures and temperatures. Am J Sci 278: 930 - 942.

Wood BJ & Banno S (1973) Garnet-orthopyroxene and orthopyroxene-clinopyroxene relationships in simple and complex systems. Contrib Mineral Petrol 42: 109 - 124.

Yoder SH Jr, Steward DB & Smith JR (1957) Ternary feldspars. Carnegie Inst Washington Geophy Lab Yearbook 56: 206 - 214.

Yund RA, Ackermand D & Seifert F (1980) Microstructures in the alkali feldspars from the granulite complex of Finnish Lapland. N Jahrb Mineral Monatsh 1980: 109 - 117.

Yund RA & Tullis J (1983) Subsolidus phase relations in the alkali feldspars with emphasis on coherent phases. In: PH Ribbe (ed) Feldspar Mineralogy. Reviews in Mineralogy. Vol 2 (2nd ed), Mineral Soc Am. pp 141 - 176.